Recent advances in catalyst-modified Mg-based hydrogen storage materials

Yaxiong Yang[a,†], Xin Zhang[b,†], Lingchao Zhang[b], Wenxuan Zhang[b], Huifeng Liu[b], Zhenguo Huang[c], Limei Yang[c], Changdong Gu[b], Wenping Sun[b], Mingxia Gao[b], Yongfeng Liu[a,b]*, Hongge Pan[a,b*]

[a]Institute of Science and Technology for New Energy, Xi'an Technological University, Xi'an, 710021, China.

[b]State Key Laboratory of Silicon Materials, Key Laboratory of Advanced Materials and Applications for Batteries of Zhejiang Province and School of Materials Science and Engineering, Zhejiang University, Hangzhou 310058, China.

[c]School of Civil & Environmental Engineering, University of Technology Sydney, 81 Broadway, Ultimo, NSW, 2007, Australia.

[†]These authors contributed equally to this work.

*Corresponding author:

Email: mselyf@zju.edu.cn (Y.F.L.); hgpan@zju.edu.cn (H.G.P.)

Abstract:

The storage of hydrogen in a compact, safe and cost-effective manner can be one of the key enabling technologies to power a more sustainable society. Magnesium hydride (MgH_2) has attracted strong research interest as a hydrogen carrier because of its high gravimetric and volumetric hydrogen densities. However, the practical use of MgH_2 for hydrogen storage has been limited due to high operation temperatures and sluggish kinetics. Catalysis is of crucial importance for the enhancement of hydrogen cycling kinetics of Mg/MgH_2 and considerable work has been focused on designing, fabricating

and optimizing catalysts. This review covers the recent advances in catalyzed Mg-based hydrogen storage materials. The fundamental properties and the syntheses of MgH_2 as a hydrogen carrier are first briefly reviewed. After that, the general catalysis mechanisms and the catalysts developed for hydrogen storage in MgH_2 are summarized in detail. Finally, the challenges and future research focus are discussed. Literature studies indicate that transition metals, rare-earth metals and their compounds are quite effective in catalyzing hydrogen storage in Mg/MgH_2. Most metal-containing compounds were converted *in situ* to elemental metal or their magnesium alloys, and their particle sizes and dispersion affect their catalytic activity. The *in-situ* construction of catalyzed ultrasmall Mg/MgH_2 nanostructures (< 10 nm in size) is believed to be the future research focus. These important insights will help with the design and development of high-performance catalysts for hydrogen storage in Mg/MgH_2.

Keywords: hydrogen storage, magnesium hydride, kinetics, catalysts, reversibility

1. Introduction

As an ideal energy carrier, hydrogen in the energy system can help to realize carbon neutrality because of its abundance, highest fuel energy density (142 MJ/kg), being environmentally friendly and renewable in nature [1-5]. However, the fact that hydrogen is a gaseous fuel at ambient condition with an extremely low volumetric density and highly flammable nature makes its safe, efficient and economical storage a huge challenge [6-9]. Traditionally, hydrogen can be stored and transported as

compressed gas or cryogenic liquid [10,11]. The problems encountered with compressed hydrogen storage are low volumetric hydrogen density (~40 g H_2 L^{-1} at 700 bar), high energy consumption for compression (~13–18% of the lower heating value is needed when hydrogen is compressed to 700 bar), and high safety risks. Liquid hydrogen storage has issues such as high consumption of primary energy (the energy required for liquefaction being about 40-50% of the total hydrogen energy content when taking hydrogen loss by boiling off into account), extremely low temperatures and high evaporation rates. In comparison, storing hydrogen in metal hydrides can avoid these limitations by chemically bonding hydrogen with metals to form compounds under moderate temperatures and pressures, enabling better safety and higher volumetric energy density [12,13].

Metal hydrides are usually formed through the reactions of metals and alloys with hydrogen. The typical hydrogen storage materials are intermetallic hydrides with high atomic weight [14-18]. Their hydrogen capacities are usually limited to ~2 wt% H_2, which are largely lower than the ultimate target (6.5 wt%) set by the United States Department of Energy for an on-board storage system [19]. Regarding gravimetric hydrogen density, the light metal hydrides are believed to be a better choice [12,20-23]. Among them, magnesium hydride, MgH_2, has aroused extensive interest because of several important features, including high hydrogen capacity (7.6 wt%), abundance (eighth most abundant element in the Earth' crust), low cost ($ 3/kg for Mg) and good reversibility [24-32]. However, the practical use of MgH_2 has been heavily limited by high operation temperatures and sluggish kinetics. For example, Mg can be converted

completely into hydride after several hours at 400 °C while exposed to hydrogen at 30 bar [30,31].

The Mg-H_2 reaction is a heterogeneous gas-solid reaction involving the adsorption and dissociation of dihydrogen molecules onto the metal surface, the penetration of hydrogen atoms through the metal surfaces, the diffusion of hydrogen atoms into the crystal lattice, and finally the formation of metal hydrides, along with different energy barriers [12,14,32]. The dissociation of H_2 molecules on Mg surface is of critical importance as the rate-limiting step for the initial stage of hydrogen absorption [10,31-36]. In contrast to transition metals, high energy is required for splitting H_2 molecules on Mg surface due to the lack of *d*-orbitals that can interact with the hydrogen antibonding orbital and therefore facilitate the dissociation of molecular hydrogen [37,38]. On the other hand, metallic Mg is very sensitive to air and oxygen and its surface is usually contaminated by MgO or $Mg(OH)_2$. Although this enables the potential of using Mg/MgH_2 for hydrogen purification [39], such oxide/hydroxide layer further inhibits hydrogen dissociation and blocks hydrogen diffusion from the surface to bulk [10].

To tailor hydrogen storage behaviors of Mg/MgH_2, considerable theoretical and experimental studies have been conducted [40-52], and several effective strategies have been proposed and attempted, including mechanical modification (e.g., ball milling, high-pressure torsion, ion irradiation, fast forging, and equal-channel angular pressing), alloying, nano-structuring, compositing with other metal/complex hydrides, and catalysis [52-70]. Among them, the addition of catalysts or catalytic additives has been

proven to be the simplest and effective in lowering the activation energy barrier and enhancing the hydrogen cycling kinetics of Mg/MgH_2. In this work, the recent advances in catalyzed Mg-based hydrogen storage materials are summarized and discussed. The review starts with a brief account of the basic physical and chemical properties and development of MgH_2 as a hydrogen carrier. The general catalysis mechanisms for hydrogen storage in MgH_2 are then illustrated. Subsequently, the catalysts developed in recent years are summarized. Finally, we discuss the challenges and future research. We hope that this review will help to guide the design and development of novel high-performance catalysts for hydrogen storage in Mg/MgH_2.

2. Fundamental properties of MgH_2 as a hydrogen store

Metallic Mg can reversibly store 7.6 wt% H_2 in mass and 110 g H_2 L^{-1} in volume according to the following reaction.

$$Mg + H_2 \rightleftharpoons MgH_2 \qquad (1)$$

The desorption enthalpy and entropy changes for bulk MgH_2 were determined to be approximately 76 kJ mol^{-1} H_2 and 130 J K^{-1} mol^{-1} H_2 [71], which gives rise to an operating temperature of ca. 311 °C at 1 bar of equilibrium hydrogen pressure according to the van't Hoff equation as shown below [72].

$$\ln P = \frac{\Delta H}{RT} - \frac{\Delta S}{R} \qquad (2)$$

Here, ΔH and ΔS are the enthalpy and entropy changes of the dehydrogenation reaction, respectively. T is absolute temperature and R is the gas constant. The desorption activation energy was measured to be ~160 kJ mol^{-1} for bulk MgH_2 [73,74].

As a well-industrialized product, Mg is very abundant and of low cost. Mg element

is around 2.5% of earth's crust, and also highly abundant in sea water. Metallic Mg crystallizes in a hexagonal close-packed (h.c.p.) structure, and hydrogenation typically leads to a tetragonal TiO_2 rutile-type structure (α-MgH_2), as shown in Fig. 1a and b [31,75]. This hydride will transform into metastable γ-MgH_2 with an orthorhombic α-PbO_2-type structure (Fig. 1c) when subject to pressures exceeding 0.39 GPa [76]. The orthorhombic structure goes back to the tetragonal phase at temperatures above 300 °C [77]. When the applied pressure reached 3.9 GPa, β-MgH_2 cubic modified CaF_2 structure was observed [78,79]. The formation of δ-MgH_2 (orthorhombic $Pbc2_1$ structure) at 6.73 GPa and ε-MgH_2 (cotunnite-type *Pnma* structure) at 10.26 GPa were also predicated using density-functional total-energy calculations [80].

MgH_2 was first synthesized by Jolibois et al. through the pyrolysis of ethyl magnesium iodide in vacuum at ~175 ºC in 1912 [81]. Wiberg et al. prepared MgH_2 with 68% purity from its elemental form in 1951 [82]. Dymova et al. increased the purity of MgH_2 to 97-98% in 1961 [83,84]. In 1984, Bogdanović proposed a two-step process to prepare MgH_2 using homogenous catalysis, including (i) the transformation of metallic Mg to a soluble form; and (ii) the reaction of this solution with gaseous H_2 with the presence of catalysts [85]. In 1995, Chen and Williams successfully synthesized MgH_2 by ball milling Mg powders for 47.5 h in 420 kPa H_2 at room temperature [86]. Recently, MgH_2 (97% pure) was fabricated by hydriding the pre-milled commercial Mg powders (Macklin, purity 98%, 20–100 mesh) at 380 °C under 50 bar of hydrogen [87].

The hydriding process of Mg involves a number of steps, including physisorption,

dissociation, chemisorption, the diffusion of hydrogen into subsurface sites and bulk lattice sites, and finally the nucleation and growth of the hydride phase [75,88]. The overall hydriding kinetics is controlled by the slowest step in the entire process. In general, the physisorption of H_2 is not rate-limiting because of the low energy barrier (<10 kJ mol^{-1} H_2) [89,90]. The chemisorption of H_2 requires a large energy of 432 kJ mol^{-1} to split H_2 molecules at the surface of Mg [34,35]. Once hydrogen atom is chemisorbed onto the surface, it will diffuse into the bulk to form Mg-H bond followed by nucleation and growth of MgH_2 phase. The diffusion coefficient of hydrogen in Mg was measured to be in the order of 10^{-13} m^2 s^{-1}, three orders of magnitude higher than the diffusion in MgH_2 (10^{-16} m^2 s^{-1}) [32,91]. As a result, the hydriding kinetics is related to three factors, (i) the dissociation of H_2 at the Mg surface, (ii) H penetration from the surface into the bulk, and (iii) H diffusion through MgH_2 already formed into the bulk. Correspondingly, there are also three main steps in dehydrogenation of MgH_2, including (i) dissociation of Mg-H bond, (ii) recombination of H atoms at the surface to form H_2 molecules, (iii) H atom or vacancy diffusion. Recently, several theoretical calculations identified that dissociation of Mg-H bond (also known as surface H desorption) was the most sluggish step at the initial stage because the H vacancy formed by dehydrogenation in the first layer requires high energy [92-101]. In these aspects, catalysis is believed to be of crucial importance for the enhancement of hydrogen cycling kinetics.

3. Catalytic mechanisms for hydrogen storage in MgH_2

Storing hydrogen in Mg suffers from slow hydriding and dehydriding kinetics. One of

critical factors is the lack of *d*-orbital electrons that can interact with the hydrogen antibonding (σ^*) orbital and thus facilitate the dissociation of dihydrogen [37,38]. As a result, catalyst is necessary to enable fast and effective dissociation of H_2 molecules [93,94,102], which is a typical heterogeneous catalysis process, and therefore an optimal interaction between the catalyst and Mg is very crucial. As shown in Fig. 2 [93], an effective heterogeneous catalytic process includes the adsorption and dissociation of H_2 molecules into H atoms at the surface of catalysts, which then diffuse into Mg. According to the Sabatier principle, the optimal catalysts should bind atoms and molecules with an intermediate strength: neither too strong nor too weak [103]. Transition metals, including Ti, Zr, V, Mn, Cr, Ni, Co, Nb, Fe and their compounds are typical heterogeneous catalysts for hydrogen storage in Mg. In particular, multivalent Ti has been demonstrated to facilitate the electron transfer between Mg^{2+} and H^- to promote hydrogen sorption in Mg [104]. The incompletely filled *d*-orbitals of transition metals can interact with the σ-bonding orbital of H_2 upon dissociation. This interaction is stabilized by back-donation of electrons from a filled *d*-orbital to the σ^*-antibonding orbital of hydrogen, which facilitates the dissociation of H_2 molecules into H atoms [105-107]. Moreover, hydrogen diffusion and hydride formation were observed to occur simultaneously at the interface between catalysts and Mg by working as a nucleation site favoring the hydride formation [108-111]. This was confirmed by the fact that the nucleation of Mg in MgH_2 changed from continues to site saturated with the presence of VB_2 [112].

Moreover, “hydrogen pump” mechanism was proposed for the composite-based

catalysts. For example, when $CeH_{2.73}/CeO_2$ was used to catalyze Mg-based hydrides, spontaneous hydrogen release was observed at the $CeH_{2.73}/CeO_2$ interface, viz., the boundary "hydrogen pump" effect, due to the significant reduction in the formation energy of V_H (hydrogen vacancy) in the $CeH_{2.73}/CeO_2$ boundary region [113]. Ouyang et al. fabricated a $CeH_{2.73}$-MgH_2- Ni nanocomposite by hydrogenating $Mg_{80}Ce_{18}Ni_2$ and observed the presence of numerous Ni nanoparticles, high-density interfaces between $CeH_{2.73}$ and MgH_2, and grain boundaries in nanocrystalline MgH_2 [114]. These interfaces and boundaries function as H diffusion channels and nucleation sites of hydrides. In addition, the *in situ* formed Ni and $CeH_{2.73}/CeH_2$ phases are of better homogeneity and finer sizes, thus displaying much higher catalytic activity for the hydriding/dehydriding reaction of Mg. Similar mechanism was also demonstrated for the Ni- or Co-containing Mg/MgH_2 systems because of the *in-situ* formation of Mg_2Ni/Mg_2NiH_4 and Mg_2Co/Mg_2CoH_5 during initial hydrogen desorption and absorption, respectively [115-121]. Recently, Lu et al. revealed a combined hydrogen spillover and hydrogen pump effect through *in-situ* observation of the hydrogenation/dehydrogenation of core–shell nanostructured Mg@Pt composites with high resolution transmission electron microscopy (HRTEM) [122]. Their results revealed that in the early stage, Pt on Mg particles showed a "spillover" effect to improve the hydrogen absorption kinetics. After that, it transformed into H-stabilized Mg_3Pt, followed by the formation of MgH_2. The H-stabilized Mg_3Pt acted as a "hydrogen pump" for the dehydrogenation of MgH_2 and then transformed into Pt after desorption. Such mechanism is of very importance in improving the dehydriding

kinetics and reducing the onset dehydrogenation temperature of the hydrogenated Mg@Pt composite.

Traditional and extended kinetic models have been used to understand the catalytic mechanisms for hydrogen storage in MgH_2, including Johnson-Mehl-Avrami-Kolmogorov (JMAK) model [123], extended JMAK model [124], Jander diffusion model [125] and Ginstling-Brounshtein model [14]. Pan et al. demonstrated that the de-hydrogenation behaviors of MgH_2 can be fitted well with the diffusion-controlled nucleation and growth model [126]. After adding 5 wt% TiO_2 nanoparticles supported on 3D macroporous structure, the hydrogenation kinetic model of Mg transformed from two-dimensional diffusion to three-dimensional diffusion [127].

According to above discussion, it is believed that a proper catalyst facilitates not only the adsorption and dissociation of H_2 molecules at its surface but also the hydrogen diffusion and the hydride formation upon hydrogen uptake.

4. Catalysts for hydrogen storage in MgH_2

Catalysts are very effective to improve hydrogen storage kinetics of MgH_2. Considerable effort has been devoted to searching for a proper catalyst, including metals, alloys, metal oxides, metal halides, MXenes, metal sulfides, metal hydrides, and carbon materials, as summarized in Fig. 3. The improved hydrogen storage properties of Mg/MgH_2 by various catalysts and catalytic additives are shown in Tables 1-8.

4.1 Metals and Alloys

Most *d*- and *f*-block metals, including transition metals and rare earth metals, have

demonstrated catalytic effect in the dissociation of H_2 molecules and are thus the most frequently used catalysts for hydrogen storage in MgH_2 [128]. After decades of development, Ni, Ti, Nb, V and Fe have been proven to be particularly effective in catalyzing hydrogen storage in Mg/MgH_2, as indicated in Table 1 [128-162].

Over 20 years ago, Zaluska et al. studied Pd, Fe, V, Zr, Ti, Mn and their combinations as catalysts to improve hydrogen sorption properties of nano-crystalline Mg [30]. They found that a small amount of Pd and Fe could offset the negative effects of surface oxidation and thus eliminated the activation. Liang et al. reported the effects of Ti, V, Mn, Fe and Ni in hydrogen sorption of MgH_2 [108]. Their results indicate that Ti was the most effective for hydrogen absorption while V was the best for hydrogen desorption. Shang et al. ball milled MgH_2 with 8 mol% Al, Ti, Fe, Ni, Cu or Nb to improve its hydrogen storage properties [129]. When dehydrogenation operated at 300 °C under vacuum, the MgH_2+Ni mixture showed the highest hydrogen desorption and the most rapid kinetics, followed by MgH_2 with Al, Fe, Nb, Ti and Cu. Similarly, Yu et al. observed the lowest hydrogen desorption activation energy (72 kJ/mol) and the lowest onset desorption temperatures (130 °C) for the MgH_2-10 wt% Ni composite, compared with samples modified with Fe, Co, Cu and Zn [130]. Cui et al. fabricated a core–shell like structure by coating transition metals (Ti, Nb, V, Co, Mo, and Ni) on Mg cores [131]. In their case, the Mg-Ni system displayed the best hydrogenation performance again. However, the dehydrogenation performance typically depends on the electronegativities of transition metals, ranking from Ti to Mo as Mg-Ti > Mg-Nb > Mg-Ni > Mg-V > Mg-Co > Mg-Mo. Note Ni is a special case, which is possibly due to

the *in-situ* formation of ultrafine Mg_2Ni nanoparticle with high hydrogen affinity. Emami et al. investigated the effects of 21 elements (e.g. Ni, Nb, Co, Fe, V, Zr etc.) on Mg prepared by high-pressure torsion and reported that Ni and V were quite effective [132].

Zhang et al. revealed that particle size and dispersion of Ni instead of the initial morphology was decisive for the hydrogen desorption of MgH_2 [133]. Doping 5 at% nano-sized Ni catalyst enabled the hydrogen absorption kinetics 16 times higher than that of pure Mg [134]. The introduction of porous nickel nanofibers composed of 50 nm-sized nanocrystals successfully reduced the desorption temperature of MgH_2 to 143 ºC [135]. More importantly, highly dispersed Ni single atom catalyst (SAC) prepared by a quasi-solid-state template method enabled fast dehydrogenation kinetics (300 °C, 5 min, 5.4 wt%), low activation energy (87.2 ± 5.4 kJ mol^{-1}) and high cycling stability (10 cycles, 97%) for hydrogen storage in MgH_2 [136]. *ab initio* molecular dynamics simulations revealed that the electronic properties of the transition metal SACs played an essential role in determining the dehydrogenation performance of MgH_2/SACs [137]. Moreover, the good (de)hydrogenation kinetics and superior cycling stability at 200 °C (without degradation within 600 cycles) were observed for the Ni-coated (3 layers of Ni) Mg sheets prepared by cold spray coating [138].

In the MgH_2-Ti system, TiH_{2-x} and TiH_2 were always formed *in situ* as the catalytic species upon ball milling and during hydrogenation/dehydrogenation [139-141]. Through fabricating a Mg-Ti nanocomposite using a co-precipitation technique with $MgCl_2$, $TiCl_4$, and lithium naphthalide (LiNp) as raw materials, Liu et al achieved 6.2

wt% of hydrogen uptake within 2 h at room temperature [142]. Using the high-pressure torsion (HPT) process, Edalati et al. obtained metastable Mg-Ti and Mg-Zr systems and reported that Ti and Zr can influence hydrogenation through phase transformation and cluster formation, resulting in fast room-temperature hydrogenation in Mg-Zr [143,144]. Mg-Nb and Mg-V nanocomposites prepared by a hydrogen plasma-metal reaction (HPMR) technique displayed remarkably improved hydrogen storage properties [145,146]. The Mg-7.5 wt% Nb nanocomposite rapidly absorbed 4.0 wt% H_2 within 10 min at 200 °C and 5.6 wt% H_2 within 60 min. The hydrogenated product released 4.0 wt% H_2 at 300 °C within 60 min. Recently, it was found that the addition of 5 wt% two-dimensional layered Fe nanosheets with a thickness of about 30 nm reduced the onset desorption temperature to 182.1 °C and absorption temperature to 75 °C [147]. At 200 °C, hydrogen absorption amounted to 6 wt% H_2 in 10 min. In addition to transition metals, rare earth metals are also very effective in catalyzing hydrogen storage in MgH_2. Zou et al. reported superior antioxidation with the presence of Nd, Gd, and Er [148]. In particular, the Er-containing Mg delivered 7.37 wt% of hydrogen capacity, which is higher than pure Mg (6.24 wt% due to oxidation).

Benefiting from synergy, binary and multielement alloys have attracted intense interests. Zhang et al. synthesized $ZrMn_2$ nanoparticles through a wet-chemical method, which enabled MgH_2 to release hydrogen from ~182 °C and reach 6.7 wt% H_2 in 5 min at 300 °C [149]. Here, $ZrMn_2$ nanoparticles facilitated the breaking of the Mg-H bonding and served as a “hydrogen pump” upon (de)hydrogenation. During hydrogenation, the dissociated H atoms entered $ZrMn_2$ to form $Zr_4Mn_8H_{10.99}$ and then

reached Mg through $Zr_4Mn_8H_{10.99}$ with a low energy barrier to form MgH_2. Upon dehydrogenation, $Zr_4Mn_8H_{10.99}$ decomposed to $ZrMn_2$ at a lower temperature than that of MgH_2. More encouragingly, Chen et al. obtained a highly effective alloy catalyst composed of Mo and Ni for MgH_2 [150]. Due to the synergy between Mo and Ni, MoNi alloy nanoparticles showed excellent catalytic effect, which promotes the breakage of Mg-H bonds and the dissociation of H_2, thus significantly improving the hydrogen cycling kinetics of Mg/MgH_2. MoNi-catalyzed Mg/MgH_2 system absorbed and released 6.7 wt% H_2 within 60 s and 10 min at 300 °C, respectively. A similar absorption performance was observed for nano-FeCo-catalyzed MgH_2 [151]. A series of ANi_5 (A= Ce, Nd, Pr, Sm, and Y) were also evaluated for their catalytic activity [152]. At 300 °C, the reversible hydrogen capacities were measured to be 6.16, 5.7, 6.21, 6.38 and 6.5 wt% for $CeNi_5$, $NdNi_5$, $PrNi_5$, $SmNi_5$ and YNi_5, respectively, with much better kinetic performance in comparison with pure MgH_2.

El-Eskandarany et al. reported that MgH_2-5 wt% $Zr_{70}Ni_{20}Pd_{10}$ metallic glass completed dehydrogenation/rehydrogenation at 200 °C/100 °C within 3.8 min/1.18 min, respectively, with 6 wt% of H capacity and excellent stability (no degradation within 100 hydrogen cycles) [153]. The improved kinetics was attributed to a remarkable grain refinement that facilitates fast hydrogen diffusion along grain boundaries. Zhang et al. reported an excellent dehydrogenation kinetics for the 20 wt% $Ti_{0.16}Cr_{0.24}V_{0.6}$-containing nanocrystalline Mg that desorbed 5.67 wt% H_2 in 20 min at 270 °C under 0.01 MPa H_2, while it was only 0.10 wt% H_2 for pure Mg under identical conditions [154,155]. The addition of $NiMn_{9.3}Al_{4.0}Co_{14.1}Fe_{3.6}$ reduced the initial dehydrogenation

temperature to 180 ºC [156]. Similarly, the hydrogenated BCC $Ti_{0.4}Cr_{0.15}Mn_{0.15}V_{0.32}$ lowered the desorption temperature of MgH_2 due to the fine dispersion of micro-/nano-BCC particles within the MgH_2 phase after ball milling [157]. Studies revealed that the hydrogenation kinetics was controlled by a 3D growth of the hydride phase and the H diffusion through the hydride phase, while the dehydrogenation kinetics was governed by the bulk/surface nucleation and 2D growth of the Mg phase with a constant velocity of the Mg/MgH_2 interface [158]. Further *in operando* study confirmed a cooperative effect between MgH_2 and the TiVCr additive [159]. Wan et al. reported the effect of FeCoNiCrMn high entropy alloy (HEA) on the hydrogen storage properties of Mg/MgH_2 system [160]. The MgH_2–5 wt% HEA composite released 5.6 wt% of H_2 at 280 °C within 10 min, and absorbed 5.5 wt% H_2 within 0.5 min at 150 °C.

For metal and alloy catalysts, however, high strength and good ductility make their uniform and dispersive distribution a huge challenge, which is one of the critical factors for their catalytic activity. Although hydrogenation can overcome this difficulty to some degree, it is an open question to fabricate nano-sized metal and alloy catalyst, which should be a focus of future research.

4.2 Metal oxides

From the aspect of dispersibility, metal oxides can be a better choice. Metal oxides, in particular transition metal oxides, have been extensively studied for their catalytic activity for hydrogen storage in MgH_2. In comparison with elemental metals, oxides are much more brittle and thus easier to disperse upon ball milling with MgH_2. Moreover, high-valent metal oxides readily react with MgH_2, which gives rise to the *in-*

situ formation of actual catalytic species. A wide variety of metal oxides, including binary oxides and complex oxides have been studied, which are summarized in Table 2 [163-223].

In 2001, metal oxides as catalysts to improve hydrogen sorption in nanocrystalline MgH_2 were reported by Oelerich and coworkers [163]. They compared the catalytic effects of TiO_2, V_2O_5, Cr_2O_3, Mn_2O_3, Fe_3O_4, and CuO and revealed that the Fe_3O_4-containing-composite delivered the fastest desorption kinetics followed by V_2O_5, Mn_2O_3, Cr_2O_3 and TiO_2. Moreover, only 0.2 mol% of the catalyst was sufficient to provide a fast sorption kinetics. In comparison with CeO_2 and Al_2O_3, the Cr_2O_3-modified Mg showed the highest hydriding/dehydriding rates [164]. Holding at 300 ºC for 60 min, the Mg+10 wt% Cr_2O_3 absorbed 5.87 wt% H_2 under 11 bar H_2 and desorbed 4.44 wt% H_2 under 0.5 bar H_2. Li et al. observed similar phenomenon [165]. Jung et al. found a temperature sensitivity of the catalytic activity of Al_2O_3, Cr_2O_3, V_2O_5 for hydrogen absorption by Mg [166]. V_2O_5 showed the fastest kinetics and hydrogen absorption capacities amounted to 3.2 and 2.25 wt% at 250 and 200 °C, respectively. The latest results indicated 2.1 wt% and 3.8 wt% of hydrogen uptake by 5 wt% V_2O_5-containing Mg at room temperature under 30 bar H_2 within 30 and 180 min, respectively [167]. All these results are closely related to the *in-situ* formation of low-oxidation V or metallic V during ball milling and/or dehydrogenation process, which play critical roles in improving the de/re-hydrogenation kinetics of MgH_2/Mg [167,168].

TiO_2 and Nb_2O_5 were also widely studied for their catalytic activity. As early as 1987, Khrussanova and coworkers improved absorption and desorption of Mg through the

addition of TiO_2 which facilitates the nucleation of MgH_2 [169]. Wang et al. reported a remarkable hydrogenation performance of Mg, including rapid kinetics, low working temperature and excellent oxidation-resistance with the addition of rutile TiO_2 [170]. By comparison, Aguey-Zinsou demonstrated a much faster hydrogenation kinetics for nanosized TiO_2 with respect to microsized counterparts [171]. Recently, considerable work has been devoted to developing different nanostructured TiO_2 catalysts, including 0D quantum dots, 1D nanotubes, 2D nanosheets and 3D ordered microporous networks [127,172-175]. For instance, the 2.5-4.0 nm TiO_2 quantum dots-catalyzed MgH_2 started releasing hydrogen at 260 °C and absorbed ~6.10 wt% in 77 s at 280 °C [172]. Improved rehydrogenation kinetics was found even at lower temperatures by absorbing ~5.0 wt% H_2 in 30 min at 100 °C. Jardim et al. studied hydrogen sorption kinetics of MgH_2 ball milled with TiO_2 1D nanotubes and nanorods [174]. The nanorods showed much better catalytic activity. At 350 °C, the modified sample absorbed 5.5 wt% H_2 after 10 min and re-desorbed all hydrogen in 5 min. Moreover, TiO_2 nanosheets with high-surface-energy {001} facets (TiO_2 NS) showed excellent catalysis [175]. The onset temperature of MgH_2 + 5 wt% TiO_2 NS for the release of hydrogen was ~180 °C and the corresponding peak temperature was 220 °C. Ma et al. found that the anatase TiO_2 with high percentage {001} facets has much better catalytic effect than that with low percentage {001} facets [176]. In addition, oxygen vacancy-rich 2D TiO_2 nanosheets reduced the onset hydrogen desorption temperature of MgH_2 to 180 °C (295 °C for pristine MgH_2) [177]. As for nanoparticles, Zhang et al. reported that 10 wt% nanocrystalline TiO_2 with ~10 nm in size reduced the onset desorption temperature

to 205 ºC, 95 °C lower than that of pristine MgH_2 [123]. The dehydrogenated sample absorbed 6.6 wt% H_2 in 10 min at 140 °C. Superior (de)hydrogenation performance of MgH_2 catalyzed by 3D flower-like TiO_2@C nanostructures was also obtained as the 5 wt% doped sample released 6.0 wt% H_2 at 250 °C within 8 min [178]. With a graphene-like TiO_2(B) nanosheet, the dehydrogenated MgH_2 could quickly absorbed 5.32 and 5.5 wt% H_2 at 50 and 60 °C, respectively [179]. With the assistance of microwave, MgH_2 with 25 wt% TiO_2 completed dehydrogenation at 220 °C and 4.25 wt% H_2 was recharged within 10 h at 25 °C under 1 bar H_2 [180]. In general, when ball milling TiO_2 with MgH_2, Ti^{4+} was readily reduced to Ti^{3+}/Ti^{2+} and even metallic Ti^0 [181]. The multivalent Ti was believed to act as the intermediates and provide catalytic active sites for the electron transfer between Mg^{2+} and H^- during the (de)hydrogenation process, which promoted H_2 dissociation and recombination on Ti surfaces, and thus led to the significantly enhanced kinetics [172].

Nb_2O_5 is also highly effective in catalyzing hydrogen cycling by Mg/MgH_2. In 2004, MgH_2-0.5 mol% Nb_2O_5 was reported to release 6.0 wt% of H within 500 s at 250 °C under vacuum [182]. Hanada et al. observed 5.0 wt% H_2 uptake at 150 °C for 1 mol% Nb_2O_5-MgH_2 in 30 s [183,184]. At ~20 ºC, hydrogen uptake still amounted to 4.5 wt%, largely superior to reported other metal oxides [185]. Friedrichs et al. reported a significant improvement when using nanometric Nb_2O_5 instead of its micrometric form [186]. This phenomenon was further confirmed by Fátay and coworkers [187]. By combing cold rolling and reactive ball milling, El-Eskandarany et al. fabricated MgH_2-10 wt% Nb_2O_5 nanocomposite, which absorbed/desorbed ~6.1 wt% H_2 and maintained

6 wt% H_2 after 230 continuous cycles at 225 °C [188]. Shinzato et al. fabricated five types of Nb_2O_5 by different heat treatment processes, and characterized their catalytic effects on the hydrogen absorption/desorption reactions of Mg [189]. It was concluded that Nb_2O_5 with lower stability of the crystal structure and smaller particle size showed better catalysis for both hydrogen desorption and absorption. Wang et al. achieved full hydrogenation of the dehydrogenated MgH_2 at 70 ºC under 50 bar H_2 by adding unique N-containing Nb_2O_5 [87]. The *in-situ* formed $NbN_{0.9}O_{0.1}$ was believed to play the critical catalytic role because of the joint action of N and Nb. Furthermore, they obtained N-doped Nb_2O_5 nanorods with 10-20 nm in diameter through graphene-guided growth, which enabled 5.5 wt% H_2 desorption at 175 ºC and full hydrogenation at 25 ºC under 50 bar H_2 (Fig. 4) [190]. This is largely superior to the previously reported catalyst-modified MgH_2 systems.

Other transition metal oxides, including ZrO_2 and Y_2O_3, were also studied for their catalytic efficacy. In 2012, Zeng et al. observed ~110 ºC reduction in hydrogen desorption temperature of MgH_2 from 350 °C to 240 °C after being milled with 20 ZrO_2 balls for 20 h, in comparison with ball milling using steel balls [191]. More interestingly, the completely dehydrogenated sample was able to absorb ~3.5 wt% H_2 at room temperature under 10 bar H_2 within 5 hours. Chen et al. found an effective grain size reduction of Mg when it was ball milled with ZrO_2 nanoparticles [192]. Through a single-pot solvothermal process, Zhang et al. prepared a hierarchical nanostructured ZrO_2 composed of primary particles of ~4 nm in diameter, which enabled MgH_2 to release H_2 from 163 °C and Mg to absorb 4 wt% H_2 within 12 s at 100 °C under 50 bar

H_2 [193]. The unique hierarchical structure facilitated uniform distributions of *in situ* formed multivalent Zr-based species (Zr^{4+}, $Zr^{1.64+}$, Zr^0), which allowed superior catalytic activity for hydrogen storage in MgH_2. This was further confirmed by Pukazhselvan et al [194].

In addition to transition metal oxides, the efficacy of rare earth oxides in catalyzing hydrogen storage of MgH_2 was also evaluated. Gupta et al. demonstrated the catalytic effect of La_2O_3, in the range 0.5–2.0 mol%, on the hydrogen storage properties of MgH_2 [195]. The desorption rates of samples with 1 and 2 mol% La_2O_3 were measured to be about 0.010 wt% H_2 s^{-1} at 300 ºC under 0.3 bar H_2, better than for sample with 0.5 mol% La_2O_3. LaH_3 was identified after hydrogenation/dehydrogenation cycles. Sadhasivam et al. observed a much lower desorption onset temperature for mischmetal oxide-modified MgH_2 than that for mischmetal-containing sample [196]. The presence of 2 wt% CeO_2 with a particle size of ∼10–15 nm led to 50 ºC decrease in desorption temperature [197]. More importantly, $CeH_{2.73}$ was formed during milling MgH_2 with CeO_2 in Ar due to reactive hydrogen diffusion and fast hydrogen desorption was observed even after air exposure [198]. Similar phenomena were also reported by Mustafa et al [199] and Lin et al [113]. In contrast, Pukazhselvan et al. suggested that CeO_2 was partially transformed to $CeO_{1.96}$ and hcp Ce_2O_3 phases when mechanically milled with MgH_2 and eventually was converted to Ce_2O_3 upon dehydrogenation at 300 °C [200].

Recent research focus has shifted to complex oxides when considering the synergistic catalytic effect of different metallic elements. Interests in complex oxides as catalysts

for hydrogen storage in MgH_2 originated from the observation of the *in-situ* formation of ternary Mg–Nb–O phases upon hydrogen cycling of MgH_2/Nb_2O_5 system, which was believed to be responsible for the reaction kinetic improvement [201-204]. Dolci et al. demonstrated that $Mg_3Nb_6O_{11}$ was active in the absorption and desorption of molecular H_2 [205,206]. The presence of $MgNb_2O_6$, $Mg_4Nb_2O_9$ and $Mg_3Nb_6O_{11}$ all significantly accelerated the hydrogen absorption and desorption processes of MgH_2 because the ternary Mg-Nb oxide facilitated H_2 transport into the solid structure of Mg [207]. Based on these observations, a series of complex oxides, including $MnFe_2O_4$, $CoFe_2O_4$, $ZnFe_2O_4$, $LaFeO_3$, $TiVO_{3.5}$, $TiNb_2O_7$, Co_2NiO, $SrFe_{12}O_{19}$, $SrTiO_3$, MnV_2O_6, $VnbO_5$, $MgNiO_2$, $BaFe_{12}O_{19}$, $CoTiO_3$, NiV_2O_6, $NiTiO_3$, $NiMoO_4$ and $CoMoO_4$ have been studied [113,200,206-223]. In comparison with $MgFe_2O_4$ and $ZnFe_2O_4$, $CoFe_2O_4$ showed the best catalytic performance [208]. The onset desorption temperature of MgH_2 + 7 mol% $CoFe_2O_4$ was measured to be 160 °C, which is 200 °C lower than of the as-received MgH_2 [209]. The nanoflake-like $MgNiO_2$-doped MgH_2 could even absorb 6.1 wt% H_2 within 10 min at 200 °C [214]. The presence of 10 wt% $TiVO_{3.5}$ reduced the dehydrogenation onset temperature of MgH_2 by 70 °C and the dehydrogenated sample absorbed 3.9 wt% H_2 in 5 s at 100 °C [216]. The addition of 7 wt% $TiNb_2O_7$ reduced the dehydrogenation onset temperature from 300 to 177 °C, and hydrogen uptake was detected at room temperature under 50 bar hydrogen [217]. In particular, 2D nanoflake-shape $TiNb_2O_7$ enabled 96% of capacity retention after 30 cycles [218]. Using nano-silica as a catalyst, the desorption kinetics of MgH_2 was also improved [224].

Overall, metal oxides can be effective catalysts for hydrogen storage in Mg/MgH_2. During ball milling and initial (de)hydrogenation, the high-valent metal ions are readily reduced to the low-valent species or even zero-valent metal. The interconversion among multivalent metal ions acts as a carrier for electron transfer, which catalyzes hydrogen cycling by Mg. Moreover, the interfaces between the *in situ* formed Mg alloys and their hydride phases function as a "hydrogen pump" and make the hydrogen release easier. All these are responsible for the enhanced performance. However, the formation of inert MgO by-product decreases the practical hydrogen storage capacity of the whole catalyst-modified composites. It is therefore necessary to balance the hydrogen storage capacity and the high catalytic activity of the oxides in MgH_2.

4.3 Metal halides

Similar to oxides, a wide range of metal halides, particularly chlorides and fluorides have been studied for their catalytic activity in hydrogen storage of Mg/MgH_2 [225-250]. Table 3 lists their catalytic effects on hydrogen storage properties of Mg/MgH_2. By comparing the performance of MgH_2 containing $NbCl_5$, CaF_2 or Nb_2O_5 additives, Bhat et al. found that the addition of $NbCl_5$ and CaF_2 improved the sorption capacity to 5.2 and 5.6 wt% within 50 min at 300 °C, respectively, in contrast to 80 min required in the case of Nb_2O_5 [225]. Ismail reported that the onset dehydrogenation temperature of 10 wt.% $FeCl_3$-doped MgH_2 sample was reduced by about 90 °C [226]. For Ti-based halides, Ma et al. reported superior catalytic effect for TiF_3 over $TiCl_3$ in improving the hydrogen sorption kinetics of MgH_2 [227]. Such phenomenon was also confirmed by Malka and coworkers who further compared the catalytic effects of ZrF_4, NbF_5, TaF_5,

FeF_2, FeF_3, $TiCl_3$ and VCl_3 [228-231]. This was primarily attributed to that the presence of F anions weakened the Mg-H bond and led to the formation of MgF_2 [232]. Moreover, group IV and V metal halides delivered higher catalytic activity with respect to other halides [228-231]. Ball milling TiF_4 with MgH_2 induced a conversion of TiF_4 to TiH_2 and MgF_2, which reduced the onset desorption temperature of MgH_2 to 200 °C [233]. Similarly, due to the formation of Mg_2Ni and MgF_2 on Mg particles, the NiF_2-modified Mg absorbed 3.26 wt% of H_2 at 100 ºC in 2 h [234]. The H_2 absorption for SrF_2-containing Mg was found to be 6.0 wt% in 5 min at 290 °C [235]. The onset desorption temperature of MgH_2 modified with CsF was measured to be 249 °C, 106 °C lower than that of ball-milled MgH_2 without any additives measured under identical conditions [236]. MgF_2 was also used as a catalyst to improve the hydrogen storage properties of MgH_2 [237]. In addition, $ZrCl_4$, VCl_3, $HfCl_4$ and $PdCl_2$ have been widely investigated [238-241]. The results showed that the dehydrogenation peak temperature of $ZrCl_4$-doped MgH_2 system was 257 °C, reduced by 100 °C with respect to the ball-milled MgH_2 [238]. This was attributed to the grain refinement of the $ZrCl_4$-doped system and the reduction of Zr^{4+} to Zr^{3+} and Zr^0. For the MgH_2-$HfCl_4$ composites, the reduction in particle sizes and the *in-situ* generation of $MgCl_2$ and Hf-containing species during milling led to the synergistic catalytic effects [240]. Various phases, including β-MgH_2, Mg_6Pd, $MgCl_2$ and $PdH_{0.778}$ were identified in the $PdCl_2$-modified MgH_2 composites, which were believed to be the catalytic species for the improved performance [241].

Ternary metal fluorides have also attracted considerable attention as catalysts for hydrogen storage by Mg/MgH_2, such as K_2TiF_6, K_2NiF_6, K_2ZrF_6, K_2NbF_7, K_2SiF_6 and

Na_3AlF_6 [242-247]. Inspired by Liu's report [248], Mustafa et al. studied the influence of K_2TiF_6 additive on the hydrogen sorption properties of MgH_2 in 2014 [242]. The addition of 10 wt% K_2TiF_6 to MgH_2 enabled an onset desorption temperature of 245 °C, about 105 °C and 205 °C lower than the as-milled and as-received MgH_2, respectively. It was reasonable to conclude that the K_2TiF_6 additive played a catalytic role through the formation of active species of KH, TiH_2, MgF_2 and Ti during the ball milling or heating process. Similar phenomenon was also observed for K_2NiF_6, K_2ZrF_6, K_2NbF_6, K_2SiF_6 and Na_3AlF_6 [244-247]. K_2NbF_7 was converted to MgF_2, KH and Nb; K_2SiF_6 to KH, MgF_2 and Mg_2Si; and Na_3AlF_6 to $NaMgF_3$, NaF and AlF_3. These were believed to be active in reducing the onset temperature of hydrogen desorption to 255~290 ºC.

The same as oxides, metal halides are also particularly effective in catalyzing hydrogen storage in Mg/MgH_2 due to the *in-situ* formation of catalytic species and their dispersive distribution. However, the strong affinity between Mg^{2+} and halide anions resulted in the generation of the inert by-products, i.e., $MgCl_2$, which induced the unacceptable reduction in the practical hydrogen storage capacity. As a result, how to alleviate this adverse effect requires further investigation.

4.4 MXenes

MXenes as a new family of 2D transition metal (e.g., Ti, V, Nb, etc.) carbides, carbonitrides and nitrides have attracted considerable attention as catalysts because of their high surface areas, good electronic and thermal conductivity behaviors [250-260]. For catalyzed hydrogen storage in Mg/MgH_2 by MXenes, the reported results are summarized in Table 4. In 2016, Liu et al. conducted the first attempt to evaluate the

catalytic effect of 2D Ti_3C_2 on the reversible hydrogen storage behaviors of MgH_2 [253]. The 5 wt% Ti_3C_2-containing MgH_2 released 6.2 wt% H_2 within 1 min at 300 °C and absorbed 6.1 wt% H_2 within 30 s at 150 °C, exhibiting largely enhanced (de)hydrogenation kinetics. The enhanced kinetics was attributed to the unique layered structure and Ti species, which remarkably facilitated the dissociation and recombination of hydrogen on the surface of Ti. Shen et al. fabricated a novel solid-solution MXene $(Ti_{0.5}V_{0.5})_3C_2$ by exfoliating a solid-solution MAX phase $(Ti_{0.5}V_{0.5})_3AlC_2$ and studied its catalytic effect on the hydrogen storage of Mg [254]. The 10 wt% $(Ti_{0.5}V_{0.5})_3C_2$-containing MgH_2 released approximately 5.0 wt% H_2 within 20 min at 250 °C and the dehydrogenated sample rapidly absorbed 4.8 wt% H_2 within 5 s at 120 °C. XPS results revealed that during ball milling, $(Ti_{0.5}V_{0.5})_3C_2$ reacted with MgH_2 and was converted to metallic Ti and V, which behaved as catalysts in the subsequent thermal dehydrogenation because their chemical states remained unchanged. Following these reports, Wu et al. demonstrated that the presence of 6 wt% multilayer Ti_3C_2 decreased the initial desorption temperature of MgH_2 to 142 °C with a capacity of 6.56 wt% [255]. The introduction of 5 wt%Ti_2C decreased the onset desorption temperature by 37 °C [256]. Theoretical calculations revealed that the catalytic effects of 2D Ti_2C on MgH_2 included two factors: electron transfer and *in situ* formed TiH_2 [257]. Wang et al. synthesized a novel solid-solution NbTiC MXene that enabled 195 °C of initial desorption temperature [258]. Similar catalytic efficacy was also attained by introducing $Nb_4C_3T_x$ or V_2C [259,260]. The post-activated MgH_2-5 wt% Nb_4C_3Tx composite started releasing hydrogen at ~150 °C, representing a ~146 °C reduction in

the onset temperature [259]. The onset desorption temperature of MgH_2 doped with V_2C was reduced by 128 °C to 190 °C [260]. As an effective catalyst, V_2C elongated the bond length of Mg-H from 1.71 Å for pure MgH_2 to 2.14 Å for MgH_2 doped with V_2C, therefore destabilizating MgH_2.

4.5 Metal sulfides

Transition metal sulfides have also shown remarkable catalytic effect on the hydrogen cycling of MgH_2, as seen in Table 4 [261-270]. In 2013, Jia et al. compared the catalytic effect of MoS_2 and MoO_2 and found that MoS_2 presented a much better catalytic effect than MoO_2 on improving the hydrogen cycling kinetic of MgH_2 [261]. The enhanced kinetics was attributed to the presence of MgS/Mo or MgO/Mo that catalyzed the hydrogen absorption/desorption behavior. After that, Wang et al. studied the (de)hydrogenation kinetics of the MgH_2-WS_2 composites [262]. The co-catalytic effect between the new phases W and MgS formed during ball milling resulted in 58 ºC reduction in the onset dehydrogenation temperature of MgH_2. With the addition of Fe_3S_4, the dehydrogenation temperature of MgH_2 was reduced by 90 ºC [263]. The MgH_2–16.7 wt% FeS_2 composite absorbed 3.71 wt% H_2 at 150 ºC, which is 3.59 times higher than that of the as-milled pure MgH_2 [264]. The synergistic effects of the *in situ* formed Fe active species and MgS enhanced the hydrogen storage properties of MgH_2. With a solvothermal method, Xie et al. fabricated flower-like NiS particles and evaluated its catalytic activity for hydrogen storage in Mg nanoparticles [265]. After ball milling with Mg nanoparticles, the NiS was converted into Ni, MgS and Mg_2Ni, which enabled the quick uptake of 3.5 wt% H_2 within 10 min at 150 ºC and the release

of 3.1 wt% H_2 within 10 min at 300 ºC. The MgH_2-5 wt% NiS_2 composite absorbed more than 5.1 wt% H_2 within 1 h at 100 ºC [266]. Here, the doped NiS_2 was transformed into MgS and Mg_2NiH_4 during the heating process, which led to the catalytic effects. Further comparison on TiS_2, NbS_2, MoS_2, MnS, CoS_2 and CuS revealed the best (de)hydrogenation kinetics for MgH_2–TiS_2 because its onset dehydrogenation temperature was measured to be about 204 °C, lowered by about 126 °C than that of MgH_2 [267]. By using CoS-nanoboxes as multifunctional scaffolds, Ma et al. achieved the dual-tailoring of thermodynamics and kinetics of hydrogen storage in MgH_2, thanks to the "nano-sizing effect" of nanoconfined Mg/MgH_2 crystals, the catalyzing effect of MgS and the multifunctional role of the CoS-nanobox scaffold [268]. Lately, Fu et al. demonstrated the catalytic effect of a carbon-supported transition metal compound, FeCoS@C, on hydrogen storage of Mg [270]. Their results shown in Fig. 5 indicated that MgH_2-FeCoS@C rapidly absorbed 6.78 wt% H_2 within 60 s at 300 ºC. The *in-situ* formed Mg_2Co, α-Fe and Co_3Fe_7 acted as "hydrogen channels" to accelerate hydrogen transfer, and MgS with excellent catalytic effect contributed a strong and stable catalytic effect. In addition, the carbon skeleton obtained by the carbonization of MOF not only served as a dispersant for the multiphase catalytic system, but also provided more active sites for the catalysts. It is therefore believed that the multiphase and multiscale catalytic systems are particularly favorable for improving the hydrogen storage performance of MgH_2.

4.6 Metal hydrides

Taking consideration of the practical hydrogen capacity, metal hydrides should be more

preferable as catalysts for hydrogen storage in Mg/MgH_2 [271-287]. The hydrogen storage properties of metal hydride-modified Mg/MgH_2 systems are shown in Table 5. In 2009, Lu et al. prepared a nanostructured MgH_2−$0.1TiH_2$ system by ultrahigh-energy high-pressure mechanical milling and obtained the lowest dehydrogenation onset temperature (∼110 °C) for MgH_2 based on TGA analysis [271]. More importantly, there was only little loss in hydrogen storage capacity after 80 cycles. The nanosize coupled with the addition of TiH_2 contributed to the improvement in the kinetics of (de)hydrogenation. This stimulated considerable studies on TiH_2-catalyzed MgH_2 [140,272-275]. Jangir et al. revealed that as a hydrogen saturated catalyst, TiH_2 provided abundant active sites for H_2 adsorption and dissociation [273]. Hao and Sholl found that epitaxial contact between MgH_2 and TiH_2 was formed with favorable interface energies by using first-principles density functional theory calculations [274]. The strain induced by TiH_2 (111) on MgH_2 and Mg in these interfaces reduced the enthalpy for H_2 release from MgH_2. However, Cuevas et al. demonstrated experimentally that the presence of TiH_2 did not modify the thermodynamics of the Mg/MgH_2 system [275]. Through the high-pressure torsion (HPT) method, Kitabayashi and coworkers fabricated metastable hydrides in the MgH_2–TiH_2 system with low hydrogen binding energy, therefore favoring low-temperature hydrogen storage [276]. The MgH_2–TiH_2 composite nanoparticles prepared by reactive gas-phase condensation of Mg–Ti vapors under He/H_2 atmosphere even achieved reversible hydrogen sorption below 150 ºC [277]. It was believed that TiH_2 acted as a catalyst promoting the generation and diffusion of H vacancies in MgH_2 [278]. Co-catalysis effect was

obtained by ball-milling MgH_2 and TiH_2 anchored on graphene [279].

Recently, Rizo-Acosta et al. systematically compared the catalytic effects of early transition metals (ETM) hydrides (ScH_2, YH_3, TiH_2, ZrH_2, VH and NbH) on the hydrogenation properties of Mg [280]. Their results demonstrated that on desorption, ETM hydrides could catalyze the recombination of hydrogen atoms, and on absorption, the formation of coherent interfaces between ETM hydrides and MgH_2 favored the nucleation of the latter. The best hydrogen cycling properties were found for the MgH_2–5 wt% TiH_2 nanocomposite with a reversible capacity of 4.8 wt% H_2 after 20 cycles. This was mainly attributed to the lattice mismatch between Mg and TiH_2 that limited Mg grain growth and facilitated the fast absorption kinetics of the MgH_2–TiH_2 nanocomposite on cycling. For ScH_2 catalyzed MgH_2, the optimal catalyst content was ca. 12 mol% to achieve the lowest activation energy [281]. Luo et al. reported hydrogen storage properties of nano-structured $0.65MgH_2/0.35ScH_2$ which was produced by hydriding $Mg_{0.65}Sc_{0.35}$ [282]. $Mg_{0.65}Sc_{0.35}$ showed ca. 6.4 wt% H_2 uptake in the first cycle at 150 °C and 4.3 wt% H_2 of reversible capacity in the following (de)hydrogenation cycles. Similarly, NdH_2-Mg-Mg_2Ni nanocomposite formed by hydriding $Nd_{4.3}Mg_{87.0}Ni_{8.7}$ alloy also delivered fast hydrogen storage kinetics because of the abundant grain boundaries and “hydrogen pump” effect of NbH_2 [283]. Chen et al. observed that ZrH_2-doped MgH_2 composite started to release H_2 at 203 °C, and the dehydrided sample quickly absorbed 5.90 wt% H_2 at 65 °C [284]. Mechanistic investigations revealed that H atoms preferentially accumulated around ZrH_2 because of the lower hydrogen dissociation energy on the surfaces of ZrH_2 (1.421 eV) than that

of pure Mg (2.301 eV). Moreover, the large lattice disorder zone between ZrH_2 and Mg phases enabled H atoms to diffuse easily into the lattice of Mg nearby, therefore facilitating the formation of MgH_2. Lately, Zhang et al. studied the hydrogen storage behaviors of nano-VH_x-modified MgH_2 and found that hydrogen release commenced from 182 °C and the release of hydrogen amounted to 6.3 wt% H_2 within 10 min at 230 °C [286]. The dehydrogenated product rapidly absorbed 5.2 wt% H_2 within 3 min at 50 °C under 50 bar H_2 and even 4.3 wt% H_2 within 30 min at 25 °C under 10 bar H_2. Upon hydrogen cycling, the reversible transformation between V and V-H species was observed, indicating that the homogeneously distributed V-based species worked as a hydrogen pump and nucleation sites for MgH_2 and Mg, respectively, thus enhancing hydrogenation/dehydrogenation kinetics.

4.7 Other compounds

Metal nitrides, carbides, borides and metal-organic frameworks (MOFs) have also been employed to improve hydrogen storage performance of MgH_2 [235,287-307]. The reported results are summarized in Table 5. In 2014, Wang et al. synthesized TiN decorated graphene (TiN@rGO) and found that 10 wt% TiN@rGO doped MgH_2 started to release hydrogen at ~167 °C, and up to 6.0 wt% H_2 was discharged within 18 min when isothermally heated to 300 °C [287]. NbN nanoparticles (~20 nm) also exhibited superior catalytic effect on (de)hydrogenation kinetics. Approximately 6.0 wt% H_2 was liberated from the MgH_2+5NbN sample within 12 min at 275 °C and the dehydrogenated sample absorbed 6.0 wt% H_2 within 16 min at 150 °C. In particular, the high chemical stability of TiN and NbN ensured a stable catalytic effect upon

cycling.

Similarly, metal carbides have also attracted attention. Shin et al. observed considerable catalytic effects of TiC on the (de)hydrogenation of MgH_2 [288]. 50 nm TiC-modified MgH_2 desorbed about 6.2 wt% H_2 within 20 min and absorbed more than 90% of hydrogen capacity within 5 min at 300 ºC. Such phenomenon was further confirmed by Tian and Shang [289]. With respect to Ni_3N, NiO and Ni_2P, MgH_2-Ni_3C system featured the lowest activation energy for hydrogen desorption [290]. Tian et al. indicated that Ti_3C_2 showed the highest catalytic effect on dehydrogenation of MgH_2, followed by Ni_3C, NbC, Mo_2C and Cr_3C_2 [291]. The 10 wt% Ta_2C-doped Mg took about 5 min to reach full hydrogenation at 300 ºC, and a full dehydrogenation was realized within 15 min at 350 ºC [292]. The MgH_2-7 wt% Ti_3AlC_2 sample liberated ~6.9 wt% H_2 starting from 205 °C, and the dehydrogenated sample absorbed 5.8 wt% H_2 within 60 s at 150 °C [293]. The improved hydrogen absorption−desorption kinetics was attributed to the catalytic effect of metal carbides and their role in inhibiting crystal growth [235,290,292,294].

Metal borides were also employed to improve the hydrogen storage performance of MgH_2. For example, TiB_2 could decrease the dissociation temperature of MgH_2 by about 50 °C [295]. This was further confirmed by the result that the peak desorption temperature of MgH_2–5wt%TiB_2/GNSs was lowered to 319 °C [296]. They also observed that the MgH_2–10 wt% NiB mixture desorbed 6.0 wt% H_2 within 10 min at 300 °C [297]. The presence of 10 wt% CoB/CNTs lowered the initial dehydrogenation temperature of MgH_2 by 166 °C, and the isothermal dehydrogenation rate was increased

by 572 times [298]. Recently, the catalytic efficacy of FeB and CoFeB was also evaluated [299,300]. The results indicated that the MgH_2−10 wt% CoFeB/CNTs composite started to release H_2 at 177 °C and a dehydriding rate of 29.7 wt% H_2 h^{-1} was achieved at 300 °C [300]. The *in-situ* formation of Co_3MgC, Fe, CoFe and B due to the introduction of CoFeB/CNTs provided active and nucleation sites for the (de)-hydrogenation reactions of MgH_2. Meanwhile, CNTs also facilitated hydrogen diffusion and improved the thermal conductivity. All of these improved the (de)hydrogenation performance and cyclic stability of MgH_2. La-Ni-B composites showed much higher structural and catalytic stability than Ni-B during hydrogen cycling of MgH_2 at high temperatures [301]. MgH_2 with 5 wt% 2La-3Ni-B liberated about 6.0 wt% H_2 within 5 min at 300 °C.

Metal organic frameworks (MOFs) have also attracted wide attention because they can not only directly store hydrogen as sorbents by physisorption but also nanoconfine metal hydrides as scaffolds and function as catalysts or catalytic precursors for catalyzing hydogen storage [302-307]. Wang et al. demonstrated the catalytic effects of ZIF-8(Zn), ZIF-67(Co) and MOF-74(Mg) on hydrogen storage properties of Mg [304]. The Mg/ZIF-67(Co) composite exhibited the best (de)hydrogenation kinetics with a good cyclability within 100 cycles. The excellent cyclic stability primarily resulted from the core-shell structure of the Mg/ZIF-67 nanocomposite. Ma et al. fabricated three kinds of MOFs with Co(II), Fe(II) and Ni(II) as metal ions and trimasic acid (TMA) as the organic linker and evaluated their catalytic activity for hydrogen storage in Mg/MgH_2 [305,306]. The TMA-Ni MOF-modifed MgH_2 delivered the lowest

absorption activation energy (51.2 kJ/mol H_2). The onset desorption temperature was reduced by 167.8 ºC with respect to that of the pure MgH_2 at 10 ºC/min of heating rate [306].

4.8 Composite catalysts

Composite catalysts have been studied and developed by combining two or more kinds of catalysts to improve activity (Table 6) [115,308-328]. The enhanced efficacy is mainly attributed to the synergistic effect of different catalytic species. As early as 1999, Zaluska et al. demonstrated that the addition of 4 wt% (Mn +Zr) was especially effective, enabling ~7 wt% of hydrogen absorption at 190 ºC under 10 bar H_2 [30]. Chen et al. performed first-principles calculations to understand the interaction between a H atom and transition metal-doped Mg (0001) surface, including Sc, Ti, V, Cr, Mn, Fe, Co, Ni, Cu, Zn, Y, Zr, Nb, Mo, Tc, Ru, Rh, Pd, Ag, Cd, Au and Pt [308]. Their results suggested that all these transition metal atoms preferred to replace Mg atoms in the second layer rather than those in the outermost layer of the Mg surface. Co-doping with Ti well stabilized Co, Ni, Pd, Ag, Pt and Au within the first layers, and Ni and Co entered into the first layer of Mg surface when co-doped with Ti, V and Nb, consequently favoring the hydrogenation of Mg. Compared with Ni alone, the Ni-TiO_2 combination offered much better catalytic activity for hydrogen storage in MgH_2, thanks to the synergistic effect of reversible transformation of Mg_2Ni/Mg_2NiH_4 that acts as a "hydrogen pump" and the multi-valent Ti compounds ($Ti^{4+/3+/2+}$) that promote the electron transfer [115].

Although doping with nano-Y_2O_3 has only limited effect [309], the Y_2O_3–YH_2

composite showed higher catalytic efficacy for hydrogen storage in MgH_2, especially with dehydrogenation rate dramatically increasing by 3 times [310]. Liu et al. synthesized an intersected Y_2O_3–NiO hybrid spherical hollow structure, which enabled ca. 6.6 wt% H_2 release at 275 °C within 60 min and 5.9 wt% H_2 uptake at 150 °C within 150 min [311]. About 5.2 wt% H_2 was desorbed after 50 cycles at a moderate cycling condition. The *in-situ* formation of Al_3Ti, MgF_2 and Al enabled 100 °C reduction in the peak temperature from 329 °C to 228 °C for hydrogen desorption of the MgH_2-10 wt% ($Mg(AlH_4)_2$-0.5TiF_4) system [312]. In the MgH_2–PrF_3–Al–Ni system, Pr_3Al_{11}, MgF_2, PrH_3 and Mg_2NiH_4 nanoparticles were *in situ* formed and enhanced hydrogen desorption kinetics [313]. The Mg+Mg_2Ni+YH_2 nanocomposite absorbed maximum ~5.2 wt% H_2 at 40th cycle and 4.3 wt% H_2 after 620th cycle [314]. The improvement was ascribed to the relatively high interface energy of YH_2/Mg, the low diffusion energy barrier for H at YH_2/Mg interface and the high affinity between YH_2 and H. It was believed that minimizing the separation between Mg/MgH_2 matrix and YH_2 nano-catalysts was of crucial importance to maintain the high capacity of the Mg+Mg_2Ni+YH_2 nanocomposite.

A series of MXene-based composites have been prepared as catalysts to improve hydrogen cycling in Mg/MgH_2. Gao et al. prepared a sandwich-like Ti_3C_2/TiO_2(A)-C through a facile gas–solid method [315]. The peak desorption temperature of MgH_2-5 wt% Ti_3C_2/TiO_2(A)-C was measured to be 308 °C, much lower than that of MgH_2-5 wt% Ti_3C_2 (340 °C) and MgH_2-5 wt% TiO_2(A)-C (356 °C). Similarly, Lu et al. reported that the hydrogen absorption and desorption kinetics of Mg/MgH_2 can be significantly

improved due to the synergy between Nb_2CT_x MXene and ZrO_2 [316]. Several Ni-Ti_3C_2 composite catalysts were also demonstrated by different groups [317,318]. Gao et al. synthesized a composite of layered $Ti_3C_2T_x$ with nano-Ni particles, which adopted an interconnected and interlaced structure [317]. This unique structure displayed superior catalytic activity for MgH_2 because MgH_2-5 wt% Ni_{30}/FL-$Ti_3C_2T_x$ released approximately 5.83 wt% H_2 within 30 min at 250 °C and absorbed 5 wt% H_2 within ~28 min at 100 °C, as shown in Fig. 6. Ni nanoparticles self-assembled onto the surface of Ti_3C_2 nanosheets enabled the MgH_2 + Ni@Ti-MX composite to absorb 5.4 wt% H_2 in 25 s at 125 °C and to release 5.2 wt% H_2 in 15 min at 250 °C [318]. The largely improved hydrogen storage kinetics was further confirmed by Gao et al. and Peng et al [319,320]. The combination of V_2C/Ti_3C_2 MXenes initiated hydrogen desorption of MgH_2 at around 180 °C with 5.1 wt% H_2 desorbed within 60 min at 225 °C. Under 60 bar H_2, the dehydrided MgH_2–V_2C/Ti_3C_2 absorbed 5.1 wt% H_2 within 20 s at 40 °C [321]. Also, the N-Nb_2O_5@Nb_2C-doped MgH_2 composite could absorb hydrogen at room temperature [322]. Lately, Wang et al. reported that Ti_3C_2-supported PrF_3 nanoparticles (PrF_3/Ti_3C_2) prepared by a hydrothermal method exhibited superior catalytic activity toward hydrogen storage by MgH_2 [323]. The onset temperature of dehydrogenation was reduced to 180 °C after adding 5 wt% PrF_3/Ti_3C_2, corresponding to a reduction of 107 °C compared with pristine MgH_2. About 7.0 wt% H_2 was rapidly desorbed within 3 min at 260 °C and 6.6 wt% H_2 was absorbed within 36 s at 200 °C for MgH_2-5 wt% PrF_3/Ti_3C_2. The synergistic effects between Ti-species and PrF_3 and the favorable electron transfer among multivalent Ti-species (Ti^0, Ti^{2+}, and Ti^{3+}) are

responsible for the markedly enhanced hydrogen storage properties of MgH_2.

MOFs-based composite catalysts have also been developed recently. By using ball milling, Ma et al. prepared TMA-Ni MOF and TMA-Fe-MOF co-doped MgH_2, which benefited from the synergy between nano α-Fe and Mg_2NiH_4/Mg_2Ni generated during the (de)hydrogenation of MgH_2 [324]. The hydriding activation energy of the MgH_2-TM MOF was reduced to 45.3 kJ mol^{-1} H_2. A bi-metal Ni-Co-MOF-74 was mixed with MgH_2 as a catalyst, which provided more active sites and improved the hydrogen sorption properties of the composite [325]. At 280 °C, the Ni-Co-MOF-containing MgH_2 released 4.7 wt% H_2 within 30 min and absorbed 6.3 wt% in 2 min at 200 °C. Zhang et al. synthesized a MOF-supported Nb_2O_5 composite catalyst (Nb_2O_5@MOF), which reduced the onset desorption temperature of MgH_2 from 347 °C to 185.3 °C [326]. The fully dehydrogenated composite absorbed hydrogen starting from 25 °C and picked up 6.5 wt% hydrogen within 6 min at 175 °C. Here, MOF acted as a matrix to enable the homogeneous dispersion of Nb_2O_5 nanoparticles, thus creating more active sites for catalysis.

4.9 Carbon-based catalysts

4.9.1 Various carbon materials

With high specific surface areas, abundant reactive sites and superior heat conductivity, carbon-based materials are also a good choice to increase the electron transfer and improve the hydrogen cycling kinetics [329-356]. The corresponding results are listed in Table 7. In 2002, Imamura and coworkers fabricated Mg/G nano-composites by mechanical grinding of Mg and graphite with organic additives (benzene, cyclohexane

or tetrahydrofuran), which led to not only a decrease in the onset decomposition temperature of MgH_2, but also the formation of additional hydrogen uptake sites [329]. In contrast, the results by Shang and Guo showed that graphite had little influence on the desorption properties of MgH_2 but largely facilitated the absorption process [330]. The dehydrogenated sample reabsorbed 5 wt% of H within 30 min at 250 °C. Improvement in hydrogen cycling properties was also achieved through adding graphite [331]. Interestingly, the rehydrogenated MgH_2/graphite composite exhibited 35 °C reduction in the desorption temperature compared with that of the as-prepared composite [332]. Wu et al. observed much superior catalytic effect for single-walled carbon nanotubes (SWNTs) as an additive in improving the hydrogen absorption performance of Mg to other carbon materials, including activated carbon, carbon black, fullerene and graphite [333]. The 5 wt% SWNTs-modified Mg absorbed 6.0 wt% H_2 within 60 min at 150 ºC [334]. Lillo-Ródenas et al. studied hydrogen storage performance of MgH_2 with different carbon materials, including graphite, activated carbon, multi-walled carbon nanotubes (MWCNTs), carbon nanofibres (CNFs) and activated carbon fibres (ACFs) [335]. They concluded that the presence of carbon materials prevented MgH_2 particle growth which, in turn, enhanced its dehydrogenation. Singh et al. demonstrated ~65 ºC decrease in the desorption temperature of MgH_2 mixed with 2 wt% twisted carbon nanofibers [336]. The nanodiamond-containing MgH_2 composite exhibited more than 100 °C decrease in the decomposition temperature compared with the ball-milled pure MgH_2 [337]. The formation of high density of defects (dislocations and grain boundaries) owing to the incorporation of carbon into

the MgH_2 particles was supposed to be the most possible reason for the decrease in dehydrogenation temperature.

Fuster et al. revealed that the catalytic effect of carbon was independent of its morphology and was more pronounced when the additive was incorporated from the beginning of milling, as well as with a higher weight proportion [338,339]. Lototsky et al. further confirmed that the hydrogenation behaviour strongly depended on the nature and amount of carbon additive [340]. Based on the time-resolved studies, they believed that carbon acted as a carrier of the activated hydrogen through spill-over and proposed that high energy reactive ball milling destroyed the original carbon structure to form stacked graphene layers, which encapsulated MgH_2 nanoparticles and prevented the grain growth, therefore favoring hydrogen cycling. After mixing with helical carbon nanofibers, nano Mg took up ~5.25 wt% H_2 within 10 min [341]. With a large quantity of exposed carbon edges, helical form of graphene nanofibres (HGNF) dramatically improved hydrogen desorption from MgH_2 at lower temperatures compared with graphene [342]. Their theoretical calculations suggested that graphene edges with high electronegativity and reactivity, in both the zigzag and armchair geometry, facilitated the electron transfer from Mg to carbon and weakened Mg-H bonds in MgH_2. Furthermore, mixing with 10 wt% rGO shortened the incubation period because ball milling established Mg–C interactions through electron-transfer from Mg to π^* of C, which changed the hybridization of C from sp^2 to sp^3, consequently weakening the Mg–H bond and enhancing hydrogen release from MgH_2 [343].

The 5 wt% activated carbon-modified Mg absorbed about 6.5 wt% H_2 within 7 min

at 300 °C [344]. After milling with highly crumpled graphene nanosheets for 20 h, MgH_2 released 6.1 wt% H_2 at 300 °C within 40 min and absorbed 6.6 wt% H_2 within 1 min [345]. Even at 150 °C, it also absorbed 6.0 wt% H_2 within 180 min. The graphene nanosheets provided more edge sites and hydrogen diffusion channels and prevented the nanograins from sintering and agglomerating, thus improving (de)hydrogenation kinetics of MgH_2. Carbon could prevent Mg particles from coalescing into big bulk during heating for hydrogen release [346-348]. With 1500 W of microwave, the post 5 min-milled 10 wt% carbon fibers-containing MgH_2 released more than 90% of after only 10 s [349]. Improvement in (de)hydrogenation was also obtained by mixing MgH_2 with fluorographene nanosheets [350]. The highly curved surface of CNTs firmly adhering to MgH_2 particles helped to alter the charge distributions in MgH_2 and weaken the interaction between Mg and H atoms [351]. The addition of carbon nanotubes increased the number of grain boundaries and facilitated the nucleation, meaning that the dehydrogenation of MgH_2 powders possibly led to a "chain" of nucleation at elevated temperatures [352]. The addition of 5 wt% of carbon nanotubes to MgH_2 has also proven very important to the enhancement of hydrogen adsorption as well as its kinetics [353]. With microwave irradiation, the hydrogen absorption capacity and kinetics of the MgH_2–10 wt% carbons fibers (CFs) mixture increased after dehydriding [354]. The microwave irradiated sample released 5.8 wt% H_2 within 1 h at 330 °C, while the as-prepared MgH_2–10 wt% CFs mixture desorbed only 4.4 wt% H_2 even within 3 h. Recently, Chawla et al. achieved 7.45 wt% of dehydrogenation capacity for the MgH_2-5 wt% AC nanocomposite at 140 °C via TGA analysis [355]. Through co-

sintering 2-methylnaphthalene (CMN) with pure Mg followed by hydriding combustion synthesis, Zhou et al. prepared amorphous carbon-modified MgH_2, which started releasing hydrogen from 287 °C, 90 °C lower than that of pure MgH_2 [356]. At 200 ºC, the composite remarkably absorbed 4.54 wt% H_2 within 42 s while the absorption was only 0.71 wt % H for pure MgH_2. In particular, hydrogenation was changed from a 3D diffusion process to a 1D diffusion process due to the formation of the amorphous carbon.

As a result, the improved performance of MgH_2 in the presence of carbon materials have been attributed to several factors, including: i) preventing surface oxidation; ii) acting as a channel/pathway for rapid hydrogen atom diffusion; iii) inhibiting growth of Mg particles and agglomeration of catalyst nanoparticles; iv) maintaining the material microstructure during phase transformation; v) promoting electron transfer and activating hydrogen dissociation/recombination.

4.9.2 Carbon-based composite materials

Carbon materials have also been widely used as supports to further enhance the catalytic activity of transition metals and their compounds. Considerable studies demonstrated the synergistic effect of metals and carbons (Table 8). In 2006, Kojima et al. reported excellent hydrogen cycling properties for the nano-Ni/Al_2O_3/C-catalyzed MgH_2 [357]. After that, the MgH_2-Ni@C composites were systematically studied by several groups [118, 19,357-361]. The sequential-doping of Ni and graphene not only accelerated the refinement of MgH_2 grains and particles, but also significantly decreased its dehydrogenation temperature [358]. The carbon supported nano-Ni (Ni@C) obtained

by calcination of dimethylglyoxime dinickel chelate enabled hydrogen desorption at 187 °C, which was 113 °C lower than that of as-milled MgH_2, and the hydrogen desorption completed within only 500 s at 300 ºC [270]. Meng et al. fabricated Ni nanoparticles *in-situ* encapsulated in carbon nanofibers using electrospinning and disclosed that the MgH_2-10 wt %Ni@C delivered 5.91 wt% H_2 in 500 s at 325 °C, as shown in Fig. 7 [360]. Uniformly dispersed Ni nanoparticles anchored on reduced graphene oxide (Ni@rGO) reduced the initial dehydrogenation temperature from 251 °C to 190 °C and enabled 5.0 wt% H_2 absorption in 20 min at 100 °C [361]. The *in-situ* formed Mg_2Ni/Mg_2NiH_4 exhibited better catalytic effect than Ni. Huang et al. observed 5.6 wt% H_2 release from the MgH_2 + 10 wt% Ni@C-MXene composite within 2 min at 300 °C, thanks to the synergistic nano-confinement and favorable hydrogen pump effect [118]. The MgH_2–Ni/hollow g-C_3N_4 tube composite released hydrogen from 252 ºC with 98% of capacity retention after 10 cycles [362]. Nano Ni particles dispersed over mesoporous carbon material CMK-3 resulted in 170 ºC decrease in the dehydrogenation onset temperature of MgH_2 [363]. MXene $Ti_3C_2T_x$ supported Ni@C nanoflakes also enabled superior hydrogen desorption kinetics and excellent cycling stability due to the *in situ* formed Mg_2NiH_4, highly-dispersed Ti nanoparticles and FL-$Ti_3C_2T_x$ nanosheets themselves [319]. More importantly, highly dispersed single atom Ni on nitrogen-doped carbon (Ni@N-C) reduced the desorption activation energy from 156.5 ± 3.2 kJ mol^{-1} to 87.2 ± 5.4 kJ mol^{-1} [136].

Similarly, enhanced catalytic activity was also observed for Co/carbon nanotubes [364], hierarchical Co@C nanoflowers [365], ZIF-67 derived Co@CNTs nanoparticles

[366], and multi-wall carbon nanotubes supported Pd (Pd/MWCNTs) [367]. Coupling effects were obtained for PdNi bimetallic nanoparticles supported by mesoporous carbon ($Pd_{30}Ni_{70}$/CMK-3) [368], multi-wall carbon nanotubes supported nano-nickel and TiF_3 (Ni/MWCNTs-TiF_3) [369], bimetallic NiCo on functional graphene (NiCo/rGO) [370], TiFe on carbon nanotubes [371], Fe–Ni catalyst modified three-dimensional graphene (Fe–Ni @3DG) [372], carbon-encapsulated iron-nickel nanoparticle ($Fe_{0.64}Ni_{0.36}$@C) [373], rGO supported NiCu (NiCu/rGO) [374], $Zr_{0.4}Ti_{0.6}Co$ nanosheets and carbon nanotubes ($Zr_{0.4}Ti_{0.6}Co$/CNTs) [375], VTi/CNTs [376], YH_2-Co@C [377] and Co/Pd supported by few-walled carbon nanotubes (Co/Pd@B-CNTs) [378]. For instance, the MgH_2+10 wt%Fe–Ni@3DG composite absorbed 6.35 wt% H_2 within 100 s (300 °C, 50 atm H_2) and released 5.13 wt% H_2 within 500 s (300 °C, 0.5 atm H_2) [372]. MgH_2-5 wt% NiCu/rGO started to desorb hydrogen at 185 °C, which was 115 °C lower than that of as-milled MgH_2, and desorbed 5.8 wt% H_2 within 20 min at 300 °C [374]. MgH_2–Co/Pd@B-CNTs composite started releasing hydrogen at 198.9 °C, 132.4 °C lower than that of as-milled MgH_2, with a special “bidirectional catalyst” mechanism [378]. During hydrogenation, Pd played a dominant role in accelerating the preferential diffusion of H atoms at the Pd/Mg interface. However, for dehydrogenation, the transformation between Mg_2Co and Mg_2CoH_5 as well as a Mg–Pd alloy became the crucial factor, facilitating hydrogen release by decreasing the diffusion barrier.

Moreover, the catalytic activity of carbon materials supported metal oxides, including Nb_2O_5, TiO_2, TiO, NiO, Fe_3O_4, V_2O_3, ZrO_2, MnO, CuO, $CoMoO_4$ were also

studied [123,222,315,379-388]. In 2010, Milanese et al. fabricated ternary Mg–Nb_2O_5–graphitic C mixtures by high-energy ball milling which reversibly delivered up to 6.8 wt% H_2 at 350 ºC [379]. Chuang et al. observed 5.81–4.88 wt% H_2 uptake under initial hydrogen pressure of 30 bar, and 5.14–4.01 wt% H_2 release within 600 s at 300 ºC by Mg–Nb_2O_5-SWCNT and Mg–Nb_2O_5-MWCNT [380]. In particular, the Mg–Nb_2O_5-SWCNT sample absorbed hydrogen up to 1.71 wt% at 25 ºC. Carbon remarkably improved the catalysis of ZrO_2 towards MgH_2. The onset desorption temperature of a MgH_2–ZrO_2/C composite was reduced to 208 °C, much lower than that of MgH_2–ZrO_2 (248 °C) and undoped MgH_2 (309 °C) [381]. ZrO_2/SWCNT-containing MgH_2 absorbed 4.5 wt% H_2 within 700 s at 25 °C, 1.5-fold higher than that of ZrO_2-doped MgH_2 under the same conditions [382]. Liu et al. synthesized graphene-supported TiO_2 nanoparticles via a solvothermal method with ethylene glycol as the solvent [383]. The MgH_2-70TiO_2@rGO-EG composite milled for 10 h desorbed 6.0 wt% H_2 within 6 min at 300 °C. Gao et al. observed that the dehydrogenated MgH_2-5 wt% Ti_3C_2/TiO_2(A)-C absorbed approximately 4 wt% H_2 within 800 s at 125 °C [315]. They suggested that the synergetic effects between the layered structure and multivalent titanium compounds (Ti^{4+}, Ti^{3+}, Ti^{2+}, Ti^0) were responsible for the improved performance. The hydrogen sorption behaviors of MgH_2 catalyzed by graphene sheet templated Fe_3O_4 nanoparticles (Fe_3O_4@GS) were reported by Bhatnagar et al [384]. MgH_2-Fe_3O_4@GS absorbed 6.2 wt% H_2 in 2.50 min at 290 °C under 15 atm H_2, while only 4.4 wt% H_2 and 5.5 wt% H_2 were uptaken by MgH_2:GS and MgH_2:Fe_3O_4, respectively. Additionally, MgH_2 catalyzed by Fe_3O_4@GS showed negligible degradation in the storage capacity

after 25 cycles.

By using MIL-47(V) as a precursor, Wang et al. synthesized vanadium oxide nanoparticles supported on cubic carbon nanoboxes (nano-V_2O_3@C) [385]. MgH_2-9 wt% nano-V_2O_3@C sample started releasing hydrogen at 215 °C, which was 60 °C lower than that of the additive-free MgH_2. Rehydrogenation was completed within 700 s at 150 °C under 50 bar H_2. The apparent activation energy of hydrogenation of MnO@C-doped MgH_2 was calculated to be 22.5 kJ mol^{-1}, lowered by 67.2% compared with undoped sample [386]. The onset desorption temperature of CuO@Gr-catalyzed MgH_2 was measured to be 229 °C, which is 121 °C and 12 °C lower than those of MgH_2 and MgH_2-CuO [387]. The graphene addition was critical for an excellent cyclability because the storage capacity remained ~6 wt% after 10 cycles without any substantial deterioration. MgH_2–10 wt% $CoMoO_4$/rGO started releasing hydrogen at around 204 °C, which was about 36 °C and 156 °C lower than that of MgH_2 −10 wt%$CoMoO_4$ and pure MgH_2, respectively [222]. The fully dehydrogenated sample absorbed H_2 below 80 °C. The synergistic effect between the *in-situ* generated MgO, Co_7Mo_6 and Mo promoted the diffusion of H_2, thereby improving the MgH_2 hydrogen storage properties.

The multi-component catalysts of activated carbon supported nanosized Pd-VO_x (Pd–VO_x/AC) and Ni-VO_x (Ni-VO_x/AC) were also prepared and evaluated [389,390]. The MgH_2+Ni-VO_x/AC composites desorbed 6.5 wt% H_2 within 10 min at 300 °C under an initial hydrogen pressure of 1 kPa and absorbed 6.2 wt% H_2 within only 1 min at 150 °C under a hydrogen pressure of 20 bar [390]. Such superior hydrogen storage

properties were further confirmed by Lan et al. who reported that 10 wt% (Ni-V_2O_3)@C-containing MgH_2 could release 6.05 wt% H_2 at 275 °C in 10 min and absorb 5.50 wt% H_2 at 25 °C [391]. Here, V_2O_3 was partially converted into VO during milling with MgH_2, and Ni reacted with Mg to form Mg_2Ni after the first dehydrogenation. The *in situ* Mg_2Ni/Mg_2NiH_4 coating around Mg/MgH_2 acted as a "hydrogen pump" to drive hydrogen diffusion and dissociation, and the presence of C inhibited the agglomeration of Mg/MgH_2 particles. Similar results were also observed for Ni-CeO_x/GNS-catalyzed MgH_2 [392]. Moreover, MgH_2 co-catalyzed with NbF_5 and single-walled carbon nanotubes absorbed 5.2 wt% H_2 within 10 min even at 100 ºC [393].

5. MgH_2 prototype tanks

In the past decades, hydrogen storage properties of the Mg/MgH_2 system have been improved remarkably by introducing suitable catalysts or catalytic additives, including the reduced (de)hydrogenation temperatures and enhanced reaction kinetics. This facilitates the exploration of prototype Mg/MgH_2 based hydrogen storage systems contained in various reactors/tanks. In 2007, de Rango et al. constructed a small stainless-steel cylindrical tank (V = 260 cm^3) filled with 110 g of post-8 h milled MgH_2-5 at% V powders [394]. Starting at 280 ºC, this unit absorbed 60 normal litres (NL) H_2, corresponding to 4.9 wt% of H_2 capacity. Following this, a variety of tanks have been developed, which contained several grams to 10 kg of MgH_2-based materials, with capacities varying from 2 NL to 7 normal cubic metres H_2, or 550 to 700 NL H_2 per kg of the hydrogen storage material (4.7 – 5.9 wt% H_2) [395-407]. Chaise et al. fabricated compacted disks with 68 mm in diameter and 9.5 mm in thickness by consolidating a

mixture MgH_2-4 at% Ti–V–Cr and expanded natural graphite (ENG) under about 100 MPa [395]. The incorporation of ENG remarkably improved the radial thermal conductivity of the compacted MgH_2 disks, which largely facilitate heat dissipation during hydrogenation.

By designing a heat exchanger composed of a double-walled tube cooled down by forced air and copper fins alternately stacked with MgH_2 disks, the new cylindrical tank filled with 5 compacted disks was able to absorb 100 NL hydrogen within 25 min starting at 300 °C under 1 MPa H_2. Based on this design, Garrier et al. developed a tank with about 2 L of internal volume (Fig. 8) [396]. The loading of the Ti-V-Cr-catalyzed MgH_2 amounted to 1.8 kg, which was compacted into disks with 5 wt% of ENG. This unit absorbed 1170 NL H_2, corresponding to 270 Wh/kg of specific energy and 42 g/L of system volumetric density. To improve mechanical stability of MgH_2-based pellets upon cycling, Al powders were introduced into Nb_2O_5 (5 wt%) and graphite (1 wt%) co-catalyzed MgH_2 as binders [397,398]. The best cycling behavior and mechanical stability were obtained for pellets with 5 wt% Al annealed at 450 °C in vacuum before cycling measurement [397]. Similarly, Capurso et al. designed a small reactor filled with ~10 g of catalyzed MgH_2 powders mixed with 5 wt% Al powders in the form of cylindrical pellets [398]. The heat flow was managed via an oil circulation system. Carbon paper was used to ensure good heat conductivity between the pellets and the inner wall of the reactor and between two adjacent pellets. Their results indicated that the use of pellets in a reactor instead of a powder bed facilitated the heat exchange and prevented local overheating and subsequent detrimental strong compaction of the

powders. A new MgH_2 tank concept was proposed by using Mg-Zn eutectic alloy as a heat exchanger [399]. A cylindrical tank with 10 kg of MgH_2 catalyzed by 4 at% Ti-V-Cr alloys was fabricated, which absorbed and released 7050 NL H_2 within 3 h. When integrating with a 1.2 kW PEMFC, a hydrogen flow of 13 NL/min was obtained. A much larger hydrogen storage system based on catalyzed MgH_2 was developed by McPhy Energy, which stored 8 kg H_2 in the standard configuration [400].

Moreover, an oil-free diaphragm pump was introduced to forcibly desorb hydrogen from a small pilot MgH_2–TiH_2 based hydride reactor [401]. At a H_2 flow rate of 25 mL min^{-1} g^{-1}, the reactor absorbed 2.9–5.2 wt% at 25–300 °C after 22 min. The hydrogenated reactor dehydrogenated at 250 °C at an average rate of 5 mL min^{-1} g^{-1} via a diaphragm pump, which successfully powered a small PEMFC with a measured conversion efficiency of 18%. El-Eskandarany et al. developed a simple hydrogen storage prototype system by incorporating various catalyst-modified MgH_2 composites into a metallic Ti tank, including $MgH_2/TiMn_2$, MgH_2/TiH_2, MgH_2/Nb_2O_5/Ni and MgH_2/Zr_2Pd [402-406]. The unit was able to power a commercial 40 W/4.5 A PEMFC, which successfully charged a battery of a cell phone. Lately, Nyamsi et al. built a 200 NL hydrogen storage tank by loading 300 g of MgH_2-TiH_2-C nanocomposite as hydrogen storage medium [407]. It delivered up to 185 NL H_2 in a temperature range from 150 °C (H_2 absorption) to 370 °C (H_2 desorption). All these sufficiently indicate the great potential of the catalyst-modified Mg-based materials for solid-state hydrogen storage.

6. Summary and perspectives

MgH_2 with 7.6 wt% H_2 in mass and 110 g H_2 L^{-1} in volume offers a potential solution to hydrogen storage. The reaction between Mg and H_2 is a heterogeneous gas-solid reaction and large energy needed to split H_2 molecules at the surface of Mg (432 kJ mol^{-1} H_2). As a result, a proper catalyst that facilitates not only the adsorption and dissociation of H_2 molecules at its surface but also the hydrogen diffusion and the hydride formation upon hydrogen uptake is necessary. Considerable work has proven Ni, Ti, Nb, Zr and V particularly effective toward catalyzing hydrogen storage in MgH_2. However, the high strength and good ductility of metals and alloys make it hard to achieve uniform and dispersive distribution. In this regard, metal oxides, halides, sulfides, hydrides, nitrides, carbides, borides and even MXenes have been studied since they are much more brittle and thus easier to disperse upon ball milling with MgH_2. For instance, N-doped Nb_2O_5 nanorods with 10-20 nm in diameter enabled 5.5 wt% of H desorption from MgH_2 at 175 ºC and full hydrogenation at 25 ºC under 50 bar H_2. MgH_2 mixed with 2D nanoflake-shaped $TiNb_2O_7$ featured 96% of capacity retention after 30 cycles. Few-layered Ti_3C_2Tx supported nano-Ni particles with an interconnected and interlaced structure enabled the release of approximately 5.83 wt% H_2 within 30 min at 250 °C and the absorption of 5 wt% H_2 within ~28 min at 100 °C. Studies revealed that high-valent metal cations were readily reduced to low-valent and even zero-valent metals when they were ball milled with MgH_2. The multivalent metals functioned as the intermediate and catalytic active sites for the electron transfer between Mg^{2+} and H^- during the (de)hydrogenation process, consequently promoting the H_2 dissociation and recombination, and leading to the significantly enhanced kinetics. However, the strong

affinity between Mg^{2+} and O^{2-} or halide anions resulted in the generation of inert by-products, i.e., MgO or $MgCl_2$, which largely decreased the practical hydrogen storage capacity of the catalyst-modified composites. Therefore, metal hydrides are more preferable as catalysts for hydrogen storage in Mg/MgH_2. For example, MgH_2–TiH_2 displayed reversible hydrogen sorption below 150 ºC. Using 0.9 MgH_2 + 0.1 TiH_2 +5 wt%C nanocomposite, a hydrogen storage tank that delivered up to 185 NL H_2 in a temperature range from 150 °C (H_2 absorption) to 370 °C (H_2 desorption) has been successfully built, indicating the potential of the catalyzed Mg-based materials for practical solid-state hydrogen storage applications. Furthermore, carbon materials were employed as supports to further enhance the catalytic activity of transition metals and their compounds. MgH_2-10 wt% (Ni-V_2O_3)@C released 6.05 wt% of H at 275 °C in 10 min and absorbed 5.50 wt% of H at 25 °C.

Although the reported catalysts and catalytic additives have significantly improved the hydrogen storage kinetics of Mg/MgH_2 system, their overall properties are still not good enough for practical mobile applications. More advanced and effective catalysts are desired to achieve simultaneously the high hydrogen capacity and the low operation temperature for hydrogen storage in MgH_2. In this regard, we believe that the ultrahigh-loading single metal atom catalysts or metal cluster catalysts should be the future research focus, which not only largely increase the utilization efficiency of catalytic active species by increasing active sites and enhancing the homogeneous dispersibility, but also effectively suppress the side reactions that give rise to the formation of inert by-products. The development of the metal multicomponent nanocatalysts should be

another promising direction.

However, the catalysts do not alter the reaction thermodynamics. The high thermal stability of MgH_2 is still a big obstacle for practical applications because it gives rise to a quite low equilibrium pressure. Moreover, the hydrogenation of a large quantity of Mg remains challenging since it is difficult to effectively dissipate heat caused by the fast charging (3-5 min). To solve these problems, the simultaneous tailoring of thermodynamics and kinetics is much more important in the future. The *in-situ* construction of catalyzed Mg/MgH_2 nanostructures offer some hopes, but also present a number of new challenges. The most important is how to controllably fabricate ultrasmall Mg/MgH_2 nanostructures (<10 nm in size) decorated with homogenously dispersed highly active catalysts. Novel external field-assisted strategies (i.e., microwave, photocatalysis, etc.) can also be explored to promote the hydrogen storage reaction of Mg/MgH_2 systems, since the external fields help with activating hydrogen storage reaction at lowered temperatures. We hope that future efforts will lead to breakthrough in improving the hydrogen cycling performance of MgH_2 and make it as a practical hydrogen carrier.

Notes

The authors declare no competing financial interest.

Acknowledgements

We gratefully acknowledge the financial support received from the National Key R&D

Program of China (2022YFB3803700), the National Outstanding Youth Foundation of China (52125104), the Natural Science Foundation of Zhejiang Province (LD21E010002), the National Natural Science Foundation of China (52001277, U22A20120), the Fundamental Research Funds for the Central Universities (2021FZZX001-09, 226-2022-00246), and the National Youth Top-Notch Talent Support Program.

References

[1] L. Schlapbach, A. Züttel, Nature 414 (2001) 353-358.

[2] T. He, P. Pachfule, H. Wu, Q. Xu, P. Chen, Nature Rev. Mater. 1 (2016) 1-17.

[3] J. Zheng, C.G. Wang, H. Zhou, E. Ye, J. W. Xu, Z.B. Li, X. J. Loh, Research 2021 (2021) 3750689.

[4] I. P. Jain, Int. J. Hydrogen Energy 34 (2009) 7368-7378.

[5] Z. Abdin, A. Zafaranloo, A. Rafieed, W. Méridab, W. Lipińskic, K.R. Khalilpour, Renew. Sustain. Energy Rev. 120 (2020) 109620.

[6] S. Singh, S. Jain, P.S. Venkateswaran, A.K. Tiwari, M.R. Nouni, J.K. Pandey, S. Goel, Renew. Sustain. Energy Rev. 51 (2015) 623-633.

[7] S. Sharma, S.K. Ghoshal, Renew. Sustain. Energy Rev. 43 (2015) 1151-1158.

[8] B. Mahant, P. Linga, R. Kumar, Energy & Fuels 35 (2021) 15424-15454.

[9] F. Qureshi, M. Yusuf, H. Kamyab, S. Zaidi, M.J. Khalil, M.A. Khan, M.A. Alam, F. Masood, L. Bazli, S. Chelliapan, B. Abdullah, Sustain. Energy Technol. Assess. 53 (2022) 102677.

[10] P. Selvam, B. Viswanathan, C.S. Swamy, V. Srinivasan, Int. J. Hydrogen Energy 11 (1986) 169-192.

[11] M. Felderhoff, C. Weidenthaler, R. Helmolt, U. Eberle, Phys. Chem. Chem. Phys. 9 (2007) 2643-2653.

[12] B. Sakintuna, F. Lamari-Darkrim, M. Hirscher, Int. J. Hydrogen Energy 32 (2007) 1121-1140.

[13] A. Gupta, G. V. Baron, P. Perreault, S. Lenaerts, R. G. Ciocarlan, P. Cool, P.G.M. Mileo, S. Rogge, V.V. Speybroeck, G. Watson, P.V.D. Voort, M. Houlleberghs, E. Breynaert, J. Martens, J.F.M. Denayer, Energy Storage Mater. 41 (2021) 69-107.

[14] Y.P. Pang, Q. Li, Int. J. Hydrogen Energy 41 (2016) 18072-18087.

[15] N.A.A. Rusman, M. Dahari, Int. J. Hydrogen Energy 41 (2016) 12108-12126.

[16] U. Eberle, M. Felderhoff, F. Schüth, Angew. Chem. Int. Ed. 48 (2009) 6608-6630.

[17] Q. Luo, Y.L. Guo, B. Liu, Y.J. Feng, J.Y. Zhang, Q. Li, K. Chou, J. Mater. Sci. Technol. 44 (2020) 171-190.

[18] Q. Li, X. Lin, Q. Luo, Y.A. Chen, J.F. Wang, B. Jiang, F.S. Pan. Int. J. Min. Met. Mater. 29 (2022) 32-48.

[19] https://www.energy.gov/eere/fuelcells/doe-technical-targets-onboard-hydrogen-storage-light-duty-vehicles.

[20] S. Orimo, Y. Nakamori, J.R. Eliseo, A. Züttel, C.M. Jensen, Chem. Rev. 107 (2007) 4111-4132.

[21] Ping Chen, Min Zhu, Mater. Today 11 (2008) 36-43.

[22] H. Wang, H.J. Lin, W.T. Cai, L.Z. Ouyang, M. Zhu, J. Alloys Compd. 658 (2016) 280-300.

[23] Q.W. Lai, M. Paskevicius, D.A. Sheppard, C.E. Buckley, A.W. Thornton, M.R. Hill, Q.F. Gu, J.F. Mao, Z.G. Huang, H.K. Liu, Z.P. Guo, A. Banerjee, S. Chakraborty, R. Ahuja, K.F. Aguey-Zinsou, ChemSusChem 8 (2015) 2789-2825.

[24] Y.H. Sun, C.Q. Shen, Q.W. Lai, W. Liu, D.W. Wang, K.F. Aguey-Zinsou, Energy Storage Mater. 10 (2018) 168-198.

[25] J.F. Zhang, Z.N. Li, Y.F. Wu, X.M. Guo, J.H. Ye, B.L. Yuan, S.M. Wang, L.J. Jiang, RSC Adv. 9 (2019) 408-428.

[26] Z. Chen, Z.L. Ma, J. Zheng, X.G. Li, E. Akiba, H.W. Li, Chin. J. Chem. Eng. 29 (2021) 1-12.

[27] Q. Luo, J.D. Li, B. Li, B. Liu, H.Y. Shao, Q. Li, J. Magnes. Alloy 7 (2019) 58-71.

[28] H.Y. Shao, L.Q. He, H.J. Lin, H.W. Li, Energy Technol. 6 (2018) 445-458.

[29] Q. Li, Y.F. Lu, Q. Luo, X.H. Yang, Y. Yang, J. Tan, Z.H. Dong, J. Dang, J.B. Li, Y. Chen, B. Jiang, S.H. Sun, F.S. Pan, J. Magnes. Alloy 9 (2021) 1922-1941.

[30] A. Zaluska, L. Zaluski, J.O. Ström–Olsen, J. Alloys Compd. 288 (1999) 217-225.

[31] I.P. Jain, C. Lal, A. Jain, Int. J. Hydrogen Energy 35 (2010) 5133-5144.

[32] K.F. Aguey-Zinsou, J.R. Ares-Fernμndez. Energy Environ. Sci. 3 (2010), 526-543.

[33] N.B. Arboleda, H. Kasai, K. Nobuhara, W. A. Diño, H. Nakanishi, J. Phys. Soc. Jpn. 73 (2004) 745-748.

[34] F.Y. Cheng, Z.L. Tao, J. Liang, J. Chen, Chem. Commun. 48 (2012) 7334-7343.

[35] W. Liu, K. -F. Aguey-Zinsou, J. Mater. Chem. A, 2014, 2, 9718-9726.

[36] J.G. Novaković, N. Novaković, S. Kurko, S.M. Govedarović, T. Pantić, B.P. Mamula, K. Batalović, J. Radaković, J. Rmuš, M. Shelyapina, N. Skryabina, P. Rango, D. Fruchart, ChemPhysChem 20 (2019) 1216-1247

[37] D. Kecik, M.K. Aydinol, Surf. Sci. 603 (2009) 304-310.

[38] K. Christmann, Prog. Surf. Sci. 48 (1995) 15-26.

[39] H.G. Wang, Y.F. Liu, J. Zhang, Adsorption 28 (2022) 85-95.

[40] K. Edalati, E. Akiba, W. J. Botta, Y. Estrin, R. Floriano, D. Fruchart, T. Grosdidier, Z. Horita, J. Huot, H.W. Li, H.J. Lin, Á. Révész, M. J. Zehetbauer, J. Mater. Sci. Technol. 146 (2023) 221-239.

[41] J. Huot, F. Cuevas, S. Deledda, K. Edalati, Y. Filinchuk, T. Grosdidier, B.C. Hauback, M. Heere, T.R. Jensen, M. Latroche, S. Sartori, Materials 12 (2019) 2778.

[42] Z. Jalil, A. Rahwanto, H. Akhyar, R. Razali, E. Handoko, IOP Conf. Ser.: Earth Env. Sci. 105 (2018) 012098.

[43] A. Rahwanto, Z. Jalil, Akhyar, E. Hand, IOP Conf. Ser.: Mater. Sci. Eng. 931 (2020) 012012.

[44] Malahayati, E. Yufita, M. Ismail, R. Idroes, Z. Jalil, J. Ecol. Eng. 22 (2021) 79-85.

[45] Z. Jalil, A. Rahwanto, Ismail, H. Sofyan, E. Handoko, Mater. Res. Express 5 (2018) 064002.

[46] P.E. de Jongh, P. Adelhelm, ChemSusChem 3 (2010) 1332.

[47] T.K. Nielsen, F. Besenbacher, T.R. Jensen, Nanoscale 3 (2011) 2086-2098.

[48] S. Bahou, H. Labrim, H. Ez-Zahraouy, Int. J. Hydrogen Energy 48 (2023) 8179-8188.

[49] S. Bahou, H. Labrim, M. Lakhal, M. Bhihi, B. Hartiti, H. Ez-Zahraouy, Int. J. Hydrogen Energy 46 (2021) 2322-2329.

[50] S. Bahou, H. Labrim, M. Lakhal, M. Bhihi, B. Hartiti, H. Ez-Zahraouy, Int. J. Hydrogen Energy 45 (2020) 10806-10813.

[51] O. Mounkachi, A. Akrouchi, G. Tiouitchi, M. Lakhal, E. Salmani, A. Benyoussef, A. Kara, A.E. Kenz, H. Ez-Zahraouy, A E. Moutaouakil, Energies 14 (2021) 7737.

[52] M. Abdellaoui, M. Lakhal, H. Benzidi, M. Garara, A. Benyoussef, A.E. Kenz, O. Mounkachi, M. Loulidi, H. Ez-Zahraouy, Appl. Phys. A 125 (2019) 760.

[53] T. Czujko, E.E. Oleszek, M. Szot, Materials 13 (2020) 4550.

[54] Á. Révész, M, Gajdics, Energies 14 (2021) 6400.

[55] R.A. Varin, T. Czujko, Ch. Chiu, Z. Wronski, J. Alloys Compd. 424 (2006) 356-364.

[56] Q. Li, J. Mater. Res. 19, (2004) 2871-2876.

[57] Z.W. Zheng, C. Peng, Q.A. Zhang, J. Mater. Sci. Technol. 145 (2023) 148-155.

[58] Q. Li, Q. Luo, Q.F. Gu, J. Mater. Chem. A 5 (2017) 3848-3864.

[59] J. Meng, Y.B. Pan, Q. Luo, X.H. An, Y. Liu, Q. Li, K.C. Chou, Int. J. Hydrogen Energy 35 (2010) 8310-8316.

[60] Q. Luo, Q.F. Gu, J.Y. Zhang, S.L. Chen, K.C. Chou, Q. Li, Sci. Rep. 5 (2015) 15385.

[61] P. Vajeeston, P. Ravindran, M. Fichtner, H. Fjellvåg, J. Phys. Chem. C 116 (2012) 18965-18972.

[62] X.C. Wang, Y.X. Jia, X.Z. Xiao, P.P. Zhou, J.P. Bi, J.C. Qi, L. Lv, F. Xu, L.X. Sun, L.X. Chen, J. Mater. Sci. Technol. 146 (2023) 121-130.

[63] X. Zhang, Y.F. Liu, Z.H. Ren, X.L. Zhang, J.J. Hu, Z.G. Huang, Y.H. Lu, M.X Gao H.G. Pan, Energy Environ. Sci. 14 (2021) 2302-2313.

[64] S.S. Shinde, D.H. Kim, J.Y. Yu, J.H. Lee, Nanoscale 9 (2017) 7094-7103.

[65] H.Y. Leng, Y.B. Pan, Q. Li, K.C. Chou, Int. J. Hydrogen Energy 39 (2014) 13622-13627.

[66] N.A. Ali, N.A. Sazelee, M. Ismai, Int. J. Hydrogen Energy, 46 (2021) 31674-31698.

[67] N.A. Ali, M. Ismail, J. Magnes. Alloys 9 (2021) 1111-1122.

[68] N. Sazelee, N.A. Ali, S. Yahya, N.S. Mustafa, F.A.H. Yap, S.B. Mohamed, M.Z. Ghazali, S. Suwarno, M. Ismail, Front. Energy Res. 10 (2022) 875405.

[69] J.J. Vajo, S.L. Skeith, F. Mertens, J. Phys. Chem. B 109 (2005) 3719-3722.

[70] Z.Y. Li, Y.J. Sun, C.C. Zhang, S. Wei, L. Zhao, J.L. Zeng, Z. Cao, Y.J. Zou, H.L. Chu, F. Xu, L.X. Sun, H.G. Pan, J. Mater. Sci. Technol. 141 (2023) 221-235.

[71] M. Paskevicius, D.A. Sheppard, C.E. Buckley, J. Am. Chem. Soc. 132 (2010) 5077-5083.

[72] G. Sandrock, J. Alloys Compd. 293 (1999) 877-888.

[73] J.F. Fernández, C.R. Sánchez, J. Alloys Compd. 340 (2002) 189-198.

[74] N. Hanada, T. Ichikawa, H. Fujii, J. Phys. Chem. B 109 (2005) 7188-7194.

[75] J.C. Crivello, B. Dam, R.V. Denys, M. Dornheim, D.M. Grant, J. Huot, T.R. Jensen, P. de Jongh, M. Latroche, C. Milanese, D. Milčius, G.S. Walker, C.J. Webb, C. Zlotea, V. A. Yartys, Appl. Phys. A 97 (2016) 122.

[76] M. Bortz, B. Bertheville, G. Böttger, K. Yvon, J. Alloys Compd. 287 (1999) L4-L6.

[77] P. Vajeeston, P. Ravindran, B. C. Hauback, H. Fjellvåg, A. Kjekshus, S. Furuseth, M. Hanfland, Phys. Rev. B 73 (2006) 224102.

[78] D. Moser, G. Baldissin, D.J. Bull, D. J. Riley, I. Morrison, D.K. Ross,W.A. Oates, D. Noréus, J. Phys.: Condens. Matter 23 (2011) 305403.

[79] K. Edalati, K. Kitabayashi, Y. Ikeda, J. Matsuda, H.W. Li, I. Tanaka, E. Akiba, Z. Horita, Scripta Mater. 157 (2018) 54-57.

[80] P. Vajeeston, P. Ravindran, A. Kjekshus, H. Fjellvåg, Phys. Rev. Lett. (2002) 89, 175506.

[81] M. P. Jolibois, Compt. Rend. Hebdomad. Sean. Acad. Sci. 155 (1912) 353–355.

[82] E. Wiberg, H. Goeltzer, R. Bauer, Z. Naturforsch B 6 (1951) 394-395.

[83] T.N. Dymova, Z.K. Sterlyadkina, V.G. Safronov, Russ J. Inorg Chem. 6 (1961) 763.

[84] T.N. Dymova, Z.K. Sterlyadkina, N.G. Eliseeva, Zh. Neorg. Khim. 6 (1961) 768-

773.

[85] B. Bogdanović, Int. J. Hydrogen Energy 9 (1984) 937-941.

[86] Y. Chen, J.S. Williams, J. Alloys Compd. 217 (1995) 181-184.

[87] K. Wang, X. Zhang, Z.H. Ren, X.L. Zhang, J.J. Hu, M.X. Gao, H.G. Pan, Y.F. Liu, Energy Storage Mater. 23 (2019) 79-87.

[88] A.W.C. van den Berg, C.O. Areán, Chem. Commun. (2008) 668-681.

[89] B. Hammer, J.K. Nørskov, Surf. Sci.343 (1995) 211-220.

[90] A.W. Thornton, K.M. Nairn, J.M. Hill, A.J. Hill, M.R. Hill, J. Am. Chem. Soc. 131 (2009) 10662-10669.

[91] A. Borgschulte, U. Bösenberg, G. Barkhordarian, M. Dornheim, R. Bormann, Catal. Today 120 (2007) 262-269.

[92] S. Dong, C.Q. Li, J.H. Wang, H. Liu, Z. Ding, Z.Y. Gao, W.J. Yang, W. Lv, L. Wei, Y. Wu, H. Li, J. Mater. Chem. A 10 (2022) 22363-22372.

[93] M.S. Salman, C. Pratthana, Q. Lai, T. Wang, N. Rambhujun, K. Srivastava, K.F. Aguey-Zinsou, Energy Technol. 10 (2022) 2200433.

[94] V.A. Yartys, M.V. Lototskyy, E. Akiba, R. Albert, V.E. Antonov, J.R. Ares, M. Baricco, N. Bourgeois, C.E. Buckley, J.M. Bellosta von Colbe, J.C. Crivello, F. Cuevas, R.V. Denys, M. Dornheim, M. Felderhoff, D.M. Grant, B.C. Hauback, T.D. Humphries, I. Jacob, T.R. Jensen, P.E. de Jongh, J.M. Joubert, M.A. Kuzovnikov, M. Latroche, M. Paskevicius, L. Pasquini, L. Popilevsky, V.M. Skripnyuk, E. Rabkin, M.V. Sofianos, A. Stuart, G. Walker, H. Wang, C. J. Webb, M. Zhu, Int. J. Hydrogen Energy 44 (2019) 7809-7859.

[95] W.Y. Chen, J.J. Tang, Z.W. Lu, M.X. Huang, L. Liu, C.C. He, Y.J. Zhao Surf. Sci. 710 (2021) 121850.

[96] A.J. Du, S.C. Smith, G.Q. Lu, J. Phys. Chem. C 111 (2007) 8360-8365.

[97] E. German, R. Gebauer, J. Phys. Chem. C 120 (2016) 4806-4812.

[98] J.H. Dai, Y. Song, R. Yang, Int. J. Hydrogen Energy 36 (2011) 12939-12949.

[99] S. Li, P. Jena, R. Ahuja, Phys. Rev. B 74 (2006) 132106.

[100] A. J. Du, S.C. Smith, X.D. Yao, G.Q. Lu, Surf. Sci. 600 (2006) 1854-1859.

[101] J.J. Liu, J. Tyrrell, L. Cheng, Q.F. Ge, J. Phys. Chem. C 117 (2013) 8099-8104.

[102] X.L. Zhang, Y.F. Liu, X. Zhang, J.J. Hu, M.X. Gao, H.G. Pan, Mater. Today Nano 9 (2020) 100064.

[103] A.J. Medford, A. Vojvodic, J.S. Hummelshøj, J. Voss, F. Abild-Pedersen, F. Studt, T. Bligaard, A. Nilsson, J.K. Nørskov, J. Catal. 328 (2015) 36-42.

[104] Z. Ding, Y.T. Li, H. Yang, Y.F. Lu, J. Tan, J.B. Li, Q. Li, Y.A. Chen, L.L. Shaw, F.S. Pan, J. Magnes. Alloys 10 (2022) 2946-2967.

[105] L. Xie, Y. Liu, X.Z. Zhang, J.L. Qu, Y.T. Wang, X.G. Li, J. Alloys Compd. 482 (2009) 388-392.

[106] G.D. Frey, V. Lavallo, B. Donnadieu, W. W. Schoeller, G. Bertrand, Science 316 (2007) 439-441.

[107] M.M. Jiang, J. Xu, P. Munroe, Z.H. Xie, Chem. Phys. 565 (2023) 111760.

[108] G. Liang, J. Huot, S. Boily, A. Van Neste, R. Schulz, J. Alloys Compd. 292 (1999) 247-252.

[109] Q. Luo, J.D. Li, B. Li, B. Liu, H.Y. Shao, Q. Li, J. Magn. Alloy 7 (2019) 58-71.

[110] J. Liu, X. Zhang, Q. Li, K.C. Chou, K.D. Xu, Int. J. Hydrogen Energy 34 (2009) 1951-1957.

[111] Y.P. Pang, Q. Li, Scripta Mater. 130 (2017) 223-228.

[112] Y.P. Pang, Y.F. Wang, J.H. Yang, S.Y. Zheng, Compos. Commun. 26 (2021) 100781.

[113] H.J. Lin, J.J. Tang, Q. Yu, H. Wang, L.Z. Ouyang, Y.J. Zhao, J.W. Liu, W.H. Wang, M. Zhu, Nano Energy 9 (2014) 80-87.

[114] L.Z. Ouyang, X.S. Yang, M. Zhu, J.W. Liu, H.W. Dong, D.L. Sun, J. Zou, X.D. Yao, J. Phys. Chem. C 118 (2014) 7808-7820.

[115] M. Chen, X.Z. Xiao, M. Zhang, M.J. Liu, X. Huang, J.G. Zheng, Y.W. Zhang, L.J. Jiang, L.X. Chen, Int. J. Hydrogen Energy 44 (2019) 1750-1759.

[116] L.T. Zhang, Z.L. Cai, X.Q. Zhua, Z.D. Yao, Z. Sun, L. Ji, N.H. Yan, B.B. Xiao, L.X. Chen, J. Alloys Compd. 805 (2019) 295-302.

[117] X.L. Yang, Q.H. Hou, L.B. Yu, J.Q. Zhang, Dalton Trans. 50 (2021) 1797-1807.

[118] T.P. Huang, X. Huang, C.Z. Hu, J. Wang, H.B. Liu, H. Xu, F.Z. Sun, Z.W. Ma, J.N. Zou, W.J. Ding, Chem. Eng. J. 421 (2021) 127851.

[119] T. Huang, X. Huang, C. Hu, J. Wang, H. Liu, Z. Ma, J. Zou, W. Ding, Mater. Today Energy 19 (2021) 100613.

[120] Q.H. Hou, J.Q. Zhang, X.T. Guo, G.Z. Xu, X.L. Yang, Int. J. Hydrogen Energy 47 (2022) 15209-15223.

[121] Y. Zhang, F.Y. Wu, S. Guemou, H.J. Yu, L.T. Zhang, Y.J. Wang, Dalton Trans. 51 (2022) 16195-16205.

[122] C. Lu, Y.L. Ma, F. Li, H. Zhu, X.Q. Zeng, W.J. Ding, T. Deng, J.B. Wu, J.X. Zou, J. Mater. Chem. A 7 (2019) 14629-14637.

[123] X. Zhang, Z.H. Leng, M.X. Gao, J.J. Hu, F. Du, J.H. Yao, H.G. Pan, Y.F. Liu, J. Power Sources 398 (2018) 183-192.

[124] Y.P. Pang, D.K. Sun, Q.F. Gu, K.C. Chou, X.L. Wang, Q. Li, Cryst. Growth Des. 16 (2016) 2404-2415.

[125] Q. Li, K.C. Choua, Q. Lin, L.J. Jiang, F. Zhan, Int. J. Hydrogen Energy 29 (2004) 843-849.

[126] Y.B. Pan, Y.F. Wu, Q. Li, Int. J. Hydrogen Energy 36 (2011) 12892-12901.

[127] Y.T. Shao, H.G. Gao, Q.K. Tang, Y.N. Liu, J.C. Liu, Y.F. Zhu, J.G. Zhang, L.Q. Li, X.H. Hu, Z.X. Ba, Applied Surf. Sci.585 (2022) 152561.

[128] D.R. Aireddy, K. Ding, ACS Catal. 12 (2022) 4707-4723.

[129] C.X. Shang, M. Bououdina, Y. Song, Z.X. Guo, Int. J. Hydrogen Energy 29 (2004) 73-80.

[130] H. Yu, S. Bennici, A. Auroux, Int. J. Hydrogen Energy 39 (2014) 11633-11641.

[131] J. Cui, J.W. Liu, H. Wang, L.Z. Ouyang, D.L. Sun, M. Zhu, X.D. Yao, J. Mater. Chem. A 2 (2014) 9645-9655.

[132] H. Emami, K. Edalati, A. Staykov, T. Hongo, H. Iwaoka, Z. Horita, E. Akiba, RSC Adv. 6 (2016) 11665-11674.

[133] J.G. Zhang, S.Y. Li, Y.F. Zhu, H.J. Lin, Y.N. Liu, Y. Zhang, Z.L. Ma, L.Q. Li, J. Alloys Compd. 715 (2017) 329-336.

[134] T.Z. Si, X.Y. Zhang, J.J. Feng, X.L. Ding, Y.T. Li, Rare Met. 40 (2021) 995-1002.

[135] J. Chen, G. L. Xia, Z.P. Guo, Z.G. Huang, H.K. Liu, X.B. Yu, J. Mater. Chem. A 3 (2015) 15843-15848.

[136] Y.K. Huang, C.H. An, Q.Y. Zhang, L. Zang, H.X. Shao, Y.F. Liu, Y. Zhang, H.T. Yuan, C.Y. Wang, Y.J. Wang, Nano Energy 80 (2021) 105535.

[137] S. Dong, C.Q. Li, E. Lv, J.H. Wang, H. Liu, Z.Y. Gao, W. Xiong, Z. Ding, W.J. Yang, H. Li, J. Mater. Chem. A 10 (2022) 19839-19851.

[138] M.S. El-Eskandarany, M. Banyan, F. Al-Ajmi, Int. J. Hydrogen Energy 44 (2019) 16852-16861.

[139] Y. Wang, Q.Y. Zhang, Y.J. Wang, L.F. Jiao, H.T. Yuan, J. Alloys Compd. 645 (2015) S509-S512.

[140] D. Pukazhselvan, K.S. Sandhya, D. Ramasamy, A. Shaula, D.P. Fagg, ChemPhysChem 21 (2020) 1195-1201.

[141] Y.J. Choi, J.W. Choi, H.Y. Sohn, T. Ryu, K.S. Hwang, Z.Z. Fang, Int. J. Hydrogen Energy 34 (2009) 7700-7706.

[142] Y.N. Liu, J.X. Zou, X.Q. Zeng, W.J. Ding, RSC Adv. 4 (2014) 42764-42771.

[143] K. Edalati, H. Emami, Y. Ikeda, H. Iwaoka, I. Tanaka, E. Akiba, Z. Horita, Acta Mater. 108 (2016) 293-303.

[144] K. Edalati, H. Emami, A. Staykov, D. J. Smith, E. Akiba, Z. Horita, Acta Mater. 99 (2015) 150-156.

[145] T. Liu, X.J. Ma, C.G. Chen, L. Xu, X. G. Li, J. Phys. Chem. C 119 (2015) 14029-14037.

[146] T. Liu, T.W. Zhang, C.G. Qin, M. Zhu, X.G. Li, J. Power Sources 196 (2011)

9599-9604.

[147] L.T. Zhang, L. Ji, Z.D. Yao, N.H. Yan, Z. Sun, X.L. Yang, X.Q. Zhu, S.L. Hu, L.X. Chen, Int. J. Hydrogen Energy 44 (2019) 21955-21964.

[148] J.X. Zou, X.Q. Zeng, Y.J. Ying, X. Chen, H. Guo, S. Zhou, W.J. Ding, Int. J. Hydrogen Energy 38 (2013) 2337-2346.

[149] L.T. Zhang, Z.L. Cai, Z.D. Yao, L. Ji, Z. Sun, N.H. Yan, B.Y. Zhang, B.B. Xiao, J. Du, X.Q. Zhu, L.X. Chen, J. Mater. Chem. A 7 (2019) 5626-5634.

[150] M. Chen, Y.H. Pu, Z.Y. Li, G. Huang, X.F. Liu, Y. Lu, W.K. Tang, L. Xu, S.Y. Liu, R.H. Yu, J.L. Shui, Nano Res. 13 (2020) 2063-2071.

[151] X.L. Yang, L. Ji, N.H. Yan, Z. Sun, X. Lu, L.T. Zhang, X.Q. Zhu, L.X. Chen, Dalton Trans. 48 (2019) 12699-12706.

[152] W.F. Liao, W.B. Jiang, X.S. Yang, H. Wang, L.Z. Ouyang, M. Zhu, J. Rare Earths 39 (2021) 1010-1016.

[153] M.S. El-Eskandarany, Sci. Rep. 6 (2016) 1-13.

[154] J.F. Zhang, Z.N. Li, Y.F. Wu, X.M. Guo, J.H. Ye, B.L. Yuan, H.P. Yuan, S.M. Wang, L.J. Jiang, J. Phys. Chem. C 123 (2019) 15963-15976.

[155] J.F. Zhang, Z.N. Li, Y.F. Wu, X.M. Guo, J.H. Ye, B.L. Yuan, S.M. Wang, L.J. Jiang, J. Alloys Compd. 798 (2019) 597-605.

[156] P. Meena, R. Singh, V.K. Sharma, I.P. Jain, J. Magnes. Alloy 6 (2018) 318-325.

[157] X.B. Yu, Z.X. Yang, H.K. Liu, D.M. Grant, G.S. Walker, Int. J. Hydrogen Energy 35 (2010) 6338-6344.

[158] A.L. Yonkeu, I.P. Swainson, J. Dufour, J. Huot, J. Alloys Compd. 460 (2008) 559-

564.

[159] L. Laversenne, J. Andrieux, D. Plante, L. Lyard, S. Miraglia, Int. J. Hydrogen Energy 38 (2013) 11937-11945.

[160] H.Y. Wan, X. Yang, S.M. Zhou, L. Ran, Y.F. Lu, Y.A. Chen, J.F. Wang, F.S. Pan, J. Mater. Sci. Technol. 149 (2023) 88-98

[161] A. Rahwanto, I. Ismail, N. Nurmalita, Mustanir, Z. Jalil, J. Phys. Conf. Ser. 1882 (2021) 012010.

[162] Malahayati, Nurmalita, Ismail, M. N. Machmud, Z. Jalil, J. Phys. Conf. Ser. 1882 (2021) 012005.

[163] W. Oelerich, T. Klassen, R. Bormann, J. Alloys Compd. 315 (2001) 237-242.

[164] M.Y. Song, J.L. Bobet, B. Darriet, J. Alloys Compd. 340 (2002) 256-262.

[165] Q. Li, K.D. Xu, K.C. Chou, Q. Lin, J.Y. Zhang, X.G. Lu, Intermetallics 13 (2005) 1190-1194.

[166] K.S. Jung, E.Y. Lee, K.S. Lee, J. Alloys Compd. 421 (2006) 179-184.

[167] M. Dai, G.T Lei, Z. Zhang, Z. Li, H.J Cao, P. Chen, Acta Chim. Sin. 80 (2022) 303-309.

[168] D. Korablov, T.K. Nielsen, F. Besenbacher, T.R. Jensen, Powder Diffr. 30 (2015) S9-S15.

[169] M. Khrussanova, M. Terzieva, P. Peshev, E.Y. Ivanov, Mater. Res. Bull. 22 (1987) 405-412.

[170] P. Wang, A.M. Wang, H.F. Zhang, B.Z. Ding, Z.Q. Hu, J. Alloys Compd. 313 (2000) 218-223.

[171] K.F. Aguey-Zinsou, T. Nicolaisen, J.R. Ares Fernandez, T.Klassen, R. Bormann, J. Alloys Compd. 434 (2007) 738-742.

[172] S.K. Pandey, A. Bhatnagar, V. Shukla, R.Kesarwani, U. Deshpandey, T.P. Yadav, Int. J. Hydrogen Energy 46 (2021) 37340-37350.

[173] M.C. Brum, P.M. Jardim, M.O.T. da Conceicao, D.S. Santos, Mater. Res. 16 (2013) 647-649.

[174] P.M. Jardim, M.O.T. da Conceição, M.C. Brum, D.S. dos Santos, Int. J. Hydrogen Energy 40 (2015) 17110-17117.

[175] M. Zhang, X.Z. Xiao, X.W. Wang, M. Chen, Y.H. Lu, M.J. Liu, L.X. Chen, Nanoscale 11 (2019) 7465-7473.

[176] Z.L. Ma, J.C. Liu, Y.F. Zhu, Y.Y. Zhao, H.J. Lin, Y. Zhang, H.W. Li, J.G. Zhang, Y.N. Liu, W.T. Gao, S.S. Li, L.Q. Li, J. Alloys Compd. 822 (2020) 153553.

[177] L. Ren, W. Zhu, Y.H. Li, X. Lin, H. Xu, F.Z. Sun, C. Lu, J.X. Zou, Nano-Micro Lett. 14 (2022) 144.

[178] M. Zhang, X. Xiao, B. Luo, M. Liu, M. Chen, L. Chen, J. Energy Chem. 46 (2020) 191-198.

[179] M. Chen, X. Xiao, M. Zhang, J.F. Mao, J.G. Zheng, M.J. Liu, X.C. Wang, L.X. Chen, Mater. Today Energy 16 (2020) 100411.

[180] R. Zou, J.A. Bolarin, G. Lei, W.B. Gao, Z. Li, H.J. Cao, P. Chen, Chem. Eng. J. 450 (2022) 138072.

[181] J. Cui, H. Wang, J.W. Liu, L.Z. Ouyang, Q.G. Zhang, D.L. Sun, X.D. Yao, M. Zhu, J. Mater. Chem. A 1 (2013) 5603-5611.

[182] G. Barkhordarian, T. Klassen, R. Bormann, J. Alloys Compd. 364 (2004) 242-246.

[183] N. Hanada, T. Ichikawa, H. Fujii, J. Alloys Compd. 404 (2005) 716-719.

[184] N. Hanada, T. Ichikawa, H. Fujii, Physica B: Cond. Matter 383 (2006) 49-50.

[185] N. Hanada, T. Ichikawa, S. Hino, H. Fujii, J. Alloys Compd. 420 (2006) 46-49.

[186] O. Friedrichs, T. Klassen, J.C. Sánchez-López, R. Bormann, A. Fernández, Scripta Mater. 54 (2006) 1293-1297.

[187] D. Fátay, Á. Révész, T. Spassov, J. Alloys Compd. 399 (2005) 237-241.

[188] M.S. El-Eskandarany, N. Ali, F. Al-Ajmi, M. Banyan, A.A. Al-Duweesh, Processes 10 (2022) 1017.

[189] K.Shinzato, H. Gi, T. Murayama, M. Sadakane, Y. M. Wang, S. Isobe, T. Ichikawa, H. Miyaoka, ACS omega 6 (2021) 23564-23569.

[190] K. Wang, X. Zhang, Y.F. Liu, Z.H. Ren, X.L. Zhang, J.J. Hu, M.X. Gao, H.G. Pan, Chem. Eng. J. 406 (2021) 126831.

[191] L. Zeng, T. Kimura, S. Hino, H. Miyaoka, T. Ichikawa, Y. Kojima, Appl. Mech. Mater. 117 (2012) 1195-1198.

[192] B.H. Chen, Y.S. Chuang, C.K. Chen, J. Alloys Compd. 655 (2016) 21-27.

[193] X.L. Zhang, X. Zhang, L.C. Zhang, Z.G. Huang, F. Fang, J.J. Hu, Y.X. Yang, M.X. Gao, H.G. Pan, Y. F. Liu, Mater. Today Nano 18 (2022) 100200.

[194] D. Pukazhselvan, K. S. Sandhya, D. Ramasamy, A. Shaula, I. Bdikin, D. P. Fagg, J. Magnes. Alloy 10 (2022) 786-796.

[195] R. Gupta, F. Agresti, S. L. Russo, A. Maddalena, P. Paladeb, G. Principi, J. Alloys

Compd. 450 (2008) 310-313.

[196] T. Sadhasivam, M.S. L. Hudson, S.K. Pandey, A. Bhatnagar, M.K. Singh, K. Gurunathan, O.N. Srivastava, Int. J. Hydrogen Energy 38 (2013) 7353-7362.

[197] R.K. Singh, T. Sadhasivam, G.I. Sheeja, P. Singh, O.N. Srivastava, Int. J. Hydrogen Energy 38 (2013) 6221-6225.

[198] L.S. Xie, J.S. Li, T.B. Zhang, L. Song, Mater. Character. 133 (2017) 94-101.

[199] N.S. Mustafa, M. Ismail, J. Alloys Compd. 695 (2017) 2532-2538.

[200] D. Pukazhselvan, K. S. Sandhya, N. Nasani, D.P. Fagg, Appl. Surf. Sci. 561 (2021) 150062.

[201] O. Friedrichs, J.C. Sánchez-López, C. López-Cartes, T. Klassen, R. Bormann, A. Fernández, J. Phys. Chem. B 110 (2006) 7845-7850.

[202] D. Pukazhselvan, I. Antunes, S.L. Russo, J. Pérez, D.P. Fagg, Int. J. Hydrogen Energy 39 (2014) 18984-18988.

[203] D. Pukazhselvan, I. Bdikin, J. Pérez, E. Carbó-Argibay, I. Antunes, D.G. Stroppa, D.P. Fagg, Int. J. Hydrogen Energy 41 (2016) 2677-2688.

[204] D. Pukazhselvan, G. Otero-Irurueta, J. Pérez, B. Singh, I. Bdikin, M.K. Singh, D.P. Fagg, Int. J. Hydrogen Energy 41 (2016) 11709-11715.

[205] F. Dolci, M. Baricco, P.P. Edwards, E. Giamello, Int. J. Hydrogen Energy 33 (2008) 3085-3090.

[206] M.W. Rahman, S. Livraghi, F. Dolci, M. Baricco, E. Giamello, Int. J. Hydrogen Energy 36 (2011) 7932-7936.

[207] W. Rahman, J. Aust. Ceram. Soc. 55 (2019) 579-586.

[208] J. Zhang, J.W. Shan, P. Li, F.Q. Zhai, Q. Wan, Z.J. Liu, X.H. Qu, J. Alloys Compd. 643 (2015) 174-180.

[209] J.W. Shan, P. Li, Q. Wan, F.Q. Zhai, J. Zhang, Z.L. Li, Z.J. Liu, A.A. Volinsky, X.H. Qu, J. Power Sources 268 (2014) 778-786.

[210] M. Ismail, N.S. Mustafa, N.A. Ali, N.A. Sazelee, M.S. Yahya, Int. J. Hydrogen Energy 44 (2019) 318-324.

[211] N.A. Sazelee, N.H. Idris, M.F. M. Din, M.S. Yahya, N.A. Ali, M. Ismail, Results in Phys. 16 (2020) 102844.

[212] N.A. Sazelee, N.H. Idris, M.F.M. Din, N.S. Mustafa, N.A. Ali, M.S. Yahya, F.A. H. Yap, N.N. Sulaiman, M. Ismail, Int. J. Hydrogen Energy 43 (2018) 20853-20860.

[213] N.S. Mustafa, N.N. Sulaiman, M. Ismail, RSC Adv. 6 (2016) 110004-110010.

[214] M. Lototskyy, M.W. Davids, J.M. Sibanyoni, J. Goh, B.G. Pollet, J. Alloys Compd. 645 (2015) S454-S459.

[215] N.A. Ali, N.H. Idris, M.F.M. Din, M.S. Yahya, M. Ismail, J. Alloys Compd. 796 (2019) 279-286.

[216] X. Zhang, Z.Y. Shen, N. Jian, J.J. Hu, F. Du, J.H. Yao, M.X. Gao, Y.F. Liu, H.G. Pan, Int. J. Hydrogen Energy 43 (2018) 23327-23335.

[217] L.C. Zhang, K. Wang, Y.F. Liu, X. Zhang, J.J. Hu, M.X. Gao, H.G. Pan, Nano Res. 14 (2021) 148-156.

[218] K.C. Xian, M.H. Wu, M.X. Gao, S. Wang, Z.L. Li, P.Y. Gao, Z.H. Yao, Y.F. Liu, W.P. Sun, H.G. Pan, Small 18 (2022) 2107013.

[219] G.B. Tian, F.Y. Wu, H.Y. Zhang, J. Wei, H. Zhao, L.T. Zhang, J. Phys. Chem.

Solids 174 (2023) 111187.

[220] N.A. Ali, M. S. Yahya, N. Sazelee, M. F. M. Din, M. Ismail, Nanomaterials 12 (2022) 3043.

[221] X. Huang, X.Z. Xiao, X.C. Wang, C.T. Wang, X.L. Fan, Z.C. Tang, C.Y. Wang, Q.D. Wang, L.X. Chen, J. Phys. Chem. C 122 (2018) 27973-27982.

[222] J.Q. Zhang, Q.H. Hou, X.T. Guo, X.L. Yang, J. Alloys Compd. 911 (2022) 165153.

[223] H.R. Liang, Z.Z. Xie, R.L. Zhao, X. B. Wen, F.F. Hong, W.T. Shi, H.Q. Chen, H.Z. Liu, W.Z. Zhou, J. Guo, Z.Q. Lan, Int. J. Hydrogen Energy 47 (2022) 32969-32980.

[224] Z. Jalil, A. Rahwanto, F. Mulana, Mustanir, Int. J. Technol. 8 (2016) 1301-1306.

[225] L.P. Ma, P. Wang, H.M. Cheng, Int. J. Hydrogen Energy 35 (2010) 3046-3050.

[226] M. Ismail, Int. J. Hydrogen Energy 39 (2014) 2567-2574.

[227] L.P. Ma, X.D. Kang, H.B. Dai, Y. Liang, Z.Z. Fang, P.J. Wang, P. Wang, H.M. Cheng, Acta Mater. 57 (2009) 2250-2258.

[228] I.E. Malka, T. Czujko, J. Bystrzycki, Int. J. Hydrogen Energy 35 (2010) 1706-1712.

[229] I.E. Malka, J. Bystrzycki, T. Płociński, T. Czujko, J. Alloys Compd. 509 (2011) S616-S620.

[230] I.E. Malka, M. Pisarek, T. Czujko, J. Bystrzycki, Int. J. Hydrogen Energy 36 (2011) 12909-12917.

[231] I.E. Malka, J. Bystrzycki, Int. J. Hydrogen Energy 39 (2014) 3352-3359.

[232] J.C. Wang, Y. Du, L.X. Sun, X. H. Li, Int. J. Hydrogen Energy, 39 (2014) 877-883.

[233] M. Jangir, A. Jain, S. Yamaguchi, T. Ichikawa, C. Lal, I. P. Jain, Int. J. Hydrogen Energy 41 (2016) 14178-14183.

[234] J.F. Mao, J.X. Zou, C. Lu, X.Q. Zeng, W.J. Ding, J. Power Sources 366 (2017) 131-142.

[235] V. Shukla, A. Bhatnagar, S.K. Verma, A.P. Pandey, A.K. Vishwakarma, P. Srivastava, T.P. Yadav, O.N. Srivastava, Mater. Adv. 2 (2021) 4277-4290.

[236] R. Kesarwani, V. Shukla, M.S.L. Hudson, M.A. Shaz, Int. J. Hydrogen Energy 47 (2022) 27049-27058.

[237] J.S. Youn, D.T. Phan, C.M. Park, K.J. Jeon, Int. J. Hydrogen Energy 42 (2017) 20120-20124.

[238] S. Kumar, A. Jain, S. Yamaguchi, H. Miyaoka, T. Ichikawa, A. Mukherjee, G. K. Dey, Y. Kojima, Int. J. Hydrogen Energy 42 (2017) 6152-6159.

[239] S. Kumar, P.K. Singh, G.N. Rao, Y. Kojima, V. Kain, Int. J. Hydrogen Energy 43 (2018) 15330-15337.

[240] M. Ismail, Int. J. Hydrogen Energy 46 (2021) 8621-8628.

[241] K. Chawla, D.K. Yadav, A. Bajpai, S. Kumar, I.P. Jain, C. Lal, Sustain. Energy Technol. Assess. 51 (2022) 101981.

[242] N.S. Mustafa, M. Ismail, Int. J. Hydrogen Energy 39 (2014) 15563-15569.

[243] N.N. Sulaiman, N. Juahir, N.S. Mustafa, F.A.H. Yap, M. Ismail, J. Energy Chem. 25 (2016) 832-839.

[244] F.A.H. Yap, N.S. Mustafa, M. Ismail, RSC Adv. 5 (2015) 9255-9260.

[245] M.S. Yahya, N.N. Sulaiman, N.S. Mustafa, F.A.H. Yap, M. Ismail, Int. J. Hydrogen Energy 43 (2018) 14532-14540.

[246] M. Ismail, M.S. Yahya, N.A. Sazelee, N.A. Ali, F.A.H. Yap, N.S. Mustafa, J. Magnes. Alloy 8 (2020) 832-840.

[247] F.A.H. Yap, N.N. Sulaiman, M. Ismail, Int. J. Hydrogen Energy 44 (2019) 30583-30590.

[248] Y.F. Liu, C. Liang, H. Zhou, M.X. Gao, Q.D. Wang, Chem. Commun. 47 (2011) 1740-1742.

[249] V.V. Bhat, A. Rougier, L. Aymard, X. Darok, G. Nazri, J.M. Tarascon, J. Power Sources 159 (2006) 107-110.

[250] M. Naguib, M. Kurtoglu, V. Presser, J. Lu, J.J. Niu, M. Heon, L. Hultman, Y. Gogotsi, M.W. Barsoum, Adv. Mater. 23 (2011) 4248-4253.

[251] M. Naguib, V.N. Mochalin, M.W. Barsoum, Y. Gogotsi, Adv. Mater. 26 (2014) 992-1005.

[252] J.A. Bolarin, R. Zou, Z. Li, Z. Zhang, H.J. Cao, Appl. Mater. Today 29 (2022) 101570.

[253] Y.F. Liu, H.F. Du, X. Zhang, Y.X. Yang, M.X. Gao, H.G. Pan, Chem. Commun. 52 (2016) 705-708.

[254] Z.Y. Shen, Z.Y. Wang, M. Zhang, M.X. Gao, J.J. Hu, F. Du, Y.F. Liu, H.G. Pan, Mater. 1 (2018) 114-120.

[255] Z.J. Wu, J.H. Fang, N. Liu, J. Wu, L.L. Kong, Micromachines 12 (2021) 1190.

[256] J.X. Li, S. Wang, Y.L. Du, W.H. Liao, Int. J. Hydrogen Energy 44 (2019) 6787-6794.

[257] Z.N. Huang, Y.Q. Wang, M.G. Zhang, Int. J. Hydrogen Energy 46 (2021) 33176-33185.

[258] Z.Y. Wang, X.L. Zhang, Z.H. Ren, Y. Liu, J.J. Hu, H.W. Li, M.X. Gao, H.G. Pan, Y.F. Liu, J. Mater. Chem. A 7 (2019) 14244-14252.

[259] Y.N. Liu, H.G. Gao, Y.F. Zhu, S.Y. Li, J.G. Zhang, L.Q. Li, Appl. Surf. Sci.493 (2019) 431-440.

[260] C.L. Lu, H.Z. Liu, L. Xu, H. Luo, S.X. He, X.Q. Duan, X.T. Huang, X.H. Wang, Z.Q. Lan, J. Guo, J. Magnes. Alloy 10 (2022) 1051-1065.

[261] Y.H. Jia, S.M. Han, W. Zhang, X. Zhao, P.F. Sun, Y.Q. Liu, H. Shi, J.S. Wang, Int. J. Hydrogen Energy 38 (2013) 2352-2356.

[262] J.S. Wang, W. Zhang, Y. Cheng, D.D. Ke, S.M. Han, J. Wuhan Univ. Techn.-Mater. Sci. Ed., 30 (2015) 670-673.

[263] W. Zhang, Y. Cheng, D. Han, S.M. Han, Energy 93 (2015) 625-630.

[264] W. Zhang, G. Xu, Y. Cheng, L.J. Chen, Q. Huo, S.Y. Liu, Dalton Trans. 47 (2018) 5217-5225.

[265] X.B. Xie, X.J. Ma, P. Liu, J.X. Shang, X.G. Li, T. Liu, ACS Appl. Mater. Interfaces 9 (2017) 5937-5946.

[266] P. Wang, Z.X. Wang, Z.H. Tian, C.Q. Xia, T. Yang, C.Y. Liang, Q. Li, Renew. Energy 160 (2020) 409-417.

[267] P. Wang, Z.H. Tian, Z.X. Wang, C.Q. Xia, T. Yang, X.L. Ou, Int. J. Hydrogen

Energy 46 (2021) 27107-27118.

[268] Z.W. Ma, S. Panda, Q.Y. Zhang, F.Z. Sun, D. Khan, W.J. Ding, J.X. Zou, Chem. Eng. J. 406 (2021) 126790.

[269] L.X. Wang, Y. Hu, J.Y. Lin, H.Y. Leng, C.H. Sun, C.Z. Wu, Q. Li, F.S. Pan, J. Magnes. Alloy. 10 (2022) 1401-1718.

[270] Y.K. Fu, L. Zhang, Y. Li, S.Y. Guo, Z.C. Yu, W.F. Wang, K.L. Ren, Q.M. Peng, S.M. Han, J. Mater. Sci. Technol. 138 (2023) 59-69.

[271] J. Lu, Y.J. Choi, Z.Z. Fang, H.Y. Sohn, E. Rönnebro, J. Am. Chem. Soc. 131 (2009) 15843-15852.

[272] B. Andrés T, M.Z. Luis, M. Marcos, Int. J. Hydrogen Energy 45 (2020) 27421-27433.

[273] M. Jangir, A. Jain, S. Agarwal, T.F. Zhang, S. Kumar, S. Selvaraj, T. Ichikawa, I. P. Jain, Int J Energy Res. 42 (2018) 1139-1147.

[274] S.Q. Hao, D.S. Sholl, J. Phys. Chem. C 116 (2012) 2045-2050.

[275] F. Cuevas, D. Korablov, M. Latroche, Phys. Chem. Chem. Phys. 14 (2012) 1200-1211.

[276] K. Kitabayashi, K. Edalati, H.W. Li, E. Akiba, Z. Horita, Adv. Energy Mater. 22 (2020) 1900027.

[277] N. Patelli, M. Calizzi, A. Migliori, V. Morandi, L. Pasquini, J. Phys. Chem. C 121 (2017) 11166-11177.

[278] Y.Y. Chen, J.H. Dai, Y. Song, Int. J. Hydrogen Energy 45 (2020) 21600-21610.

[279] S. K.rVerma, A. Bhatnagar, V. Shukla, P. K. Soni, A. P. Pandey, T. P. Yadav, O. N.

Srivastava, Int. J. Hydrogen Energy 45 (2020) 19516-19530.

[280] P. Rizo-Acosta, F. Cuevas, M. Latroche, J. Mater. Chem. A 7 (2019) 23064-23075.

[281] X.L. Luo, D.M. Grant, G.S. Walker, J. Alloys Compd. 622 (2015) 842-850.

[282] X.L. Luo, D.M. Grant, G.S. Walker, Int. J. Hydrogen Energy 38 (2013) 153-161.

[283] Q. Luo, Q.F. Gu, B. Liu, T.F. Zhang, W.Q. Liu, Q. Li, J. Mater. Chem. A 6 (2018) 23308-23317.

[284] M. Chen, Y. Q. Wang, X. Z. Xiao, Y. H. Lu, M. Zhang, J. G. Zheng, L. X. Chen, Appl. Sur. Sci. 541 (2021) 148375.

[285] X.L. Ding, Y.T. Li, F. Fang, D.L. Sun, Q.G. Zhang, J. Mater. Chem. A 5 (2017) 5067-5076.

[286] X.L. Zhang, X.Z. L.C. Zhang, Z.G. Huang, F. Fang, Y.X. Yang, M.X. Gao, H.G. Pan, Y.F. Liu, J. Mater. Sci. Technol. 144 (2023) 168-177.

[287] Y. Wang, L. Li, C.H. An, C.C. Chen, L.F. Jiao, H.T. Yuan, Nanoscale 6 (2014) 6684-6691.

[288] J.H. Shin, G.J. Lee, Y.W. Cho, K.S. Lee, Catal. Today 146 (2009) 209-215.

[289] M. Tian, C.X. Shang, J. Chem. Technol. Biotechnol. 86 (2011) 69-74.

[290] Q.Y. Zhang, L. Zang, Y.K. Huang, P.Y. Gao, L.F. Jiao, H.T. Yuan, Y.J. Wang, Int. J. Hydrogen Energy 42 (2017) 24247-24255.

[291] Z.H. Tian, Z.X. Wang, P.F. Yao, C.Q. Xia, T. Yang, Q. Li, Int. J. Hydrogen Energy 46 (2021) 40203-40216.

[292] C. Xu, Q.A. Zhang, Int. J. Hydrogen Energy 44 (2019) 24792-24799.

[293] K. Wang, H.F. Du, Z. Y. Wang, M.X. Gao, H.G. Pan, Y.F. Liu, Int. J. Hydrogen

Energy 42 (2017) 4244-4251.

[294] M.Q. Fan, S.S. Liu, Y. Zhang, J. Zhang, L.X. Sun, F. Xu, Energy 35 (2010) 3417-3421.

[295] V.D. Dobrovolsky, O.G. Ershova, Y.M. Solonin, O.Y. Khyzhun, V. Paul-Boncour, J. Alloys Compd. 465 (2008) 177-182.

[296] G. Liu, Y.G. Wang, L.F. Jiao, H.T. Yuan, Int. J. Hydrogen Energy 39 (2014) 3822-3829.

[297] G. Liu, F.Y. Qiu, J. Li, Y.J. Wang, L. Li, C. Yao, L.F. Jiao, H.T. Yuan, Int. J. Hydrogen Energy 37 (2012) 17111-17117.

[298] S.C. Gao, H.Z. Liu, L. Xu, S.Q. Li, X.H. Wang, M. Yan, J. Alloys Compd. 735 (2018) 635-642.

[299] S.C. Gao, X.H. Wang, H.Z. Liu, T. He, Y.Y. Wang, S.Q. Li, M. Yan, J. Power Sources 438 (2019) 227006.

[300] S.C. Gao, X.H. Wang, H.Z. Liu, T. He, Y.Y. Wang, S.Q. Li, M. Yan, Int. J. Hydrogen Energy 45 (2020) 28964-28973.

[301] Z.J. Gao, Z.P. Li, B.H. Liu, J. Alloys Compd. 888 (2021) 161520.

[302] V. Kudiiarov, J.Z. Lyu, O. Semyonov, A. Lider, S. Chaemchuen, F. Verpoort, Appl. Mater. Today 25 (2021) 101208.

[303] H. Zhou, J. Zhang, J. Zhang, X.F. Yan, X.P. Shen, A.H. Yuan, Inorg. Chem. Commun. 54 (2015) 54-56.

[304] Y.Q. Wang, Z.Q. Lan, X.T. Huang, H.Z Liu, J. Guo, Int. J. Hydrogen Energy 44 (2019) 28863-28873.

[305] Z.W. Ma, J.X. Zou, D. Khan, W. Zhu, C.Z. Hu, X.Q. Zeng, W.J. Ding, J. Mater. Sci. Technol. 35 (2019) 2132-2143.

[306] Z.W. Ma, J.X. Zou, C.Z. Hu, W. Zhu, D. Khan, X.Q. Zeng, W.J. Ding, Int. J. Hydrogen Energy 44 (2019) 29235-29248.

[307] J.S. Yang, K.M. Zhang, Z.W. Ma, X. Zhang, T.P. Huang, S. Panda, J.X. Zou, Int. J. Hydrogen Energy 46 (2021) 28134-28143.

[308] M. Chen, X.B. Yang, J. Cui, J.J. Tang, L.Y. Gan, M. Zhu, Y.J. Zhao, Int. J. Hydrogen Energy 37 (2012) 309-317.

[309] R.A. Varin, T. Czujko, E.B. Wasmund, Z.S. Wronski, J. Alloys Compd. 446 (2007) 63-66.

[310] H. Wang, J. Hu, F.G. Han, Y.S. Lu, J.W. Liu, L.Z. Ouyang, M. Zhua, J. Alloys Compd. 645 (2015) S209-S212.

[311] Y.S. Liu, S. Wang, Z.L. Li, M.X. Gao, Y.F. Liu, W.P. Sun, H.G. Pan, Processes 9 (2021) 892.

[312] Y.P. Pang, T. Yuan, J.H. Yang, M.X. Gao, H.G. Pan, Y.F. Liu, S.Y. Zheng, Catal. Today 318 (2018) 107-112.

[313] Z.H. Sun, J. Zhou, Q.G. Zhang, Prog. Nat. Sci. Mater. Int. 31 (2021) 152-158.

[314] Q. Li, Y. Li, B. Liu, X.G. Lu, T.F. Zhang, Q.F. Gu, J. Mater. Chem. A 2017, 5 (2017) 17532-17543.

[315] H.G. Gao, Y.N. Liu, Y.F. Zhu, J.G. Zhang, L.Q. Li, Nanotechnology 31 (2019) 115404.

[316] H. Lu, J.B. Li, Y.F. Lu, Y.A. Chen, T.Y. Xie, X. Zhou, Q. Li, F.S. Pan, Int. J.

Hydrogen Energy 47 (2022) 38282-38294.

[317] H.G. Gao, Y.T. Shao, R. Shi, Y.N. Liu, J.L. Zhu, J.C. Liu, Y.F. Zhu, J.G. Zhang, L.Q. Li, X.H. Hu, ACS Appl. Mater. Interfaces 12 (2020) 47684-47694.

[318] W. Zhu, S. Panda, C. Lu, Z. W. Ma, D. Khan, J.J. Dong, F.Z. Sun, H. Xu, Q.Y. Zhang, J.X. Zou, ACS Appl. Mater. Interfaces 12 (2020) 50333-50343.

[319] H.G. Gao, R. Shi, J.L. Zhu, Y.N. Liu, Y.T. Shao, Y.F. Zhu, J.G. Zhang, L.Q. Li, X.H. Hu, Appl. Surf. Sci. 564 (2021) 150302.

[320] C. Peng, C.Z. Yang, Q.G. Zhang, J. Mater. Chem. A 10 (2022) 12409-12417.

[321] H.Z. Liu, C.L. Lu, X.C. Wang, L. Xu, X.T. Huang, X.H. Wang, H. Ning, Z.Q. Lan, J. Guo, ACS Appl. Mater. Interfaces 13 (2021) 13235-13247.

[322] Z.Q. Lan, H. Fu, R.L. Zhao, H.Z. Liu, W.Z. Zhou, H. Ning, J. Guo, Chem. Eng. J. 431 (2022) 133985.

[323] Y.H. Wang, G.G. Fan, D.F. Zhang, Y.P. Fan, B.Z. Liu, J. Alloys Compd. 914 (2022) 165291.

[324] Z.W. Ma, Q.Y. Zhang, W. Zhu, D. Khan, C. Hu, T.P. Huang, W.J. Ding, J.X. Zou, Sustain. Energy Fuels 4 (2020) 2192-2200.

[325] A. Kadri, X.D. Yao, Int. J. Recent Tech. Eng. 8 (2019) 3149-3155.

[326] L.T. Zhang, F.M. Nyahuma, H.Y. Zhang, C.S. Cheng, J.G. Zheng, F.Y. Wu, L.X. Chen, Green Energy Environ. 2021, doi.org/10.1016/j.gee.2021.09.004.

[327] K.C. Tome, S.L. Xi, Y.Y. Fu, C. Lu, N. Lu, M.L. Guan, S.X. Zhou, H. Yu, Int. J. Hydrogen Energy 47 (2022) 4716-4724.

[328] N.N. Sulaiman, M. Ismail, Int. J. Hydrogen Energy 44 (2019) 30574-30582.

[329] H. Imamura, S. Tabata, N. Shigetomi, Y. Takesue, Y. Sakata, J. Alloys Compd. 330 (2002) 579-583.

[330] C.X. Shang, Z.X. Guo, J. Power Sources 129 (2004) 73-80.

[331] Z.G. Huang, Z.P. Guo, A. Calka, D. Wexler, H.K. Liu, Mater. Lett. 61 (2007) 3163-3166.

[332] Z.G. Huang, Z.P. Guo, A. Calka, D. Wexler, J. Wu, P.H.L. Notten, H.K. Liu, Mater. Sci. Eng. A 447 (2007) 180-185.

[333] C.Z. Wu, P. Wang, X. Yao, C. Liu, D.M. Chen, G.Q. Lu, H.M. Cheng, J. Alloys Compd. 414 (2006) 259-264.

[334] C.Z. Wu, P. Wang, X.D. Yao, C. Liu, D.M. Chen, G.Q. Lu, H.M. Cheng, J. Phys. Chem. B 109 (2005) 22217-22221.

[335] M.A. Lillo-Ródenas, Z.X. Guo, K.F. Aguey-Zinsou, D. Cazorla-Amorós, A. Linares-Solano, Carbon 46 (2008) 126-137.

[336] R.K. Singh, H. Raghubanshi, S.K. Pandey, O.N. Srivastava, Int. J. Hydrogen Energy 35 (2010) 4131-4137.

[337] T. Spassov, Z. Zlatanova, M. Spassova, S. Todorova, Int. J. Hydrogen Energy 35 (2010) 10396-10403.

[338] V. Fuster, F.J. Castro, H. Troiani, G. Urretavizcaya, Int. J. Hydrogen Energy 36 (2011) 9051-9061.

[339] F.J. Castro, V. Fuster, G. Urretavizcaya, J. Alloys Compd. 509 (2011) S595-S598.

[340] M. Lototskyy, J.M. Sibanyoni, R.V. Denys, M. Williams, B.G. Pollet, V.A. Yartys, Carbon 57 (2013) 146-160.

[341] R.R. Shahi, H. Raghubanshi, M.A. Shaz, O.N. Srivastava, Appl. Nanosci. 2 (2012) 195-201.

[342] M.K. Singh, A. Bhatnagar, S.K. Pandey, P.C. Mishra, O.N. Srivastava, Int. J. Hydrogen Energy 42 (2017) 960-968.

[343] S. Shriniwasan, T. Kar, M. Neergat, S.S. V. Tatiparti, J. Phys. Chem. C 122 (2018) 22389-22396.

[344] Y. Jia, Y.N. Guo, J. Zou, X.D. Yao, Int. J. Hydrogen Energy 37 (2012) 7579-7585.

[345] G. Liu, Y. G. Wang, C.C. Xu, F.Y. Qiu, C.H. An, L. Li, L.F. Jiao, H.T. Yuan, Nanoscale 5 (2013) 1074-1081.

[346] S.X. Zhou, Q.Q. Zhang, W.X. Ran, Z.Y. Han, H.L. Niu, S.N. Han, L.Q. Cui, T.H. Zhang, H.P. Chen, D. Liu, J. Alloys Compd. 581 (2013) 472-478.

[347] S.X. Zhou, H.P. Chen, W.X. Ran, N.F. Wang, Z.Y. Han, Q.Q. Zhang, X.L. Zhang, H.L. Niu, H. Yu, D. Liu, J. Alloys Compd. 592 (2014) 231-237.

[348] Y.Q. Huang, G.L. Xia, J. Chen, B.P. Zhang, Q. Li, X.B. Yu, Prog. Nat. Sci-Mater. 27 (2017) 81-87.

[349] A.S. Awad, T. Tayeh, M. Nakhl, M. Zakhour, B. Ourane, M.L. Troëdec, J.L. Bobet, J. Alloys Compd. 607 (2014) 223-229.

[350] L.T. Zhang, L.X. Chen, X.Z. Xiao, X.L. Fan, J. Shao, S.Q. Li, H.W. Ge, Q.D. Wang, Int. J. Hydrogen Energy 39 (2014) 12715-12726.

[351] W.P. Cai, X.S. Zhou, L.D. Xia, K.L. Jiang, S.M. Peng, X.G. Long, J.H. Liang, J. Mater. Chem. A 2 (2014) 16369-16372.

[352] W.P. Cai, X.S. Zhou, L.D. Xia, K.L. Jiang, S.M. Peng, X.G. Long, J.H. Liang, J.

Phys. Chem. C 119 (2015) 25282-25290.

[353] S.U. Rather, A.A. Taimoor, A. Muhammad, Y.A. Alhamed, S.F. Zaman, A.M. Ali, Mater. Res. Bull. 77 (2016) 23-28.

[354] A.S. Awad, M. Nakhl, M. Zakhour, S.F. Santos, F.L. Souza, J.L. Bobet, J. Alloys Compd. 676 (2016) 1-8.

[355] K. Chawla, D.K. Yadav, P. Sharda, N. Lal, S. Sharma, C. Lal, Int. J. Hydrogen Energy 45 (2020) 23971-23976.

[356] S.H. Zhou, W. Zhang, W.F. Wang, Y.K. Fu, H. Yu, L. Zhang, J.Z. Song, Y. Cheng, S.M. Han, ACS Appl. Energy Mater. 4 (2021) 11505-11513.

[357] Y. Kojima, Y. Kawai, T. Haga, J. Alloys Compd. 424 (2006) 294-298.

[358] J. Zhang, H. Qu, G. Wu, L.B. Song, X.F. Yu, D.W. Zhou, Int. J. Hydrogen Energy 41 (2016) 17433-17441.

[359] M.L. Ma, J.G. Zhang, Y.F. Zhu, H.J. Lin, Y.N. Liu, Y. Zhang, D.L. Zhu, L.Q. Li, ACS Appl. Energy Mater. 1 (2018) 1158-1165.

[360] Q.F. Meng, Y.Q. Huang, J.K. Ye, G.G. Xia, G.F. Wang, L.X. Dong, Z.X. Yang, X.B. Yu, J. Alloys Compd. 851 (2021) 156874.

[361] P.Y. Yao, Y. Jiang, Y. Liu, C.Z. Wu, K.C. Chou, T. Lyu, Q. Li, J. Magnes. Alloy 8 (2020) 461-471.

[362] X.J. Li, Y.K. Fu, Y.C. Xie, L. Cong, H. Yu, L. Zhang, Y. Li, Int. J. Hydrogen Energy 46 (2021) 33186-33196.

[363] G. Chen, Y. Zhang, J. Chen, X.L. Guo, Y.F. Zhu, L.Q. Li, Nanotechnology 29 (2018) 265705.

[364] M.G. Verón, H. Troiani, F.C. Gennari, Carbon 49 (2011) 2413-2423.

[365] L. Li, G.X. Jiang, H.R. Tian, Y.J. Wang, Int. J. Hydrogen Energy 42 (2017) 28464-28472.

[366] M.J. Liu, X.Z. Xiao, S.C. Zhao, S. Saremi-Yarahmadi, M. Chen, J.G. Zheng, S.Q. Li, L.X. Chen, Int. J. Hydrogen Energy 44 (2019) 1059-1069.

[367] J.G. Yuan, Y.F. Zhu, Y. Li, L. Zhang, L.Q. Li, Int. J. Hydrogen Energy 39 (2014) 10184-10194.

[368] H.H. Cheng, G. Chen, Y. Zhang, Y.F. Zhu, L.Q. Li, Int. J. Hydrogen Energy 44 (2019) 10777-10787.

[369] W. Su, Y.F. Zhu, J.G. Zhang, Y.N. Liu, Y. Yang, Q.F. Mao, L.Q. Li, J. Alloys Compd. 669 (2016) 8-18.

[370] Y. Wang, G. Liu, C. H. An, L. Li, F.Y. Qiu, Y.J. Wang, L.F. Jiao, H.T. Yuan, Chem. Asian J. 9 (2014) 2576-2583.

[371] X. Lu, L.T. Zhang, H.J. Yu, Z.J. Yu, Z.Y. Lu, J. H. He, J.G. Zheng, F.Y. Wu, L.X. Chen, Chem. Eng. J. 422 (2021) 130101.

[372] D.M. Zhou, K.X. Cui, Z.W. Zhou, C.R. Liu, W. Zhao, P. Li, X.H. Qu, Int. J. Hydrogen Energy 46 (2021) 34369-34380.

[373] Z. M. Ding, Y.K. Fu, L. Zhang, I.A. Rodríguez-Pérez, H.M. Zhang, W.F. Wang, Y. Li, S.M. Han, J. Alloys Compd. 843 (2020) 156035.

[374] J.C. Liu, Y.N. Liu, Z.B. Liu, Z.L. Ma, Y.J. Ding, Y.F. Zhu, Y. Zhang, J.G. Zhang, L.Q. Li, J. Alloys Compd. 789 (2019) 768-776.

[375] L.T. Zhang, Z. Sun, Z.L. Cai, N.H. Yan, X. Lu, X.Q. Zhu, L.X. Chen, Appl. Surf.

Sci.504 (2020) 144465.

[376] X.D. Yao, C.Z. Wu, A.J. Du, J. Zou, Z.H. Zhu, P. Wang, H.M. Cheng, S. Smith, G.Q. Lu, J. Am. Chem. Soc. 129 (2007) 15650-15654.

[377] C. Xu, H.J. Lin, J. Liu, P. Zhang, Y. Meng, Y. Liu, J. Zhang, L. Li, Y. Zhu, Chem. Select 4 (2019) 7709-7714.

[378] M. J. Liu, X.Z. Xiao, S.C. Zhao, M. Chen, J.F. Mao, B.S. Luo, L.X. Chen, J. Mater. Chem. A 7 (2019) 5277-5287.

[379] C. Milanese, A. Girella, S. Garroni, G. Bruni, V. Berbenni, P. Matteazzi, A. Marini, Int. J. Hydrogen Energy 35 (2010) 9027-9037.

[380] Y.S. Chuang, S.J. Hwang, J. Alloys Compd. 656 (2016) 835-842.

[381] M. Chen, X.Z. Xiao, X.W. Wang, Y.H. Lu, M. Zhang, J.G. Zheng, L.X. Chen, Carbon 166 (2020) 46-55.

[382] S.J. Hwang, Y.S. Chuang, J. Alloys Compd. 664 (2016) 284-290.

[383] G.H. Liu, L.X. Wang, Y. Hu, C.H. Sun, H.Y. Leng, Q. Li, C.Z. Wu, J. Alloys Compd. 881 (2021) 160644.

[384] A. Bhatnagar, S.K. Pandey, A.K. Vishwakarma, S. Singh, V. Shukla, P.K. Soni, M.A. Shaz, O.N. Srivastava, J. Mater. Chem. A 4 (2016) 14761-14772.

[385] Z.Y. Wang, Z.H. Ren, N. Jian, M.X. Gao, J.J. Hu, F. Du, H.G. Pan, Y.F. Liu, J. Mater. Chem. A 6 (2018) 16177-16185.

[386] H. Fu, J.W. Nong, X.B. Wen, H.R. Liang, J. Guo, W.Z. Zhou, X.T. Huang, H.Z. Liu, H. Ning, Z.Q. Lan, J. Alloys Compd. 887 (2021) 161380.

[387] V. Shukla, T.P. Yadav, Int. J. Energy Res. 46 (2022) 12804-12819.

[388] Q.H. Hou, X.L. Yang, J.Q. Zhang, W.J. Yang, E. Lv, J. Alloys Compd. 899 (2022) 163314.

[389] Y. Jia, J. Zou, X. D. Yao, Int. J. Hydrogen Energy 37 (2012) 13393-13399.

[390] Y. Jia, L. Cheng, N. Pan, J. Zou, G.Q. Lu, X. D. Yao, Adv. Energy Mater. 1 (2011) 387-393.

[391] Z.Q. Lan, X.B. Wen, L. Zeng, Z.Q. Luo, H.R. Liang, W.T. Shi, F.F. Hong, H.Z. Liu, H. Ning, W.Z. Zhou, J. Guo, Chem. Eng. J. 446 (2022) 137261.

[392] G. Liu, K.F. Wang, J.P. Li, Y.J. Wang, H.T. Yuan, Int. J. Hydrogen Energy 41 (2016) 10786-10794.

[393] Y. Luo, P. Wang, L.P. Ma, H.M. Cheng, Scrip. Mater. 56 (2007) 765-768.

[394] P. de Rango, A. Chaise, J. Charbonnier, D. Fruchart, M. Jehan, P. Marty, S. Miraglia, S. Rivoirard, N. Skryabina, J. Alloys Compd. 446-447 (2007) 52-57.

[395] A. Chaise, P. de Rango, Ph. Marty, D. Fruchart, S. Miraglia, R. Olivès, S. Garrier, Int. J. Hydrogen Energy 34 (2009) 8589-8596.

[396] S. Garrier, A. Chaise, P. de Rango, P. Marty, B. Delhomme, D. Fruchart, S. Miraglia, Int. J. Hydrogen Energy, 36 (2011) 9719-9726.

[397] A. Khandelwal, F. Agresti, G. Capurso, S. L. Russo, A. Maddalena, S. Gialanella, G. Principi, Int. J. Hydrogen Energy 35 (2010) 3565-3571.

[398] G. Capurso, F. Agresti, S. L. Russo, A. Maddalena, G. Principi, A. Cavallari, C. Guardamagna, J. Alloys Comp. 509 (2011) S646-S649.

[399] S. Garrier, B. Delhomme, P. de Rango, P. Marty, D. Fruchart, S. Miraglia, Int. J. Hydrogen Energy 38 (2013) 9766-9771.

[400] P. de Rango, P. Marty, D. Fruchart, Appl. Phys. A 122 (2016) 126.

[401] H.C. Cheung, D.J. Syu, N.S. Zhuang, K.C. Wu, Y.X. Lu, C.C. Shen, Int. J. Hydrogen Energy,44 (2019) 29170-29178.

[402] M.S. El-Eskandarany, E. Al-Nasrallah, M. Banyan, F. Al-Ajmi, Int. J. Hydrogen Energy 43 (2018) 23382-23396.

[403] M.S. El-Eskandarany, E. Shaban, F. Aldakheel, A. Alkandary, M. Behbehani, M. Al-Saidi, Sci. Rep. 7 (2017) 13296.

[404] M.S. El-Eskandarany, F. Al-Ajmi, M. Banyan, A. Al-Duweesh, Int. J. Hydrogen Energy, 44 (2019) 26428-26443.

[405] M.S. El-Eskandarany, A. Alkandary, F. Aldakheel, M. Al-Saidi, F. Al-Ajmi, M. Banyan, RSC Adv., 2018, 8, 38175-38185.

[406] N.N. Lei, D.Z Shen, X. Chen, RSC Adv., 2019, 9, 27987-27995.

[407] S.N. Nyamsi, M.V. Lototskyy, V.A. Yartys, G. Capurso, M.W. Davids, S. Pasupathi, Int. J. Hydrogen Energy 46 (2021) 19046-19059.

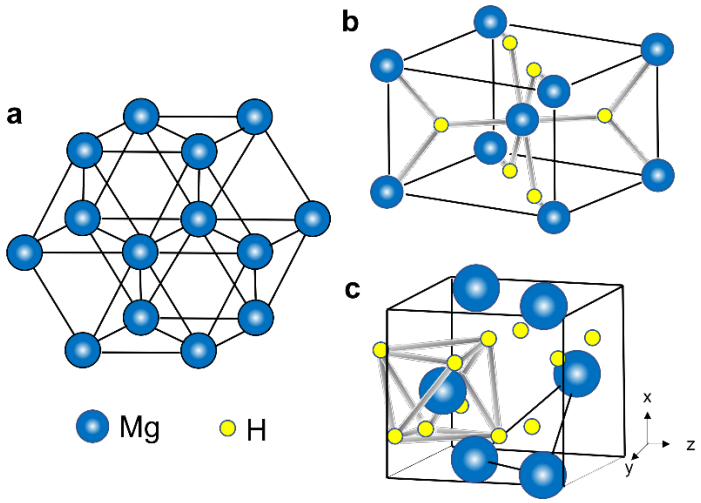

Fig. 1. (a) Mg with hexagonal close-packed (h.c.p.) structure [31], (**b**) α-MgH_2 with TiO_2 type structure (space group $P4_2/mnm$) and (c) γ-MgH_2 with PbO_2 type structure (space group Pbcn) [31,75]

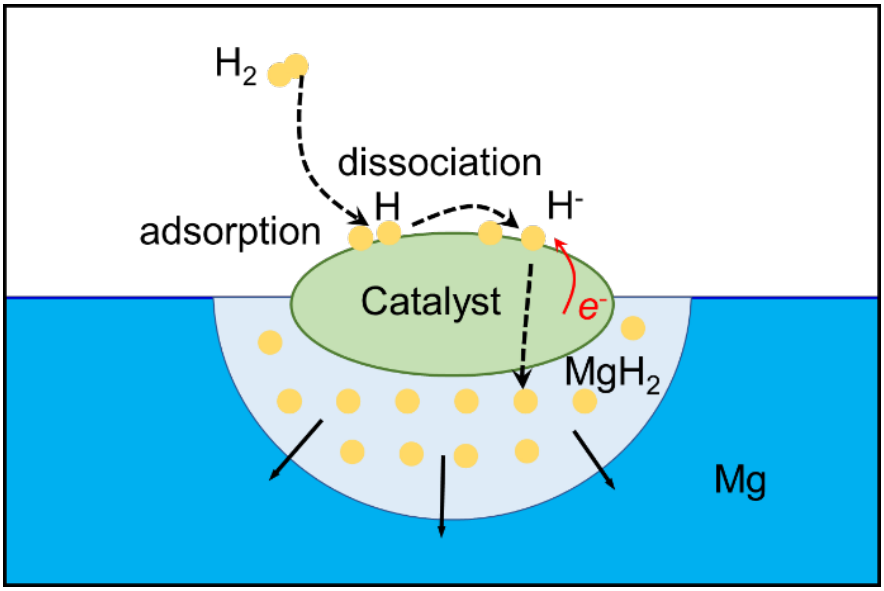

Fig. 2. Schematic drawing for the catalyzed hydrogenation of Mg [93].

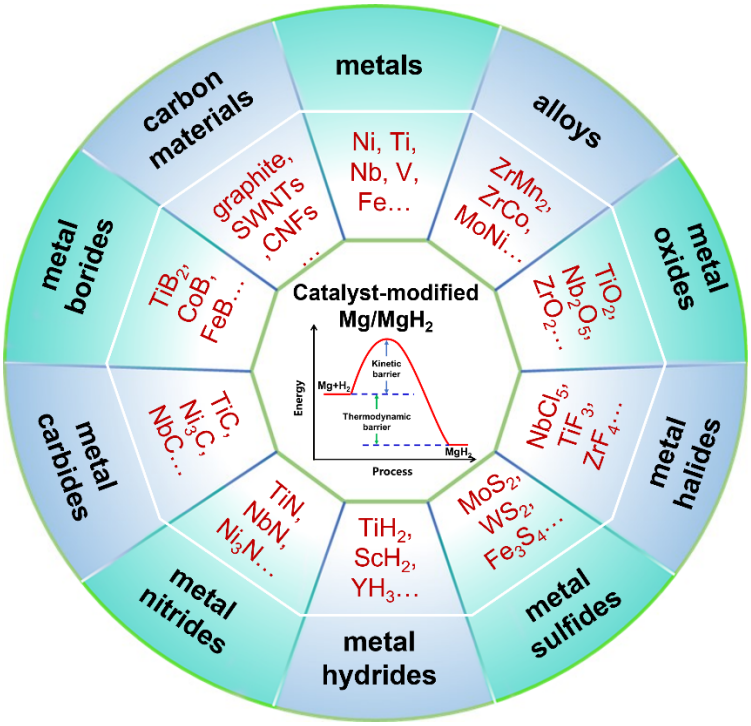

Fig. 3. The catalyst categories of Mg-based hydrogen storage systems.

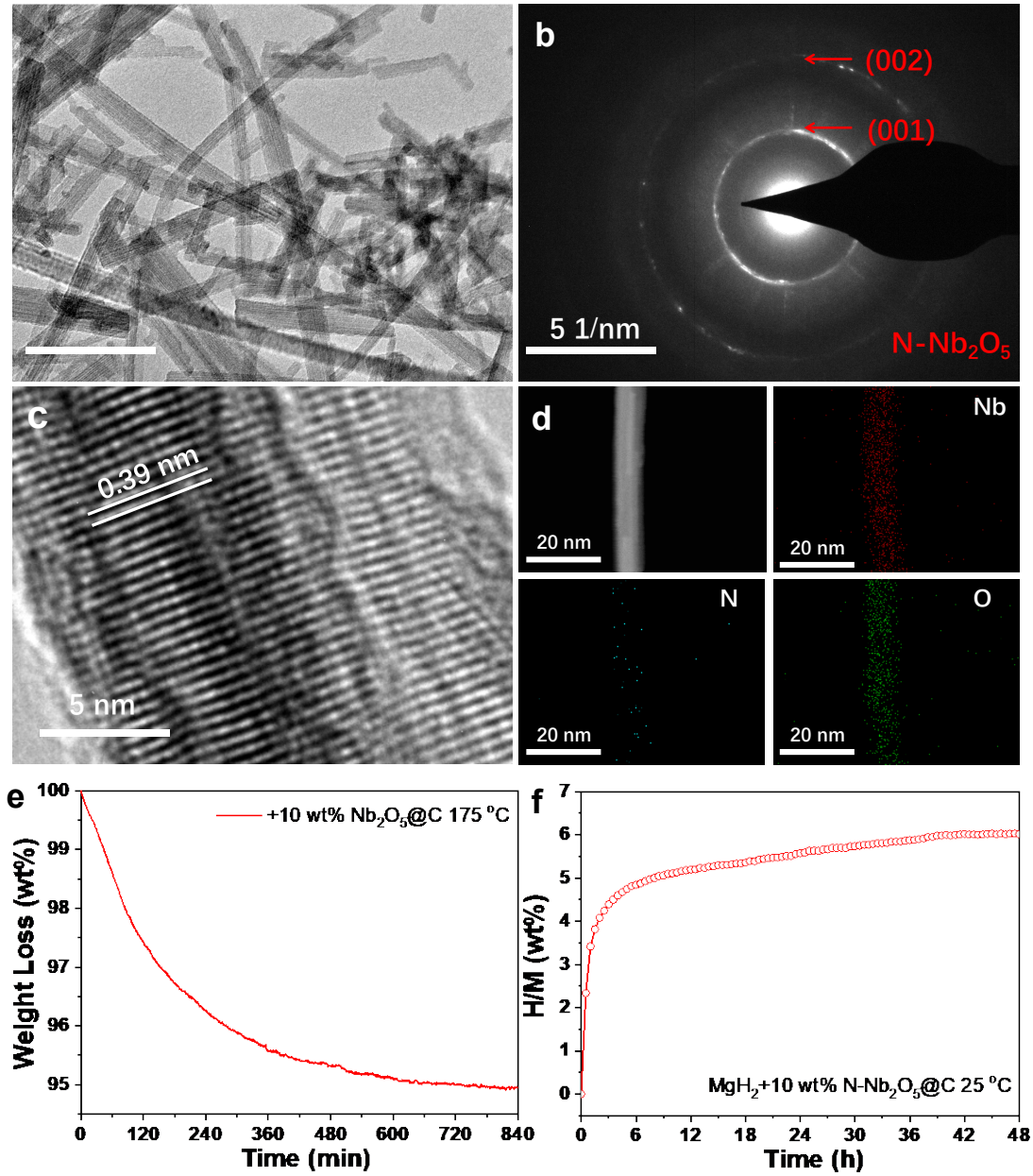

Fig. 4. (a) TEM image, (b) SAED pattern, (c) HRTEM image, and (d) EDS mapping of N-Nb_2O_5@C. Isothermal (e) dehydrogenation and (f) hydrogenation curves of MgH_2-10 wt% N-Nb_2O_5@C samples [190].

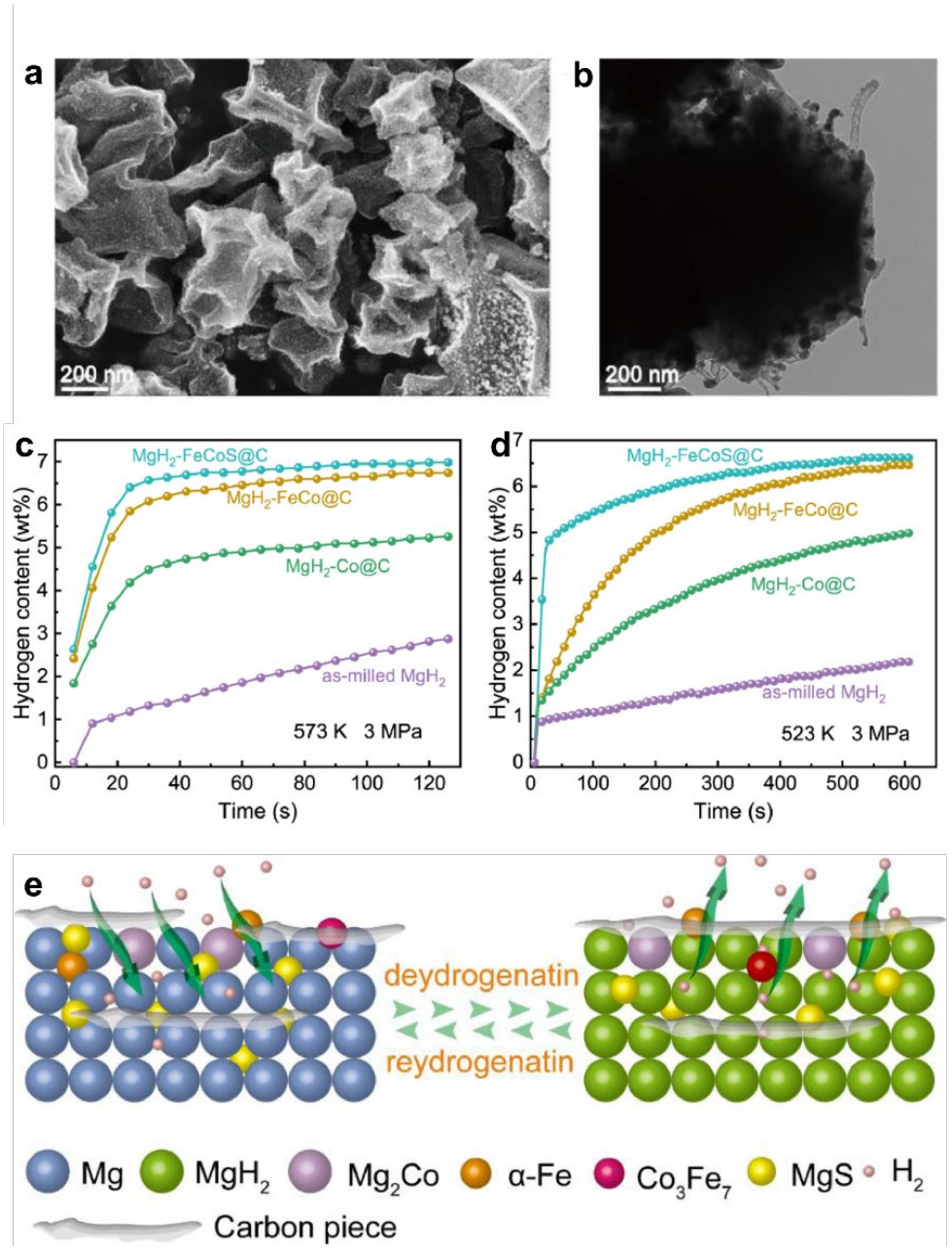

Fig. 5. (a) SEM and (b) TEM images of FeCoS@C. Isothermal absorption curves of the MgH_2 composites under 3.0 MPa H_2 at (c) 573 K and (d) 523 K. (e) Schematic diagram of the synergistic catalysis of hydrogen absorption and desorption by heterogeneous catalysts [270].

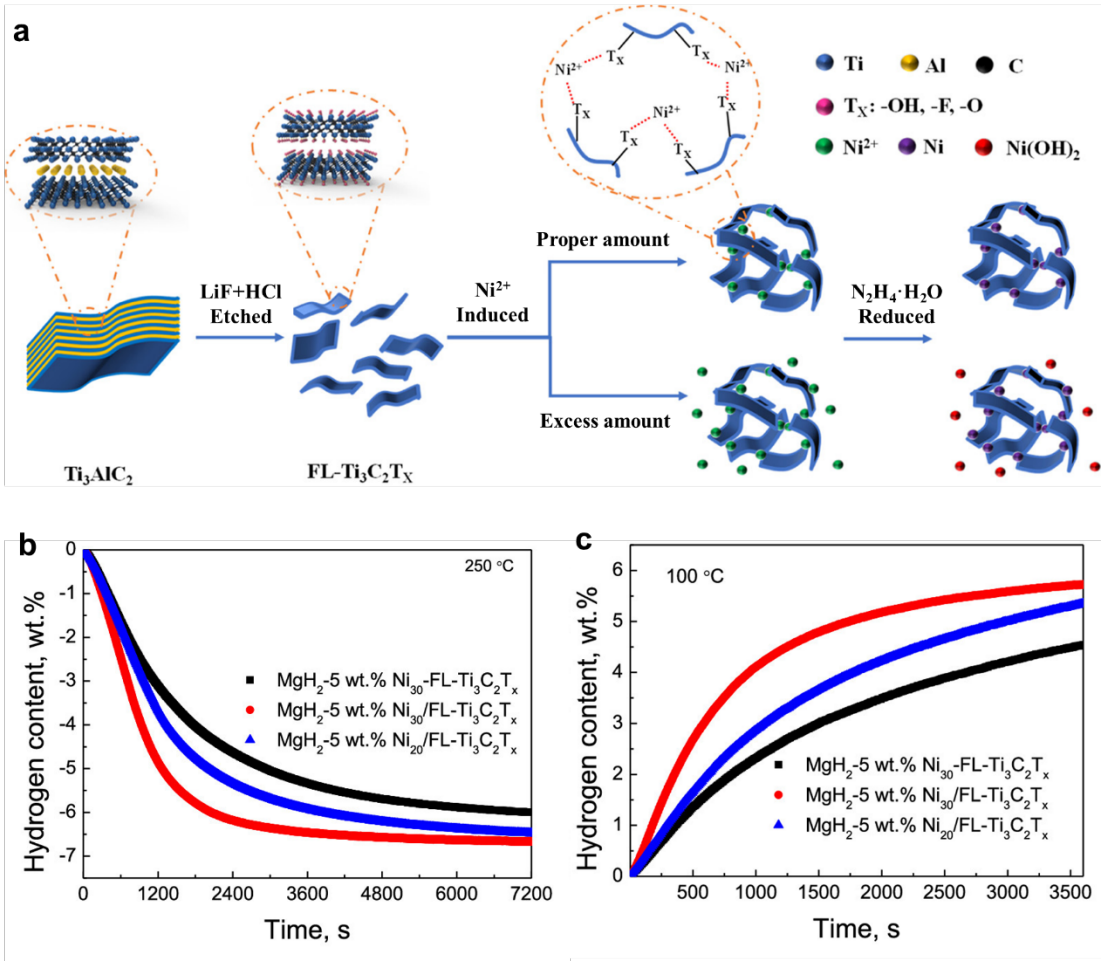

Fig. 6. (a) Schematic diagram for the preparation of Ni/FL-$Ti_3C_2T_x$. (b) Dehydrogenation and (c) hydrogenation curves of the three different catalyst-doped MgH_2 [317].

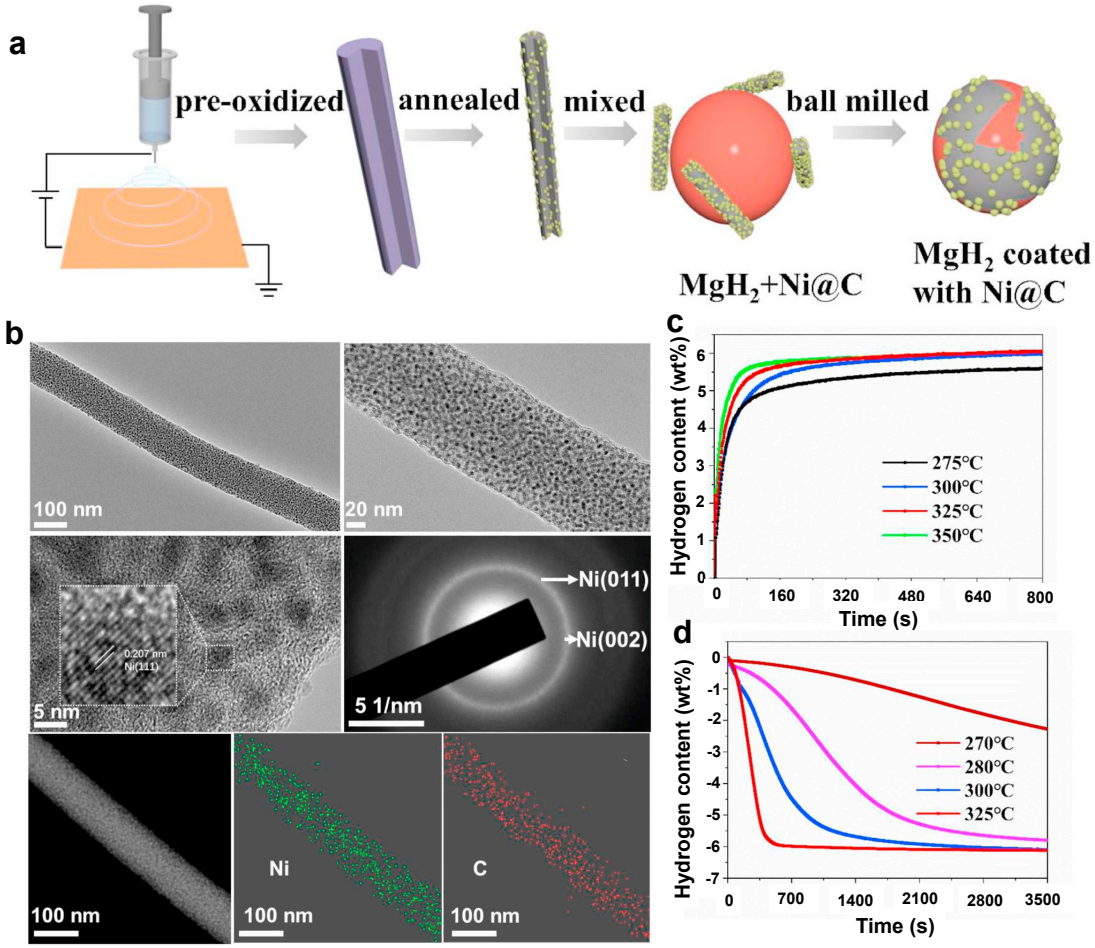

Fig. 7. (a) Schematic illustration for the formation of Ni@C and the synergistic catalytic effect on MgH_2. (b) Microstructures of the as-prepared Ni@C. (c) Hydrogen absorption and (d) desorption curves of MgH_2-10 wt %Ni@C at different temperatures [360].

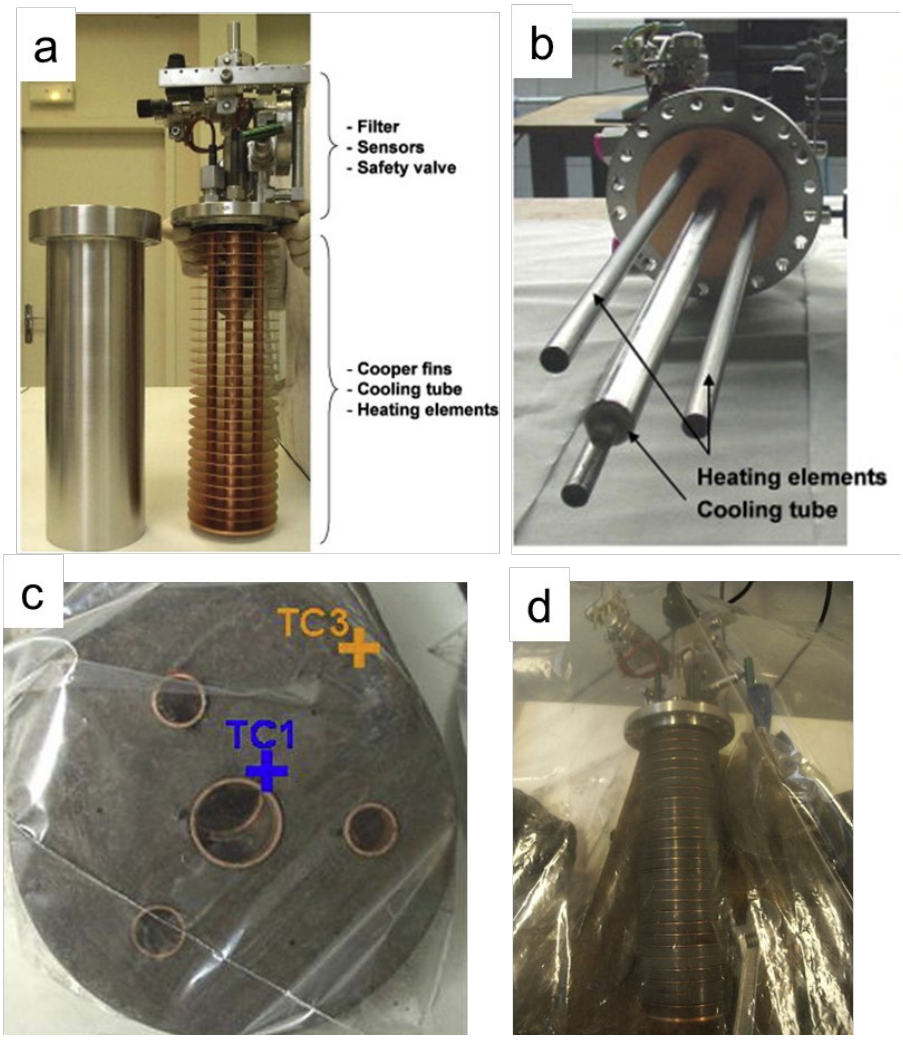

Fig. 8. Photos of a reactor with about 2 L of internal volume. (a) External stainless-steel container and stack of cooper fins connected to the vessel top. (b) Electrical heating elements and central cooling tube. (c) Photo of a drilled BM MgH_2 disk with the cooper rings. (d) Stack of 27 disks of MgH_2 + 5% ENG and copper fins [396].

Table 1. Hydrogen storage properties of MgH_2 modified with metal and alloy catalysts.

Catalyst	Non-isothermal Deh		Isothermal Deh		Isothermal Reh		Capacity (wt%)/ Cycle	Real catalytic active species	Deh E_a (kJ/mol)	Deh ΔH (kJ/mol H_2)	Ref.
	T_{Onset}/ T_{Peak} (°C)	Capacity (wt%)	T(°C)/ t(min)	Capacity (wt%)	T(°C)/ t(min)	Capacity (wt%)					
Mn+Zr	-	-	-/-	-	190/10	~7	-	Mn+Zr			30
Ni									82		105
V	-	-	250/1000s	-	250/1000s	5.5		VH	62.3	-	108
Ti	-	-	250/1000-	-	250/1000s	5		TiH_2	71.1	-	108
Ni/TiO_2	-/232	-	265/7	6.5	100/10	5	-/-	Multivalent Ti/ Mg_2Ni	43.7 ± 1.5		115
nano-$ZrMn_2$	181.9/250.8	6.7	300/5	6.7	100/3	4.3		$ZrMn_2$	82.2		116
Ni	180/245.3	-	300/3	6.7	125/20	4.6	5.6/20	Mg_2Ni	83.9 ± 9.1	67.61	117
$LiCo_2$	180/-	6.8	250/60	5.5	200/10	6.0	6.1/20	Mg_2Co/ Mg_2CoH_5		83.4	121
Mg@Pt	287.5/373.8	6	350/20	6.5	225/2h	6	-	Pt/Mg_3Pt	152.8		122
Ni	-	-	300/15	7.7	300/15	7.7		Mg_2Ni	-	-	129
Ni	130/203	6.8	350/-	6.8	350/2	5.0	5.0/4	Mg_2Ni	72	75	130
Ni			250/5	6.0	225/5	5.75		Mg_2Ni	51.2		131
Ti			250/5	4.9	225/5	4.1		TiH_2	30.9		131
$NiGS_4$	225/-	6.74	270/1800s	5.78-	250/60s	6.2	6.2/10		93.2	76.5	133
Ni NF	143/244		300/30	6.16	-	--	-	Mg_2Ni	81.5		135
Ni@Pt	210/272	6.2	300/5	5.4	102/1000s	5.7	-		89.9	69.4	136
Ni	288/	-	200/11	6.1	150/5.1	6.1	6.1/600	Mg_2Ni	74		138
Ti NP	190	5.2	350/70	5.2					104		141
Ti	-/326.9	6.8	-/-	-	75/499s	6.6	-	Ti/γ-TiH_2	50.2	75.8 ± 4.7	142
Nb	-	-	300/60	4	200/10	4	-		86.4	71	145
V	-	-	300/15	4	200/30	3.8	-	V	119.4	74.4	146
Fe NS	182.1/222.6	~6.8	300/12.8	6	200/10	6	5/50	Fe_{NS}	40.7 ± 1.0		147
Mg-Er	402.5/430	7.37	-/-	-	300/5	6	-	Er	78.7	69.9	148

$ZrMn_2$	181.9/250.8	6.7	300/5	6.7	100/10	5.3	-	$ZrMn_2$	82.2 ± 2.7		149
nano-FeCo	200/250.9	~7.0	300/9.5	6	300/1	6.7	6.4/10	Fe/Mg_2Co	65.3 ± 4.7		151
YNi_5	-/287.3		300/10	5.92				$YH_3/Mg_2NiH_4/Mg_2NiH_{0.3}$			152
$Zr_{70}Ni_{20}Pd_{10}$	418/437		200/3.8	6	100/1.18	6	6.15/100		92		153
$Ti_{0.16}Cr_{0.24}V_{0.6}$	224/285	6.05	270/20	5.67	270/10	5.93	5.4/30		76.32	54.16	154
$NiMn_{9.3}Al_{4.0}Co_{14.1}Fe_{3.6}$	180/267.	2	-/-	-	-/	-	-		131.34		155
$NdNi_5$	-/284.2		300/10	6.07							156
$TiV_{1.1}Mn_{0.9}$	362.3/368.3		300/7	6.2	300/2	6.2		BCC-$TiV_{1.1}Mn_{0.9}$			157
			270/20	4.53	200/10	5.33					
Ti-Cr-V			285/20	5.28	270/30	6.04			86.46	70.6	160
			300/20	6.3	300/10	5.97					
Nanoscale Ni					300/5	5.3					161
Microscale Ni					300/55	5.3					161
Ti			350/5	3.1	300/7	2.7					162

Table 2. Hydrogen storage properties of MgH_2 modified with oxide catalysts.

Catalyst	Non-isothermal dehydrogenation		Isothermal dehydrogenation		Isothermal hydrogenation		Available capacity (wt%)/ Cycle	real catalytic active species	Deh E_a (kJ/mol)	Deh ΔH (kJ/mol H_2)	Ref.
	T_{Onset}/ T_{peak}(°C)	Capacity (wt%)	T(°C)/ t(min)	Capacity (wt%)	T(°C)/ t(min)	Capacity (wt%)					
N-Nb_2O_5	170/	6.6	250/3 250/10	5 5.5	70/360 100/60	6.0 6.3	6.08/50	$NbN_{0.9}O_{0.1}$	98±3	76±1	87
$NiMoO_4$	243.3/-	6.51	300/10	6.0	150/10	5.5	5.6/10	Mg_2Ni/MoO/Mg_2NiH_4	85.88 ±0.36		119
$CoMoO_4$	277.6/-	6.49	300/60	3.3	150/10	4.9			108.08 ±2.57		119
Cr_2O_3	-/	-	300/60	4.44	300/60	5.87	~4.3/5				164
Al_2O_3	-/-				300/10	4.09		Al_2O_3			
Cr_2O_3	-/-	4.49	-/-	-	300/10	4.02	-	Cr_2O_3			166
V_2O_5	-/-		-/-	-	300/10	3.1	-	V/V_2O_3			
V_2O_5	175/248		300/10	6.4	30/1	6.7	6.0/20	V^0/V^{+3}	56	75.5	167
TiO_2			350/2	4.7	340/10	4					170
TiO_2 quantum dots	260/-	~6.1	300/4.5	6	280/77s 100/30	~6.1 5	~5.89/80	multivalent $Ti^{0/2+/3+/4+}$		78.56	172
1D nano-TiO_2	250/380		350/5	6	350/10	5.5					174
TiO_2	180.5/220.4	-	260/3.2	6	100/10s	5.4	-		67.6		175
TiO_2 nanosheets	220/315	6.89	275/60 300/700s	6 6.4	100/500s 200/44s	2.7 5.3	6.4/10	TiO_2 {001}facest	76.1±1.6		176
Vacancy-rich 2D TiO_2 nanosheet	200/220.2	4	300/10	2.43	200/12	2.65	2.67/100		106.7		177
fl-TiO_2@C	180.3/233.0	~6.5	200/100 225/60 250/8	3 4.9 6	50/40 100/40 150/40	3.0 5 6.3	- - -	multi-valent Ti	67.1		178

TiO_2(B)	200/227.6	6.29	210/70 250/10	4 6.16	50/80 60/80	5.32 5.5	5.9/10	TiO_2(B)	75.3±1		179
$TiO_2/TiCl_3$	175/	6.7	200/15 225/15 250/15	1.5 3 5				multivalent $Ti^{2+/3+/4+}$	75.1	75.2	181
Nb_2O_5	-/-	7	275/15 250/500s	6.05 6	300/1	7	-				182
Nb_2O_5	-/310	6.1	300/7 350/-	6.5 6.1	140/10 350/-	6.6 6.1	6.0/230	Nb_2O_5			188
Mono- Amor- Pyro- Layered- Ortho-	Nb_2O_5	247/283 242/273 242/253 237/259 232/262				1.7 2.2 3.7 3.0 2.7	45/30				189
N-Nb_2O_5@C	170/206	6.2	175/840 225/60	5.5 6.2	25/48h 100/60	6 6.2	6.08/50	Ternary $NbN_{0.9}O_{0.1}$	81±2	74.8	190
Nano-ZrO_2			300/1000s	6.24	150/100s	6.73			13.05		192
nano-ZrO_2	163/235	6.7	185/10 230/20	1.5 5.9	100/12s 200/6s	4 5.9	~5.9/10	multivalent Zr	86.4		193
$Mg_xNb_{1-x}O$	250/	6.5	265/100s	6.0	265/2	6		$Mg_xNb_{1-x}O$			202
$FeTiO_3$	200/316	5.8	-/-	-	250/7	5	-	Fe/TiFe(H_x)			214
$MgNiO_2$	285/	6.2	280/60 320/60	2.6 5.6	200/10	6.1	10/5.1		108		215
$TiNb_2O_7$	178/235	7.0	250/10	5.7	150/15	6.2	6.72/30	TiO/NbO_2/ 2D-$TiNb_2O_7$ $Ti^{2+/3+/4+}$			218
$NiTiO_3$	235/261.5	6.9						Mg_2Ni, Mg_2NiH_4	74±4		221
$CoMoO_4$	250/377.5	6.4	250/60 275/40 300/10	2.81 6.4 6.21	125/60 150/60 175/60	3.89 4.94 5.33	10/5.66		43.26 ±1.06		222

$TiVO_{3.5}$	197/230	6.8	200/10 300/30	5.0 6.8	100/5s 200/200s	3.9 6.5	6.3/50	Metallic Ti/V	62.4	223
NiV_2O_6	227/	5.75	250/75 300/75	4.5 5.2	75/50 150/50	2.2 5.59	50/5.17	Mg_2Ni V_2O_5	92.9±3.3	223

Table 3. Hydrogen storage properties of MgH_2 modified with halide catalysts.

Catalysts	Non-isothermal dehydrogenation		Isothermal dehydrogenation		Isothermal hydrogenation		Available capacity (wt%)/ Cycle	Real catalytic active species	Activation energy/ (kJ/mol)	Enthalpy change/ (kJ/mol H_2)	Ref.
	T_{Onset}/ T_{Peak} (°C)	Capacity (wt%)	T(°C)/ t(min)	Capacity (wt%)	T(°C) /t(min)	Capacity (wt%)					
ZrF_4	212/270	-	-/-	-	-/-	-	-	-	77	-	228
NbF_5	213/262	-	-/-	-	-/-	-	-	-	83	-	
TaF_5	223/270	-	-/-	-	-/-	-	-	-	97	-	
$TiCl_3$	225/274	-	-/-	-	-/-	-	-	-	75	-	
VCl_3	237/278	-	-/-	-	-/-	-	-	-	97	-	
ZrF_4	-/-	-	325/2	6	325/2	6.3	-	-	-	76.4	230
NbF_5	-/-	-	325/3	6	325/2	6.3	-	-	-	79.7	
TaF_5	-/-	-	325/7	5.9	325/3	6.3	-	-	-	79.5	
$TiCl_3$	-/-	-	325/6	6	325/2	6.2	-	-	-	79.1	
TiF_4	150/~220	~6.7	-/	-	-/-	-	-	TiH_2/MgF_2	70	-	233
NiF_2		5.22			350/2 h	5.22	-	Mg_2Ni/ MgF_2/F^-	88.61	-	
VF_3		7.25			350/2 h	7.25	-	V/MgF_2	95.56	-	234
LaF_3		6.6			350/2 h	6.6		La/MgF_2	91.04		
CeF_3		6.02			350/2 h	6.02		Ce/MgF_2	95.51		
CsF	-/-	-	300/40	5.12	300/15	5.26	4.94/25	MgF_2/CsH	98.1	63.1	236
$ZrCl_4$	-/257	~6	-/-	-	-/-	-	-	Zr^0/Zr^{4+}	92	-	238
VCl_3	250/275	~6	-/-	-	-/-	-	-	-	122	-	239
$HfCl_4$	270/-	6.5	300/5	4.5	300/5	5.5	-	$MgCl_2$/Hf	-	77.5	240
$PdCl_2$	-/-	-	350/14	4.47	300/-	6.14	9/5	-	180	57.378	241
K_2TiF_6	245/-	6.5	300/~10	4.75	-/-	-	-	KH/TiH_2/ MgF_2/Ti	132	-	242
			320/~10	5.37	-/-	-					
			350/~10	6.36	350/10	5.71					
K_2NiF_6	260/-	6.1	280/60	1.4	-/-	-	-	KF/KH/	111	70.4	243

			300/~60	4.0	-/-	-	-	Mg_2Ni			
			320/~60	5.5	320/2	3.7	5.1/10				
			340/~60	5.8	-/-	-	-				
K_2ZrF_6	250/-	6.6	300/60	4.1	-/-	-	3.9/10	KH/ZrH_2	80	-	244
K_2NbF_7	255/-	6.5	320/4.6	5.7	320/5.6	5.2	5.4/5	MgF_2/KH/Nb	96.2	-	245
K_2SiF_6	282/-	~6.75	250/2	4.5	320/30	5.1	-	KH/MgF_2/ Mg_2Si	114	-	246
Na_3AlF_6	-/-	-	300/60	5.0	-/-	-	-	$NaMgF_3$/ AlF_3/NaF	129	-	247
$NbCl_5$	-	-	300/50	5.2			-		-	-	249
CaF_2	-	-	300/50	5.8			-		-	-	

Table 4. Hydrogen storage properties of MgH_2 modified with Mxene and sulfide catalysts.

Catalyst	Non-isothermal Deh		Isothermal Deh		Isothermal Reh		Capacity (wt%)/ Cycle	Real catalytic active species	Deh E_a (kJ/mol)	Deh ΔH (kJ/mol H_2)	Ref.
	T_{Onset}/ T_{Peak} (℃)	Capacity (wt%)	T(℃)/ t(min)	Capacity (wt%)	T(℃)/ t(min)	Capacity (wt%)					
Ti_3C_2	185/-	7.2	250/10	5	50/2.5	3	6.4/10	Ti	98.9	-	253
$(Ti_{0.5}V_{0.5})_3C_2$	210/232.6	7.5	300/7	6	120/5s	4.8	6.5/10	Ti/V	77.3	-	254
ML-Ti_3C_2	142/315.2	6.56	240/10	6.45	100/1	4.86	-	Multivalent Ti	99.11	-	255
Ti_2C	423/-	-	-	-	-	-	-	Ti^{2+}/Ti	157.9	59.5	256
NbTiC	195/230	6.8	250/30	5.8	50/15	4	6.5/10	NbTi nanocrystals	80 ± 3	-	258
$Nb_4C_3T_x$	250/230.6	~6.3-	250/385s	5.45	100/2000s	4.22	-	Nb/NbH_x	81.2	-	259
V_2C	190/314	~7	300/10	6.4	-	-	6.4/10	V_2C	126.3 ± 0.4	73.6 ± 0.2	260
MoS_2	367.19/-	-	300/10	0.57	150/13	2.709	-/-	MgS/Mo	87.19±4.48	-	261
WS_2	342/-	4.5	350/21	4.24	150/21	2.818	-/-	MgS/W	-	-	262
Fe_3S_4	287/-	-	350/21	4.01	150/20	3.41	-/-	MgS/Fe	-	-	263
FeS_2	296/289.99	1.24	300/23.3	1.24	150/23.3	3.71	-/-	MgS/Fe	68.94	-	264
NiS	-	-	350/10	5.0	150/10 200/5 400/5	3.5 4.0 5.4	5/5.0	MMgS/Mg_2Ni/ Mg_2NiH_4	64.71	75.34	265
NiS_2	210/-	6.4	300/10	4.7	100/60	5.1	6.4/20	MgS/ Mg_2NiH_4	62.6	-	266
TiS_2	204/-	6.1	300/10	5.9	150/10	5.3	-/-	TiH_2/MgS	50.8±5.5	-	267
NbS_2	213/-	6.1	360/20	5.6	150/10	5.3	-/-	NbH/MgS	54.2±2.9	-	
NiS_2	225/-	6.1	360/20	5.5	150/10	5.5	-/-	-	66.1±5.4	-	
MoS_2	248/-	6	360/20	5.4	150/10	2.5	-/-	Mo/MgS	89.9±3.3	-	
MnS	263/-	6	360/20	5.4	150/10	1.3	-/-	Mn/MgS	93.7±7.3	-	
CoS_2	272/-	6	360/20	5.4	150/10	0.7	-/-	Mg_2CoH_5/	106.6±4.0	-	

CuS	287/-	6	360/20	5.4	150/10	0.2	-/-	MgS $MgCu_2$/ MgS	123.7±8.6	-	
CoS-NBs	/302.7	2.5	300/16.7	1.67	175/120	1.26	-/-	-	120.8±3.2	68.1±1.4	268
MoS_2	259/-	-	280/20	4.0	200/5	4.5	-/-	Mo	-	76.82±4.2	269
FeCoS@C	277/371	6.8	300/50	4.6	200/15 300/1	4.56 6.78	-/-	MgS/C	91.9	-	270

Table 5. Hydrogen storage properties of MgH_2 modified with hydrides and other catalysts.

Catalyst	Non-isothermal Deh		Isothermal Deh		Isothermal Reh		Capacity (wt%)/ Cycle	Real catalytic active species	Deh E_a (kJ/mol)	Deh ΔH (kJ/mol H_2)	Ref.
	T_{Onset}/ T_{Peak} (℃)	Capacity (wt%)	T(℃)/ t(min)	Capacity (wt%)	T(℃)/ t(min)	Capacity (wt%)					
TiH_2	280/335	6	316/100	6	315/200	6	-/-	Ti/TiH_2	89.4	-	140
TiH_2	180/-	6.20	240/20	4	240/1	5	6.2/80	TiH_2	58.4	68	271
TiH_2	160/250	5.1	-/-	-	300/4	4.6	-/-	Ti/TiH_2	77.58	-	273
TiH_2	230/-	5.5	250/7	5.5	175/6	5.5		TiH_2	72	75.8±0.7-	275
TiH_2	-/-	-	150/1000	1.75-2	150/1000	3.5		-	-	68.1±0.9	277
TiH_2@Gr	~204/-	~6.77	300/15	5.48	300/1.3	5.59	5.65/5 5.65/25	TiH_2@Gr	88.89±3.8 6	74.54	279
VH	-/-	-/-	300/15	6.1	300/15	5.2	3.5/20		-	-	280
TiH_2			300/15	4.5	300/15	4.1	4.8/20				280
ScH_2	288/390	5.8	-/-	-	-/-	-	-	TiH_2	62±5	76±1	281
ScH_2	250/310	4.3	290/5	3.0	290/5	3.2	4.3/55	ScH_2	82±1	77±0.7	282
$Nd_4Mg_{80}Ni_8$	-/-	-	-/-	-	-/-	-	4.77/38	NdH_2/Mg_2Ni	-	-	283
ZrH_2	203/237.7	6.42	265/10	6.49	65/60	5.74	-/-	ZrH_2	94.70±5	72	284
Zr	235/-	6	300/60	3	300/1	4.9	-/-	ZrH_2	53±6	-	285
			350/30	5.7	200/1	4.0					
VH_x	182/230	6.8	230/10	6.3	150/1	5.8	-	V/VH_x	89.0	74	286
			210/30	5.6	50/30	4.9					
Nano-TiN	218/-	6									287
TiN-graphene	167/313	6.01	300/18	6	275/60	5.8			120		287
TiC	199/-	6	300/1700s	6.6			5/6	TiC			288
TiC	190/275	6			300/50	5			104		289
			275/20	3.3							
Ni_3C	180/310.7	6.5	300/20	6.2					97.8		290
			325/20	6.3							

Ni_3C	216/-	6	300/50 300/30 360/10	5.5 5.7 5.7	100/30 200/10 300/3 360/3	5 5.5 5.8 6			72.8	73.3	291
Nano-Ta_2C	257/-	6	350/15 300/60	6.0 3.9	300/5 200/60	5.8 5.4					292
TiC	245/328	6.7	300/2000s	6.3	300/3000s	6.01	10/5.81	Ti/TiH_2	144.62		294
TiB_2	350/400	3.5									295
TiB_2/GNS	210/319	6.5	300/10 270/40 240/5h	6.5 6.3 6					90.8		296
NiB	180/	6.1	300/10	6					59.7	76.3±3	297
Nano-CoB/CNTs	225/271	6.5	300/60	6.5	200/20s	5.67		Co_3MgC/CoB/ CNTs	89.1		298
FeB	235/289	6.5	300/30	4	150/10	3.3		Fe	100.6		299
FeB-CNTs	196/274	6.5	300/30	5.9	150/10	6.2	20/6.02	Fe	89.7		
CoFeB-CNTs	177/289.2	6.5	300/30	6.5	150/10	6.2	20/6.4	Fe/CoFe/B/ Co_3MgC	83.2±1.3		300
LaNiB	200/-	6.6	300/20	6	250/20 300/5	6.6 6		$MgNi_3B_2$/ LaBNI			301
Co-MOF	362.7				300/3 h	3.5		Mg_2Co	73.9±2	78.2±3.4	305
Fe-MOF	341.6				300/3 h	3.5		Fe	66.8±3.3	77.8±3.4	
Ni-MOF	224/272	3.4	325/3h 300/3h	3.4 3	325/3 h 375/3 h	5.09 5.17	10/3.4	Mg_2Ni/ Mg_2NiH_4	126.7	78.7	306

Table 6. Hydrogen storage properties of MgH_2 modified with composite catalysts.

Catalyst	Non-isothermal Deh		Isothermal Deh		Isothermal Reh		Capacity (wt%)/ Cycle	Real catalytic active species	Deh E_a (kJ/mol)	Deh ΔH (kJ/mol H_2)	Ref.
	T_{Onset}/ T_{Peak} (℃)	Capacity (wt%)	T(℃)/ t(min)	Capacity (wt%)	T(℃)/ t(min)	Capacity (wt%)					
Ni/TiO_2	175/231	6.5	265/7 220//100	6.5 4.5	100/10 150/120s 200/120s	5 5.62 6.1	7/6.0	Multivalent-Ti/ Mg_2Ni/ Mg_2NiH_4	91.6±8.5		115
Y_2O_3/NiO	220/270	6.2	275/15m/60m 250/225	6/6.6 6.3	150/50 150/150 100/240	4.2 5.9 3	50/5.2	Y_2O_3/NiO	86±5		311
Ni/Ti_3C_2		6.75	250/2400 300/2400	5.87 6.73	200/50s 100/1200s	5.6 4.59		Multivalent-Ti	91.64		319
2D-Ni@Ti_3C_2	175/221		250/15 300/200s	5.2 5.0	75/60 125/25s	4 5.4	10/5.1	Mg_2Ni/ Mg_2NiH_4	73±3.5		318
V_2C/Ti_3C_2	180/309.3	6	225/60 300/2	5.1 5.8	40/20	5.2		V_2AlC	79.7±1.9	76.2±0.4	321
Ni_{30}/FL-$Ti_3C_2T_x$	180/262.8	6.2	250/1800s	5.83	100/1700s	5	10/5.6	Multivalent-Ti			317
NbN/Nb_2O_5	178/-	7.21	350/1	4.81	30/5h 90/1.95	5 5	100/5.30	NbN/Nb_2O_5	78.1±5.1		323
Ni@C/$Ti_3C_2T_x$	205/-	6.43	300/5	6.28			50/6.25	Ti-C/T^0	74.7		320
Ti_3C_2/TiO_2	250/308	6.1	250/1700s	5	125/800s	4		Multivalent-Ti	77.69		315
Ni/Y_2O_3	280/302.3	6.3	275/5000s 300/5000s	4 6.3				Mg_2Ni			309
YH_2/Y_2O_3		4.5	300/1800s	4.5	320/5	3		$Mg_{24}Y_5/YH_2$ /YH_3			310
$Mg(AlH_4)_2$-TiF_4	200/228	6.6	275/10 225/10	6.3 2			8/5.9	$Al_3Ti/MgF_2/Al$	73.2		312
PrF_3-Al-Ni			300/1200s	4.5				Pr_3Al_{11}/	109.1		313

			275/2400	4.3			30/4.42	$MgF_2/PrH_3/Mg_2NiH_4$			
			250/3600s	4							
			240/900s	5.69	25/1800s	2.98	30/5.1	$Zr^0/ZrH_x/Zr^{4+}$			
$ZrO_2@Nb_2CT_x$		6.5	300/150s	6.24	150/150s	5.5		$Nb^{4+}/Nb^{2+}/NbC/Nb^0$	60.0	68.64±0.67	316
Fe/Mg_2Ni	260/-	2.6			25/3h	1.36	15/2.6	Mg_2Ni	103.6		324
$Nb_2O_5@MOF$	181.9/-	6.2	250/6.3	6.2	150	4.9	20/5.7		75.57±4.16	79.07±4.19	326
			275/2.6	6.2	175	6.5					
Ni/ZrO_2	255.1/365.5	6.4	310/30	6.83	310/30	6.10	6.2/45		63.4	74.7	327
TiF_3/Cd	150/-	2.75	200/60	0.5	240/5	2.24		Cd/Mg_3Cd	107		328
			240/30	1.07							

Table 7. Hydrogen storage properties of MgH_2 modified with carbon catalysts.

Catalyst	Non-isothermal Deh		Isothermal Deh		Isothermal Reh		Capacity (wt%)/ Cycle	E_a (kJ/mol)	Ref.
	T_{Onset}/ T_{Peak} (℃)	Capacity (wt%)	T(℃)/ t(min)	Capacity (wt%)	T(℃)/ t(min)	Capacity (wt%)			
graphene	330/375	5	375/400s	5					330
CNT	350/395	6.2	350/25	6.2	300/3	6.2			331
graphene	350/395	6.6	350/20	6.2	300/2	6.2			331
graphite	-/358								332
SWNTs/C_{60}			350/10	5.9	300/2 200/120 150/150	6.7 6 5.2			333
SWNT	-/337	6.2	300/30 280/30	6.1 3.2	300/2 200/20 150/20	5.7 6.1 6.0		96	334
MWCNT	-/364		300/90	7					335
MWCNT	350/-	6.9			300/60	5.3			336
Graphite flakes	280/335	6.1	300/20	6.1	200/60	6.1	10/6.1		337
graphite			300/20	6	200/100	6			339
activated carbon	315/364	7.4						73.7	340
graphite	280/341	7.28					10/6.9	61.6	
HGNF	265/-	6.5			310/12	5.6			341
graphene	310/-	6			310/12	4.8			
rGO	-/-	-	320/300 350/60	5 5	-	-	-	-	342
Active carbon	-/350	6.7	300/120 330/30	6.5 6.5	200/120 300/7	6.5 6.7		76	343
GNS	307/334	6.6	300/60 300/120	6.2 6.5	150/180 200/40	6 6.3		76.2	345

					300/1	6.6			
Anthracite coal	250/344		350/10	4.6				76	347
Fluorographene nanosheets	-/336.6	6.5	300/60	5.9	300/5	6.0	10/6.5	156.2	350
Amorphous carbon	284/362	6.85	300/60 400/60	2.18 5.75	200/1 300/30s	4.93 6.17	10/6.82	87.1	356

Table 8. Hydrogen storage properties of MgH_2 modified with carbon-based composite catalysts

Catalysts	Non-isothermal Deh		Isothermal Deh		Isothermal Reh		Available capacity (wt%)/ Cycle	Real catalytic active species	Deh E_a (kJ/mol)	Deh ΔH (kJ/mol H_2)	Ref.
	T_{Onset}/ T_{Peak} (°C)	Capacity (wt%)	T(°C)/ t(min)	Capacity (wt%)	T(°C) /t(min)	Capacity (wt%)					
Ni@C-Mxene	230/241.1	6.5	300/2	5.5	150.2	5	10/6	$Ti^{0/2+}$/Ni/ Mg_2Ni/	54.79±4.34	74.08±3.67	118
Ni/BC-3	/263.3	6.5	300/3.5	6.04	150/60	5.28	20/6.32	Mg_2Ni/	72.41±2.37		120
Ni/Ti_3C_2	190/-	6.73	250/2400s 300/2400s	5.87 6.73	100/1200s 50/5.5 h	4.59 4.51	10/6.4	Ti^0/Ti^{2+}/ Ti^{3+}/Ti^{4+}	91.64		319
$Ni/Al_2O_3/C$		6.5	200/6 h	5.8	23/70 h	6.3-6.5			74		357
Ni/G	-/470.2										358
Ni@C	187/275	6.5	300/500s 275/1200s	6 5.8	275/800s 300/70s	6.5 6.22	10/5.5	Ni/Mg_2Ni	66.5±1.8		359
Ni@C	230/-	6.8	280/3500s 300/3500s 325/700s	5.79 6.12 6.12	300/80s 350/80s 350/800s	4.78 5.6 6.12	5.86/20	Ni	93.08		360
Ni@rGO	~180/259	6.5	300/15	6.1	100/10 100/20	3.7 5	8/6.5	Ni/Mg_2Ni	117.8±3.4	69.6±0.4	361
$Ni/g\text{-}C_3N_4$	262/332	4.29	300 350	1.72 5.04	100/3500s 150/3500s	3.56 5.25		Mg_2NiH_4/ $Mg_2NiH_{0.3}$	82.6		362
Ni/CMK3	160/245	6.6	270/8000s 300/4000s	5.8 6.5	150/40 150/60	5.7 5.9	10/5.96	Ni/Mg_2Ni	43.4±2	74.7±0.5	363
Co/CNTs	~250/323	6.5	250/85 257/1500 300/700	6.5 6.5 6.5	250/100s 275/50	6.5 6.5	15/6.5	Mg2CoH5 Mg2CoH11	108±7		364
Co@C	201/292	6.06	250/60 270/60 300/30	3.72 5.48 5.74	250/120 300/10 300/20	4.5 5.96 6.16			115		365

Co@CNTs	268.7/303.3	6.89	300/60 250/100 280/50 300/16 325/10	6.08 3.92 6.26 6.48 6.89	200/4 250/2 300/1.5	6.02 6.15 6.89	10/6.26	Mg_2Co/ Mg_2CoH_5	130.36	366
Pd/MWCNTs		6.75	200/30 300/20	0.24 6.66	200/400s 300/400s	6.67 6.75		Mg-Pd alloy	78.6	367
Pd-Ni/CMK-3	162/212	6.6	100/300 300/8	1.3 6.6	200/100 70/350	4.8 4		$MgPd_6$/ Mg_2Ni	65.9±2.0	71.9±0.5 368
Ni/MWCNTs	201/-	5.68	250/30	4.31	100/100s	5.68		$Mg_2NiH_{0.3}$/ Mg_2NiH_4		78.43 369
Co/Pd@B-CNTs	202.3/256.2	6.68	225/50 250/30 275/10	3.78 6.26 6.34	50/100 200/20s 250/10s	1.91 6.49 6.68	10/6.35	Mg_6Pd/Mg_2Co/ Mg_2CoH5	97.94	378
TiFe/CNTs	210/-	6.6	250/60 275/30 300/10	4.5 6.1 6.6	75/60 100/60 125/60	1.85 3.6 4.5	10/6.6	TiFe/Fe	60.7±8.0	80.6±1.6 371
Fe-Ni@3DG	-/254.9	6.5	300/1000s	~5.2	300/100s	~7.1	7/6.5	Fe/Ni/Mg_2Ni	83.8	72.2 372
$Fe_{0.64}Ni_{0.36}$@C	250/343	5.18	300/20 310/20 325/20	2.78 4.35 5.18	100/20 150/20	4.2 5.18	5/5.13	Fe/Mg_2Ni/ Mg_2NiH_4	86.9±4.6	373
NiCu/rGO	185/	~6.5	275/20 300/20	5.0 5.8	150/20 200/100s	4.5 5	10/6.5			374
$Zr_{0.4}Ti_{0.6}Co$/ CNTs	200/270.9	6.46	250/60 275/35 300/10	4.8 6.46 6.1	75/60 100/60 125/60	1.5 3.1 4.1	10/6.46	$Zr_{0.4}Ti_{0.6}Co$/ $Zr_{0.4}Ti_{0.6}Co_2$	77±4.8	375
YH_2/Co@C	177/270.54	6.4	300/1700s	6.0	250/150s	6.4		YH_2/YH_3	72.89	377
VTi-CNTs			300/10	6	150/30s/5m 200/30s/5m	4.2/5.1 5.2/5.8			75.6	376

Nb_2O_5/SWCNT	150/-	6.17	300/600s	5.14	300/600s	5.81			102.69	56.28	380
Nb_2O_5/MWCNT	225/-	5.29	300/600s	4.88	300/600s	4.01			141.46	98.23	
ZrO_2/C	208/226	6.57	265/10	6.48	100/10m/120m	4.01/5.09	10/6.3	Zr/ZrH_x	100.7		381
			235/70	5.38	200/10	6.23					
ZrO_2/SWCNT			300/1000s	6.24	150/100s	6.73					382
			240/1000s	3.73	25/100s/700s	1.06/4					
TiO_2@rGO	240/-	6	300/6	6.0	200/2	5.9	20/6	Ti^{2+}/Ti^{4+}	86.7±8.0	73.4±0.9	383
Fe_3O_4@G	262/-	6.5			290/2.5	6.2	6.12/25	Fe/MgFeO	90.53	60.62	384
MnO@C	195/-	6.28	275/15	5	50/160	3.21	50/6	Mn^{2+}	94.6	78.5	386
			300/6	5	100/9	4					
			325/3	5	150/10	5.8					
NiO/C	195/-	6.5	300/10	6.21	125/60	5.13	6.4/20	Mg_2Ni/ Mg_2NiH_4	84.64±2.59		388